VOL. 27 NO. 2 SEPTEMBER 1970
PUBLISHED MONTHLY

JOURNAL OF

ELECTROANALYTICAL CHEMISTRY

AND INTERFACIAL ELECTROCHEMISTRY

International Journal devoted to all Aspects of Electroanalytical Chemistry, Double Layer Studies, Electrokinetics, Colloid Stability, and Electrode Kinetics.

ELSEVIER SEQUOIA S.A.
LAUSANNE

GENERAL INFORMATION

Detailed *Suggestions and Instructions to Authors* were published in the June 1969 issue of the journal, *J. Electroanal. Chem.*, 21 (1969) 565–572. A free reprint can be obtained by application to the publisher.

Types of contributions

(a) Original research work not previously published in other periodicals (regular papers). (b) Reviews on recent developments in various fields. (c) Short communications. (d) Preliminary notes.

A Preliminary Note is a brief report of work which has progressed to the stage when it is considered that the science of chemistry would be advanced if the results were made available as soon as possible to others working on the same subject. Preliminary Notes can in general be published within 4–8 weeks of their acceptance by the editor although this implies that proofs cannot be sent to the author(s). The publisher will attend to correction of the proof but it should be remembered that errors in the manuscript will also appear in the published Note. Preliminary Notes, clearly marked as such, must be sent to Dr. R. Parsons (address given below).

Submission of papers

Papers should be sent to one of the following Editors:

Dr. R. PARSONS, Department of Chemistry, The University, Bristol BS8 1TS, England.
Dr. R. DE LEVIE, Department of Chemistry, Georgetown University, Washington, D.C. 20007, U.S.A.
Dr. R. H. OTTEWILL, Department of Chemistry, The University, Bristol BS8 1TS, England.

For rapid handling papers originating from the American continent should be sent to Dr. DE LEVIE, those of colloid interest to Dr. OTTEWILL, and all others to Dr. PARSONS.

Authors should preferably submit two copies in double-spaced typing on pages of uniform size. Legends for figures should be typed on a separate page. The figures should be in a form suitable for reproduction, drawn in Indian ink on drawing paper or tracing paper, with lettering etc. in thin pencil. The sheets of drawing or tracing paper should preferably be of the same dimensions as those on which the article is typed. Photographs should be submitted as clear black and white prints on glossy paper. Standard symbols should be used in line drawings, the following are available to the printers:

▼ ▽ ■ □ ● ◎ ▪ ◘ ⊕ ⊡ ▪ + ×

All references should be given at the end of the paper. They should be numbered and the numbers should appear in the text at the appropriate places.

A summary of 50 to 200 words should be included.

Authors are recommended to use wherever possible the "Système International d'Unités" (SI Units) approved by the Conférence Générale des Poids et Mesures in 1960. If units are used which are not SI units, authors should provide a conversion factor to SI units. Axes of graphs and headings for tables should always be given clearly with the units of the quantities concerned. It is recommended that this should be done in the form consistent with "Quantity calculus", *e.g.* time as t/min or e.m.f. as E/mV, or capacity per unit area as C/F m^{-2}.

Reprints

Fifty reprints will be supplied free of charge. Additional reprints (minimum 100) can be ordered at quoted prices. They must be ordered on order forms which are sent together with the proofs.

Publication

The *Journal of Electroanalytical Chemistry and Interfacial Electrochemistry* appears monthly. In the period November 1970–December 1971, 6 volumes will appear.

Subscription price for 1971 (covering Nov. 1970–Dec. 1971): Sfr. 476.— (U.S. $112.—) incl. postage. Additional cost for copies by air mail available on request. For subscribers in the U.S.A. and Canada, 2nd class postage paid at New York, N.Y. For advertising rates apply to the publishers.

Subscriptions should be sent to:

ELSEVIER SEQUOIA S.A., P.O. Box 851, 1001 Lausanne 1, Switzerland

NUCLEAR DESALINATION

Proceedings of a Symposium on Nuclear Desalination held by the International Atomic Energy Agency in Madrid, 18-22 November 1968

Published for the International Atomic Energy Agency, Vienna, Austria

6½ x 9½", xvi + 941 pages, 302 illus., 1969, Dfl. 110.00
SBN 444-40806-1

Water supply planners are looking more and more to desalination as a means by which supplemental and new water supplies can be offered at acceptable cost in those regions where natural water supplies are becoming fully utilized. There the water demands are relatively large, nuclear reactors can be an economic energy source for a desalination plant, especially when desalination is combined with the production of electricity in dual-purpose and multi-purpose plants.

In recognition of the growing interest, the International Atomic Energy Agency held a Symposium on Nuclear Desalination, the proceedings of which are published in this volume.

Nearly 300 participants from 36 countries and international organizations discussed more than 60 papers on desalination and reactor applications, research, recent developments and studies, and large desalination plant operating experience. Papers also described agro-industrial complexes and the potential that the energy centre concept may hold for integrated and large-scale area development in certain underdeveloped regions. This concept is of special interest to those countries which are now major importers of food and fertilizers; which possess raw materials that can be processed by energy-intensive industries; or which have climates favourable to year-round agriculture and fertile but 'under-watered' soils.

Elsevier

P.O. Box 211
Amsterdam - The Netherlands
186 E

ELECTROANALYTICAL CHEMISTRY AND INTERFACIAL ELECTROCHEMISTRY
Elsevier Sequoia S.A., Lausanne – Printed in The Netherlands

RAPID DATA ACQUISITION IN ROTATING DISK VOLTAMMETRY. II

SAMUEL C. CREASON AND ROBERT F. NELSON
Department of Chemistry, Sacramento State College, Sacramento, California 95819 (U.S.A.)
(Received February 26th, 1970)

I. INTRODUCTION

In the collection of data with the rotating disk electrode (RDE), the functional variation of interest is that of limiting current (i_{lim}) *vs.* square root of rotation rate ($\omega^{\frac{1}{2}}$). Typically, a plot or tabulation of i_{lim} *vs.* $\omega^{\frac{1}{2}}$ is built up point by point from a series of measurements of i_{lim}, each made at a different, fixed rotation rate. Depending on the number of points involved, such a process may require from 10 to 30 min to complete. However, a continuous plot of i_{lim} *vs.* $\omega^{\frac{1}{2}}$ spanning the rotation rate range of 300–10,000 rev. min^{-1} can be automatically plotted in less than a minute by the use of the technique described in brief previously[1] and more fully herein.

In a typical experiment, a voltage proportional to i_{lim} is applied to the Y-axis input of an X–Y recorder, while a voltage proportional to $\omega^{\frac{1}{2}}$ is applied to the recorder X-axis input. The potential of the electrode is stepped to a value which is sufficient to cause the desired electrode reaction well up on the limiting current plateau so charge-transfer rates are not prohibitively slow, and after the current transient has decayed, the electrode rotation is swept through the required range, producing the desired plot.

Measurement of i_{lim} while electrode rotation rate is varied was originated by Prater[2], who called the technique "rotoamperometry". In his technique, ω is varied linearly with time to produce parabolic plots of i_{lim} *vs.* ω. Although the basic information gathered by the two techniques is similar, the technique developed in the present study appears to offer two advantages. First, if the system under study departs from ideal electrochemical behavior, such departure produces deviations from a straight-line rather than a parabolic plot, so that the deviations, if small, are more apparent. Second, as discussed later, short experiment times are often desirable, in which case a non-linear variation of ω with time is useful.

II. THE TECHNIQUE

In Fig. 1 a plot is shown of i_{lim} *vs.* $\omega^{\frac{1}{2}}$ obtained, by the technique developed in the present study, for the electrolysis of a 8.0×10^{-4} *F* solution of 5,10-dihydro-5,10-dimethylphenazine (DMPZ) in acetonitrile (MeCN)/0.1 *F* tetraethylammonium perchlorate (TEAP). Points from fixed rotation rate experiments are included for comparison; the points and plot are coincident to within *ca.* 1 % over the rotation rate range of 300–7000 rev. min^{-1}.

The DMPZ system is ideal for testing a technique of this sort, since the oxidation is known to be a reversible one-electron process[3] and the oxidation products do

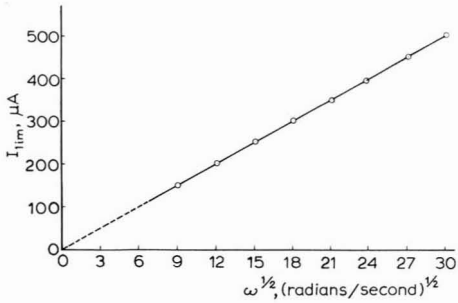

Fig. 1. Rotoamperogram of a 8.0×10^{-4} *F* solution of DMPZ in acetonitrile/0.1 *F* TEAP. (——) Exptl. curve, (------) extrapolation to the origin, (○) data obtained from individual RDE curves at fixed rotation rates.

not film the rotating disk electrode. However, the oxidation products of triphenylamines and carbazoles, systems which are of interest to the authors, tend to film the electrode to a degree, if a relatively long electrolysis time is used. Accordingly, a series of experiments was performed to determine the minimum allowable scan time consistent with accurate measurement of i_{lim}. Typically, the electrode potential was stepped to the desired potential and after the current transient had decayed, the motor rotation rate was brought to the lower limit of the desired range. When i_{lim} had reached its steady state value, the rotation rate was increased by 100 rev. min^{-1} or so and the recorder pen was observed to see if i_{lim} remained constant immediately after the change in rotation rate. This process was repeated until the maximum desired rotation rate was reached and then the entire scan was repeated with more rapid changes in rotation rate. By this means, a minimum time of about 40 s was established for a scan from 1000 to 10,000 rev. min^{-1}, using 25 ml of solution in a 40 ml cylindrical single compartment cell.

During such experiments, for a 500–7500 rev. min^{-1} scan, about 20 s were necessary to reach 1900 rev. min^{-1}, then 10 s to reach 4200 rev. min^{-1} and, finally, 5 s to reach 7500 rev. min^{-1}. Points corresponding to these rotation rates are ap-

TABLE 1. DEPENDENCE OF i_{lim} *vs.* $\omega^{\frac{1}{2}}$ FOR $Fe(CN)_6^{-4}$ ON SOLUTION VOLUME[a]

		$i_{lim}/\mu A$							
		Solution vol./l 0.025				1			
		Scan time/s							
$\omega^{\frac{1}{2}}/s^{-\frac{1}{2}}$	*Rev. min*$^{-1}$	10	30	120	*Fixed* ω	10	30	120	*Fixed* ω
6	344	9.4	11.5	11.6	11.6	8.2	11.3	11.5	11.4
9	773	16.2	17.1	17.2	17.1	16.0	17.0	17.0	17.1
12	1375	22.6	22.8	22.8	22.8	22.0	22.5	22.6	22.6
15	2149	28.5	28.6	28.5	28.6	28.1	28.1	28.1	28.2
18	3094	33.7	33.8	33.8	33.7	33.7	33.6	33.7	33.5
21	4211	39.8	39.9	39.9	39.9	39.5	39.4	39.4	39.6
24	5500	45.4	45.5	45.4	45.6	45.1	45.0	45.2	45.0

[a] 1.06×10^{-3} *F* solution in H_2O/0.2 *F* KCl.

proximately evenly spaced on a scale which is linear in the square-root of rotation rate, as is the case for a plot of i_{lim} *vs.* $\omega^{\frac{1}{2}}$. Thus, to scan between a specified set of rotation rate limits as rapidly as possible, the time derivative of rotation rate must be a function of time that is of higher than first order. No attempt was made to determine the exact nature of the optimum rotation rate–time relationship, since no theoretical basis for such a relationship was apparent.

A motor rotation rate programmer (discussed in detail later) which causes the rotation rate to change as an exponential function of time was constructed. A series of experiments was then performed to determine the minimum allowable scan time for 25 ml of solution in a 40-ml single compartment cell, and 1 l of solution in a beaker, to determine the effect of solution volume. A 1.06×10^{-3} *F* solution of $K_4Fe(CN)_6$ in H_2O/0.2 *F* KCl was used in these experiments. Points from fixed rotation rate experiments and from 10, 30 and 120 s scans were obtained and are summarized in Table 1. If the points from fixed rotation rates are used as the standard, then more than 10 s is required to scan from 344 to 5500 rev. min^{-1}, using 25 ml of solution since not until 1375 rev. min^{-1} is reached do the points from continuous scan and fixed rotation rate experiments agree within 1%. In the corresponding experiment using 1 l of solution, agreement is not reached until 2149 rev. min^{-1}. Thus, the larger volume of solution is slightly more sensitive to rotation rate changes at low rotation rates. For either solution, a 30 s scan time is acceptable since points obtained by the two techniques agree within 1%.

Using a 30 s exponential scan from 344 to 5500 rev. min^{-1} rotoamperograms were obtained for 4-nitrotriphenylamine and N-*p*-methoxyphenylcarbazole. The resultant curves, along with points from fixed rotation rate experiments for comparison, are shown in Figs. 2 and 3, respectively. The points and curves are coincident within *ca.* 1%.

These diagrams point out the potentiality of this technique as a diagnostic tool in elucidating the pathways of electrode mechanisms. Probably its greatest utility is for detecting e.c.e.-type reactions involving organic molecules. Figure 1 establishes that a reversible system will give a perfectly straight-line rotoamperogram that extrapolates to the origin. However, in Figs. 2 and 3 there is a definite bow to the curves. The magnitude of this bow is a function of the rate and extent of the intermediate chemical reaction(s). A relatively fast e.c.e. process will give a slight but

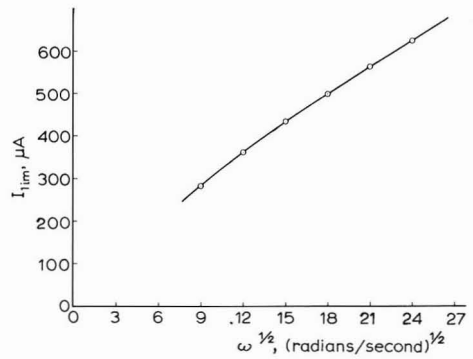

Fig. 2. Rotoamperogram of 1×10^{-3} *F* 4-nitrotriphenylamine in acetonitrile/0.1 *F* TEAP.

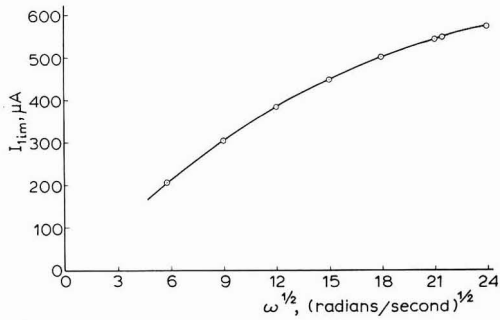

Fig. 3. Rotoamperogram of 1×10^{-3} *F* N-*p*-methoxyphenylcarbazole in acetonitrile/0.1 *F* TEAP.

perceptible bow (the case for 4-nitrotriphenylamine[5]) whereas a multistep electron transfer–chemical step process (an e.c.e.c.e., etc.) will produce a pronounced bend in the rotoamperogram, as seen in Fig. 3 for the carbazole[6]. This is certainly a useful aspect of the technique, but it should be pointed out that other tools such as cyclic voltammetry and chronopotentiometry are far superior as diagnostic tools. However, if one wishes to use rotoamperometry as a diagnostic tool, the criteria formulated for linear scan voltammetry would also hold for rotoamperometry, considering i_{lim} as a function of rotation rate analogous to peak current as a function of scan rate[7-9].

By far its greatest value in our studies has been manifested in experiments where kinetic parameters such as rate constants of homogeneous chemical reactions are desirable. When used in conjunction with the working curves of Feldberg[10,11], this technique can be used to determine the rate constants of chemical reactions associated with electron transfer processes for a large number of compounds in a minimum of time. By recording of a single curve over a time span of 30–60 s, one has data sufficient for the calculation of rate constants over a wide rotation rate range.

This instrument may seem like a great deal of work for such a limited task, but if one is at all engaged in this field, the time spent in building the instrument is repaid in short order!

It should be pointed out that this instrumentation is suitable only for studying the limiting current of an electrode process as a function of rotation rate. If one wishes to run RDE voltammograms to obtain $E_{\frac{1}{2}}$ values, this can be accomplished by simply bypassing the square-rooter and motor programmer and using the E550M master control unit directly. The rotation rate can be kept constant by manipulating the control unit while using a stroboscope (General Radio Model 1531) to monitor the rotation rate. Regulation on the motor is quite good and allows one to obtain discrete rotation rate voltammograms over a wide range of ω's.

III. THE INSTRUMENTATION

A block diagram of the instrumentation involved is shown in Fig. 4. A variable-speed motor is used to drive simultaneously the rotating disk electrode and a tachometer-generator. The output voltage of the tachometer-generator, which is proportional to motor rotation rate, is applied to the input of an analog square-root function generator, the output of which drives the recorder X-axis. The rotating disk electrode is used in a three-electrode cell in conjunction with a conventional potentiostat which

is used to drive the recorder Y-axis.

The motor rotation rate is determined by the magnitude of a control voltage which is produced by the motor rotation rate programmer.

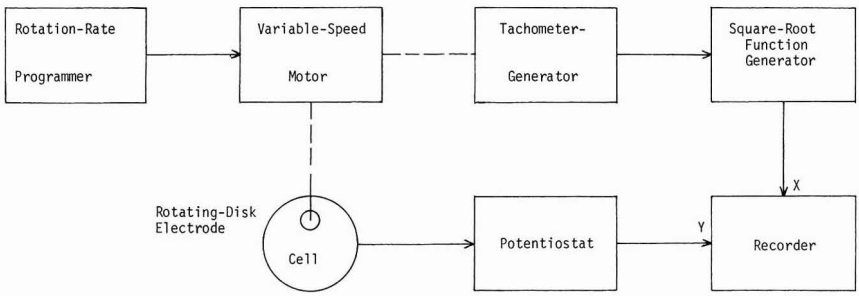

Fig. 4. Block diagram of instrumentation for rapid data acquisition with the rotating disk electrode.

A detailed description of each device follows (the potentiostat employed is the standard Booman–DeFord–Shain–Hawley type and all experimental conditions are as previously described[12]):

1. *The drive-motor assembly and tachometer-generator*

The drive motor assembly chosen consists of a Motomatic E-550 motor (Electro-Craft Corp., Hopkins, Minn.), which was modified by the manufacturer to provide a maximum rotation rate of 10,000 rev. min^{-1}, and a companion E-550M master control unit. The motor rotation rate can be adjusted to any value within the specified range by means of a potentiometer which is an integral part of the control unit, or by means of a voltage which is applied to the control unit from an external source. As it stands, the motor-control unit combination is suitable for fixed rotation rate experiments since the manufacturer specifies that the regulation of rotation rate is within 1%. This degree of regulation is obtained by use of an electromechanical servo system, part of which is a tachometer-generator winding on the motor armature, and which is potentially the source of a voltage to drive the square-root function generator. However, neither lead from this winding may be grounded, so that to obtain an output voltage compatible with the remaining instrumentation would require the use of a differential-input to ground-referenced-output converter. While such a converter may be easily constructed, its cost would approach that of an external tachometer-generator (Motomatic E300, Electro-Craft Corp., Hopkins, Minn.), belt-driven by the motor. The latter approach was chosen.

2. *The square-root function generator*

The prime requirement for this device is that its output voltage be proportional to the square-root of its input voltage over the desired range of input voltage. A tabulation of output voltage *vs.* input voltage for the device constructed is presented in Table 2 and shows that this requirement is met to within an accuracy of $\pm 1\%$ over the input voltage range of 1–25 V.

A schematic diagram of the function generator is shown in Fig. 5. The generator consists of an operational amplifier (A_2) with an analog multiplier (Integrated Circuit

TABLE 2
CHARACTERISTICS OF THE SQUARE-ROOT FUNCTION GENERATOR

e_{in}/V	e_{out}/V		% Difference
	Calcd.	*Obs.*	
1	1.00	1.01	+1.0
2	1.41	1.40	−0.7
3	1.73	1.72	−0.6
4	2.00	2.01	+0.5
5	2.24	2.26	+0.9
9	3.00	3.02	+0.7
16	4.00	3.98	−0.5
25	5.00	5.05	+1.0

IC, and amplifier A_1) in its feedback loop. Since the inputs (pins 4 and 9) of the multiplier are tied together (*via* 470 Ω resistors, to minimize the possibility of parasitic oscillation), it generates a voltage which is proportional to the square of its input voltage. This output is applied to amplifier A_1, which removes the common mode component. By placing these components in the feedback loop of amplifier A_2, a square root function generator results.

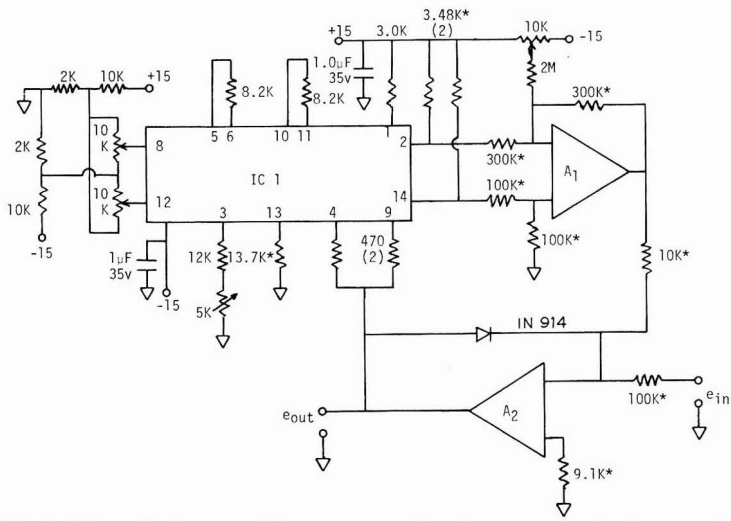

Fig. 5. Schematic diagram of the square-root function generator. Resistance values in Ω, kΩ or MΩ, as indicated. All fixed resistors are ½ W. Resistors marked * are 1% tolerance, others are 5% tolerance. Variable resistors are 1 W, 10% tolerance. IC 1 is an MC 1595L integrated circuit multiplier, Motorola Semiconductors, Phoenix, Arizona. A_1 and A_2 are ZEL-1 operational amplifiers, Zeltex, Inc., Concord, Calif.

The circuit is very similar to one which appears in an information sheet on the integrated circuit[13], except for the type of amplifier used and the inclusion of a diode in the feedback loop of amplifier A_2, which prevents driving the amplifier to saturation if a negative input voltage is applied.

The function generator is powered by a ± 15 V power supply, built according to National Semiconductor Application Notes[14,15].

The balancing procedure for the square-root function generator is critical to the proper operation of the instrument, but it is somewhat tricky. A brief description of the procedure is given in the Appendix.

3. *The motor rotation rate programmer*

The principal requirement for this device is that it be capable of producing an output voltage sufficient to drive the motor to the maximum required rotation rate along an approximately exponential rotation rate *vs.* time path in 60 s or so. A plot of output voltage *vs.* time for the device constructed, Fig. 6, shows that this requirement has been met. The plot can be directly converted to motor rotation rate *vs.* time, since the rotation rate of the E-550 motor is directly proportional to control voltage. Accordingly, an equivalent rotation rate scale has been added.

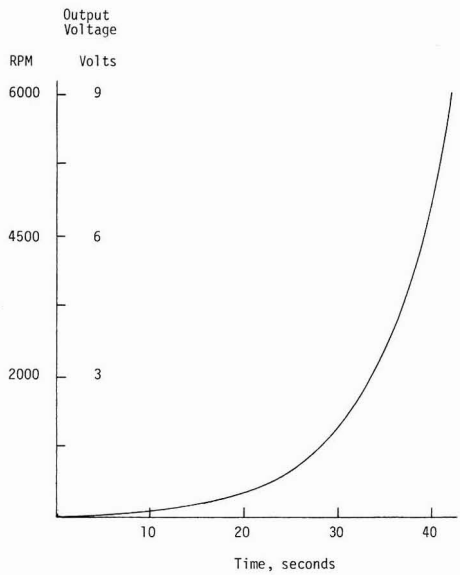

Fig. 6. Motor rotation-rate programmer output voltage and equivalent rev. min^{-1} *vs.* time.

To provide flexibility, five maximum rotation rates, from 2150 to 10,000 rev. min^{-1}, and scan times up to five min can be selected by front panel controls.

A schematic diagram of the programmer is shown in Fig. 7 and consists of an integrator, A1, a gain of minus one-half amplifier, A2, and a biased output buffer, A3. The exponential function is generated by the integrator and the inverting amplifier which injects an inverted facsimile of the integrator output back into the integrator input. A bound diode, D_1, is included in the integrator feedback circuit to reproducibily limit the integrator output voltage.

Scan time is determined by the setting of the variable feedback resistor, R1, which determines the magnitude of the variable input to the integrator, and by the fixed potential which is applied to the integrator *via* resistor R2. In practice, with

resistor R1 set to zero, resistor R2 is adjusted to provide the maximum desired scan time. When resistor R1 is then adjusted to a value other than zero, an additional input is injected into the integrator and the scan time is decreased.

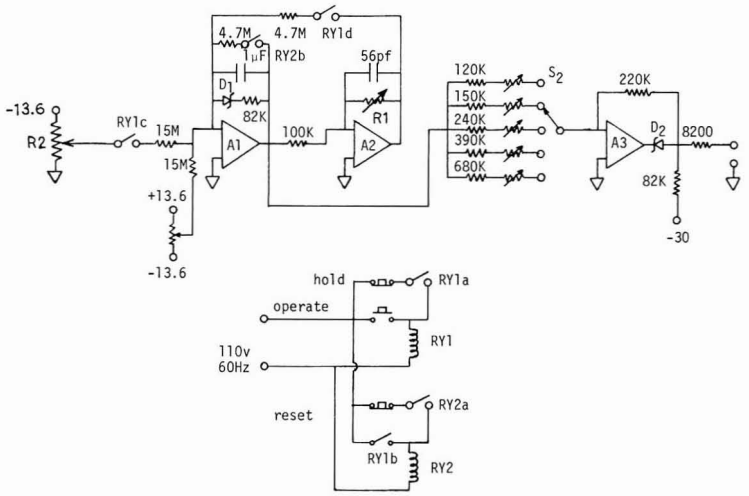

Fig. 7. Schematic diagram of the motor rotation-rate programmer. Resistance values in Ω, kΩ or MΩ, as indicated. Fixed resistors are $\frac{1}{2}$ W, 5% tolerance. Variable resistors are $\frac{1}{2}$ W, 10% tolerance, unmarked variable resistors are 50k. Amplifiers are ZEL-1 operational amplifiers, Zeltex, Inc., Concord, Calif. Relays RY_1 and RY_2 are Type 45-2703, Aemco Corp. Diodes D_1 and D_2 are 9.1 V HEP-140 Zener diodes, Motorola Semiconductors, Phoenix, Ariz.

The control voltage range necessary to drive the motor from 0 to 10,000 rev. min^{-1} is 0 to -15 V. Since the output voltage swing of typical solid state operational amplifiers is ± 10 V, a reverse biased zener diode, D_2, was placed in the feedback loop of the buffer amplifier to translate this swing to from $+1$ to -19 V[16]. An 8200 Ω resistor is included in the buffer output circuit to satisfy the source impedance requirement of the E-550M control unit.

The maximum rotation rate is determined by the value of the buffer amplifier input resistor, which depends on the position of switch S2.

As shown, the programmer can be switched to one of three states. In the operate state, which is selected by momentarily depressing the "operate" switch, relays RY1 and RY2 are actuated, which applies both the fixed and inverted inputs to the integrator. The control voltage is produced in this state.

In the hold state, which is selected by momentarily depressing the "hold" switch, relay RY1 is off, which removes both integrator inputs. Motor rotation rate is relatively constant in this mode. However, since there is some integrator drift in the hold state, motor rotation rate regulation is insufficient for fixed rotation rate experiments.

In the reset state, which is selected by momentarily depressing the "reset" switch, relay RY2 is off (as is relay RY1), which connects a 4.7 MΩ resistor across the integrator feedback capacitor to discharge it and return the motor rotation rate to zero. With this high value of resistance, discharge occurs over a period of several

seconds, so that the motor rotation rate is slowly reduced, and mechanical stress is thereby avoided.

Each amplifier can be switched to a test position in which it is connected as a gain of -10 amplifier with grounded input and floating output, for offset null adjustment. These test positions are not shown in the schematic. The programmer is powered by a simple, one-stage zener-diode-regulated ± 13.6 and -34 V supply, which is adequate for this purpose.

4. *The electrode*

The principal requirement for the electrode is that it be capable of consistent performance over the desired rotation rate range. For the electrode employed, $i_{\mathrm{lim}}/\omega^{\frac{1}{2}}C$ for the electrolysis of a 8.8×10^{-4} F solution of DMPZ in MeCN/0.1 F TEAP, which should be constant, is 21.4 ± 0.2 over the range of 500–8600 rev. min^{-1}; thus the requirement is met.

The method of electrode fabrication employed is similar to the procedure devised by Marcoux and Adams[17]. A Beckman No. 39273 platinum button electrode was cut radially about 2 in. from the button end and an extension soldered to the electrode lead. This was then mounted directly on the drive motor shaft as described below.

The shaft of the E-550 motor is $\frac{1}{4}$-in. diameter, and extends about 2 in. from either end of the motor. A $\frac{1}{8}$-in. diameter hollow extends the length of the shaft. A pair of soft-balsa washers of about $\frac{5}{8}$-in. outer diameter and $\frac{1}{4}$-in. inner diameter were placed on the motor shaft and, with the motor turning at *ca.* 2000 rev. min^{-1}, were machined to a snug fit for the inner surface of the electrode sleeve. With the electrode sleeve in place on the motor shaft and the extension lead passing through the hollow shaft, the cavity was filled with an epoxy potting resin* which was allowed to cure at room temperature. This arrangement produced an electrode assembly which shows no visible vertical wobble during rotation.

At opposite ends of the motor, the extension lead was wrapped around the shaft and secured with tape. Electrical contact for the potentiostat lead is made by a loop of number eighteen stranded wire which is pulled against the motor shaft by a small spring. Alternatively, one can fill the motor shaft with mercury and insert a wire into the hollow from the top. One can then tap off this lead for the potentiostat connection.

ACKNOWLEDGEMENT

Support for this work through National Science Foundation Grant No. GP-8941 is gratefully acknowledged. Special thanks are also due to Drs. R. N. Adams and D. E. Smith for their support and encouragement.

SUMMARY

By use of a square-root device and a motor rotation rate programmer, direct

* A 50/50 mixture of Epon 828, Shell Chemical Co., Emeryville, California, with Genamide 250, General Mills Co., Minneapolis, Minn.

plots of limiting current, i_{lim} *vs.* square root of rotation rate, $\omega^{\frac{1}{2}}$, can be obtained on an ordinary X–Y recorder. Various rates of increase in motor rotation speed are available in order to circumvent problems such as electrode filming. Optimum conditions for the rate of increase were tested, as were the effects of solution volume.

The technique can be used to detect homogeneous chemical reactions associated with electron transfer processes, but the primary use is in the rapid acquisition of large amounts of data relating limiting currents to rotation rates.

APPENDIX

Balancing procedure for the square-rooter

Once the square-rooter is set up, it should rarely need balancing, *i.e.*, e_{out} should be the exact square root of e_{in}. However, it is advisable to check the instrument occasionally as a matter of course. The following procedure is recommended.

Power off

1. Adjust the 50K offset adjust pots on A_1 and A_2 to about midrange.
2. Turn each of the remaining pots to destroy adjustment.
3. Pull A_2 from its socket and clip the output terminal of the A_2 socket to ground.

Power on

4. Adjust the 10K pot that connects to the negative input of A_1 *via* a 2M resistor until the voltage between the output of A_1 and ground is zero.
5. Unclip the A_2 output terminal from ground.
6. Apply 2 V between the A_2 output terminal and ground. Note that the negative lead of the source goes to the A_2 output terminal, and the positive lead of the source goes to ground; if this is not done, the 1N914 may conduct with unknown results.
7. Adjust the 5K potentiometer that appears in the IC1 pin 3 circuit (a Daystrom pot) until the voltage between the output of A_1 and ground is exactly 0.4 V. This makes the proportionality constant in the squarer characteristic equation to be 0.1.

Power off

8. Replace A_2 in its socket.

Power on

9. Theoretically, the square-rooter should now be operating properly, but probably e_{out} will swing a few tenths of a volt positive for $e_{in}=0$. Even if the above is true, try running an e_{in} *vs.* e_{out} curve, which should follow $e_{out}=-e_{in}^{\frac{1}{2}}$. Note that whichever recorder axis that e_{out} is applied to should be zeroed with the hot lead of e_{out} disconnected unless $e_{out}=0$ exactly for $e_{in}=0$.
10. If e_{out} hangs at a few volts positive, regardless of the value of e_{in}, then adjust the 10K pot that leads to the A_1 input *via* 2M until e_{out} is about 0.05 V when $e_{in}=0$ and try a curve. This will degrade accuracy for very low values of e_{in}, but it should be acceptable between 1 and 25 V. Recall that e_{in} must be positive and should be less than 25 V.

REFERENCES

1 S. C. CREASON AND R. F. NELSON, *J. Electroanal. Chem.*, 21 (1969) 549.
2 K. PRATER, *J. Electrochem. Soc.*, 115 (1968) 27C.
3 R. F. NELSON, D. W. LEEDY, E. T. SEO AND R. N. ADAMS, *Z. Anal. Chem.*, 224 (1967) 184.

4 V. LEVICH, *Physicochemical Hydrodynamics*, Prentice-Hall, Inc., Englewood Cliffs, N.J., 2nd ed., 1962, p. 64.
5 R. F. NELSON, *J. Electroanal. Chem.*, 18 (1968) 329.
6 J. F. AMBROSE, J. WHEELER AND R. F. NELSON, unpublished data.
7 R. S. NICHOLSON AND I. SHAIN, *Anal. Chem.*, 36 (1964) 706.
8 R. S. NICHOLSON AND I. SHAIN, *Anal. Chem.*, 37 (1965) 178.
9 D. C. POLCYN AND I. SHAIN, *Anal. Chem.*, 38 (1966) 376.
10 S. W. FELDBERG, in A. J. BARD (Ed.), *Electroanalytical Chemistry*, Vol. 3, Marcel Dekker, Inc., New York, 1969.
11 L. S. MARCOUX, R. N. ADAMS AND S. W. FELDBERG, *J. Phys. Chem.*, 73 (1969) 2611.
12 J. F. AMBROSE AND R. F. NELSON, *J. Electrochem. Soc.*, 115 (1968) 1159.
13 DS9124-MC 1595L Information Sheet, Motorola Semiconductors, Phoenix, Arizona.
14 Application Note AN-1, *Monolithic Voltage Regulator*, National Semiconductor Corporation, Santa Clara, California, 1967.
15 Specification Sheet, LM-300 Voltage Regulator, National Semiconductor Corporation, Santa Clara, California, 1968.
16 *Applications Manual for Operational Amplifiers*, Philbrick/Nexus Research, Dedham, Massachusetts, 1966, p. 22.
17 L. MARCOUX AND R. ADAMS, *Anal. Chem.*, 39 (1967) 1898.

ELECTROANALYTICAL CHEMISTRY AND INTERFACIAL ELECTROCHEMISTRY
Elsevier Sequoia S.A., Lausanne – Printed in The Netherlands

THE IMPEDANCE OF THE PbO_2/AQUEOUS ELECTROLYTE INTERPHASE

I. SULPHATE ELECTROLYTES

J. P. CARR, N. A. HAMPSON AND R. TAYLOR*
Department of Chemistry, Loughborough University of Technology, Leicestershire (England)
(Received March 3rd, 1970)

INTRODUCTION

In an earlier paper[1] we presented the results of a study of the double layer of α- and β-PbO_2 in aqueous nitrate electrolytes. It was shown that the system was not complicated by adsorption of either H^+ or NO_3^- and that the p.z.c. was located at 0.81 ± 0.01 V (SCE)** in the case of α-PbO_2 and 0.905 ± 0.01 in the case of β-PbO_2.

In sulphate electrolyte the PbO_2 electrode is of considerable technological importance and has been fairly well investigated. Kabanov *et al.*[2] and Kokarev *et al.*[3] have studied the a.c. impedance of PbO_2 electrodeposits in H_2SO_4 solutions. The value of the p.z.c. was said to be at 1.78 V(NHE). A gradual increase in electrode capacitance was observed in both investigations which was ascribed by Kabanov *et* al.[2] to a change (expansion) in the crystallographic form of the surface. Hardness studies by Leikis and Venstrem[4] of PbO_2 electrodeposits in H_2SO_4 solutions have indicated a maximum in hardness at 1.78 V(NHE) apparently confirming this value as that of the p.z.c.

Adsorption at the PbO_2 electrode of the products of reaction between PbO_2 and solutions of $HClO_4$ and H_2SO_4 has been detected by Kabanov *et al.*[2] and these results have been confirmed recently by Kokarev *et al.*[5]. From the results of other kinetic studies[6-8] in relatively concentrated solutions of H_2SO_4, adsorption of SO_4^{2-}, Pb^{2+} and H^+ appears to be well-established.

In the present paper are presented the results of a study of the impedance of α- and β-PbO_2 electrodes as a function of the pH at constant total equivalent ionic concentration. These data provide information concerning the participation of the H^+ ion in the process of adsorption at the electrode and the importance of the H^+ ion in modifying the electrode surface (time stability).

EXPERIMENTAL

The preparation of electrodes[1], electrolytic cell and experimental techniques[9] have been described. Charcoal purification of electrolytes (A.R. K_2SO_4, A.R. H_2SO_4

* Address: Joseph Lucas, Ltd., Group Research Centre, Shirley, Warwickshire (England).
** All potentials are as measured against a reference electrode with a liquid junction—the saturated calomel electrode. Present experimental data are recorded here against this reference.

and doubly distilled water) was used. Electrolytes were purified by continuous circulation through cleaned activated charcoal for 14 days before measurements were commenced. Electrolytes were maintained at 0.0344 ± 0.001 mol l^{-1} sulphate ion.

RESULTS AND DISCUSSION

Figure 1 shows the extent of the experimental polarizability. About 0.5 V is available for study, in which interval the faradaic current flow is negligible. The position of the polarizable region depended on pH; at pH 12 the range 0.7–1.2 V was available, at pH 1.8 the region had been shifted to more positive potentials, 1.2–1.7 V.

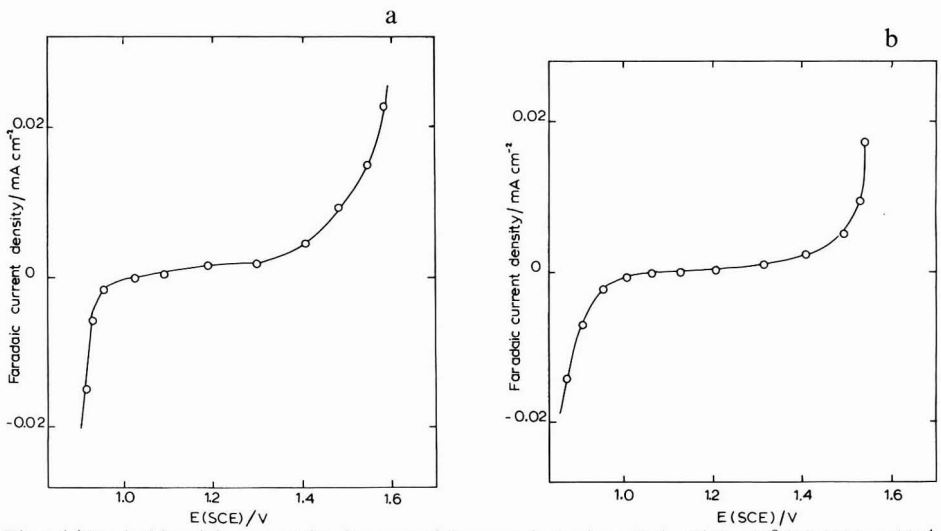

Fig. 1. (a) Typical faradaic current density–potential curve; electrodeposited α-PbO_2: 23°C, 0.0344 mol l^{-1} aq. K_2SO_4, pH 3.8. (b) As (a) for β-PbO_2.

Figure 2 shows the differential capacitance curves for a small region of pH, the range 2–4. Some time variation was observed during the first 3 h of electrode electrolyte contact, this variation amounted to about 20% of the maximum capacitance but after 3 h the electrode capacitance was constant. The form of the family of curves (Fig. 2) is completely unlike those observed for nitrate electrolytes and indicates that adsorption is occurring[10]. The rise in capacitance at the positive extremity of the polarizable region is a pseudocapacitance associated with the oxygen evolution reaction (bubbles of O_2 appearing at potentials slightly more positive than this). At the negative extremity of the polarizable region there is a rise in capacitance marking the reduction of the electrode. A very high pseudocapacitance "spike" is only observed with low pH electrolytes.

The in-phase (resistive) components of the electrode impedance (Fig. 2) are fairly constant throughout the polarizable region (indicating little change in double layer structure) but rise abruptly at the extremities. At the positive limit the increase is due to the oxygen evolution reaction and at the negative limit to the onset of the development of a layer of lead sulphate when the electrode is reduced. At potentials

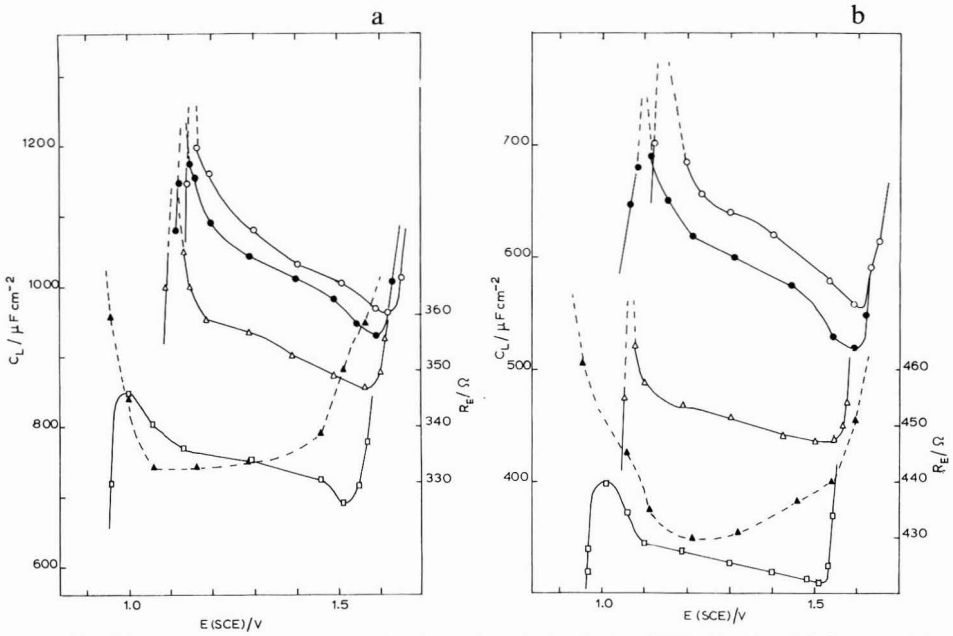

Fig. 2. (a) Differential capacitance curves for electrodeposited α-PbO_2: 23°C, 0.0344 mol l^{-1} aq. K_2SO_4 over pH range 2.5–3.8. (□) pH 3.8, (△) pH 3.4, (●) pH 3.0, (○) pH 2.5; 120 Hz. Broken line shows a typical electrode resistance, R_E, *vs.* potential curve at 23°C. Electrode area 4.9×10^{-2} cm^2, 0.0344 mol l^{-1} aq. K_2SO_4, 120 Hz, pH 3.8. (b) As (a) for β-PbO_2.

more negative than the experimentally polarizable region the capacitance decreases very significantly and at a fixed potential the extent of the decrease is time dependent. It is likely that in this region thickening of the lead sulphate film causes a capacitance reduction in accordance with the "parallel plate" formula.

Figure 3 shows differential capacitance curves for systems in the pH range 1.8–12. At the lowest pH there was evidence of a progressive although slight increase in capacitance. In view of the uncertainty this introduced, 1.8 marked the limit of pH of the present experiments, for further decrease in pH resulted in a serious progressive increase of electrode capacitance in agreement with the Russian workers[2,3]. The form of the curves (Fig. 3) is similar at each pH. The magnitude of the capacitance rises progressively as pH is decreased indicating that the participation of the H^+ ion in the structure of the interphase results in a pseudocapacitance. If the p.z.c. is 0.8–0.9 V then the direct adsorption of H^+ ion in the experimentally polarizable region is unlikely. The SO_4^{2-} ion however may be expected to be adsorbed in view of the low solubility of $PbSO_4$. As the pH is lowered the concentration of HSO_4^- at the electrode is increased. It is suggested that the observed pseudocapacitance arises from reactions of the type

$$H^+ + SO^{2-}_{4_{ads}} = HSO^-_{4_{ads}} \quad (1a)$$

$$4\,HSO^-_{4_{ads}} + PbO_2 + 2e = PbSO_{4_{ads}} + 3\,SO^{2-}_{4_{ads}} + 2\,H_2O \quad (1b)$$

In the case of uni-univalent nitrate systems reactions of the type (1) are not possible.

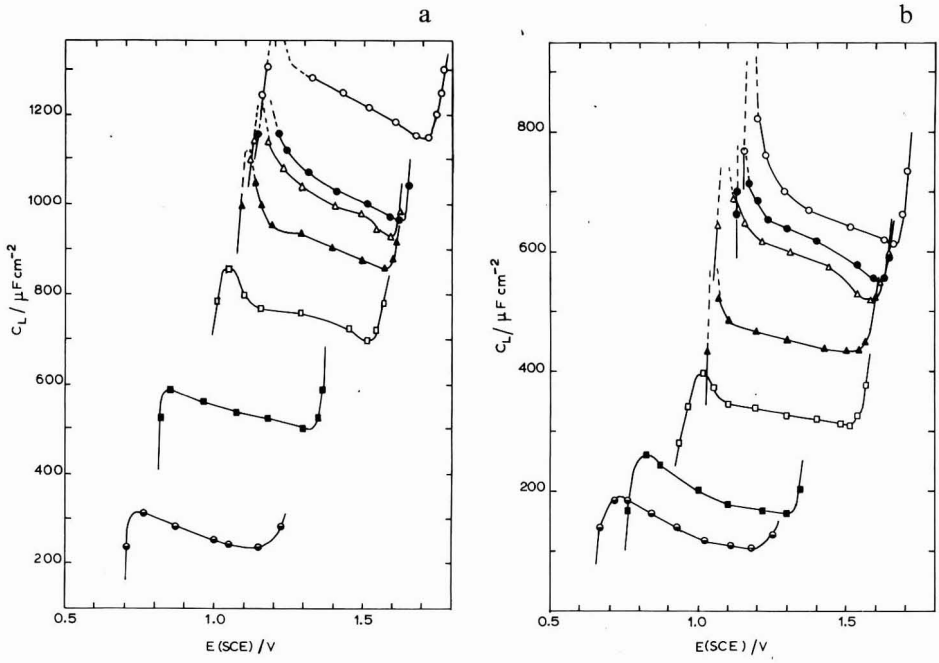

Fig. 3. (a) Differential capacitance curves for electrodeposited α-PbO_2: 23°C, 0.0344 mol l^{-1} aq. K_2SO_4 over pH range 1–12: (◒) pH 12.0, (■) pH 6.0, (□) pH 3.8, (▲) pH 3.4, (△) pH 3.0, (●) pH 2.5, (○) pH 1.8; 120 Hz. (b) As (a) for β-PbO_2.

At neutral pH, adsorption of anions is to be expected at potentials positive to the p.z.c. (0.8–0.9 V)[1]. Reference to Fig. 3 indicates that at pH 6 the negative limit of the polarizable region occurs at this potential as would be expected since reactions (1) are dependent upon the adsorption of SO_4^{2-}. The magnitude of the electrode capacitance increases with decrease in pH in acordance with eqns. (1). The negative limit of the polarizable region (and the position of the "negative" pseudocapacitance peak) is governed by the "reducibility" of the electrode. The limit is thus driven to more positive potentials at lower pH as observed (Figs. 2 and 3).

As the pH is increased from 6 the magnitude of the electrode capacitance decreases. Although it is clear that reaction (1) is less important under these conditions it is also likely that OH^- is adsorbed and may even displace adsorbed sulphate. Under these circumstances the potential of lattice reduction would be expected to occur at increasingly negative potentials as reactions (1) are suppressed as observed.

The magnitude of the dispersion of frequency is shown in Fig. 4. The dispersion is considerably greater than observed with nitrate electrolytes[1] and is found to be more extensive at low pH than high pH. This is to be expected if the reaction is as proposed (eqns. (1)).

The difference between the behaviour of α- and β-PbO_2 electrodes in these electrolytes is only marginal. This may be contrasted with α- and β-PbO_2 in nitrate electrolytes[1] where differences were significant. It seems that the adsorption of sulphate and surface reactions of type (1) obscure surface structural differences between the polymorphs.

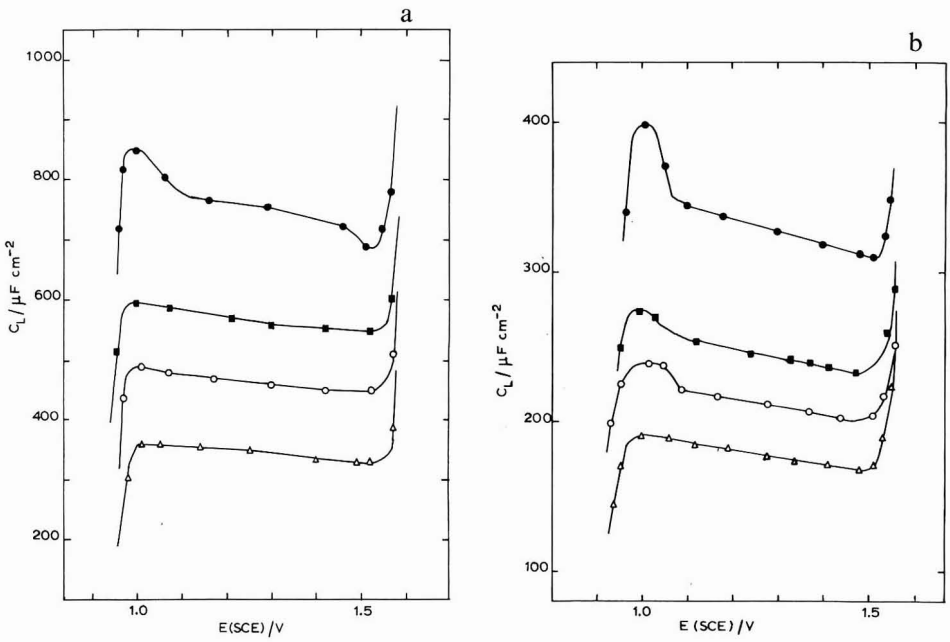

Fig. 4. (a) Typical frequency dispersion of differential capacitance curves for electrodeposited α-PbO_2: 23°C, 0.0344 mol l^{-1} aq. K_2SO_4, pH 3.8. (●) 120 Hz, (■) 300 Hz, (○) 500 Hz, (△) 1000 Hz. (b) As (a) for β-PbO_2.

CONCLUSIONS

1. Sulphate ion is adsorbed at potentials positive with respect to the p.z.c. (0.8–0.9 V).

2. The H^+ ion may interact with the adsorbed sulphate ion.

3. In the presence of significant surface concentrations of HSO_4^- a reaction in the adsorbed state occurs between HSO_4^- and the PbO_2 surface. This reaction gives rise to a pseudocapacitance.

4. A net lattice reduction reaction occurs when the potential is sufficiently negative for $PbSO_4$ to be formed on the surface as a solid phase. This potential is determined by the pH according to equations of the type

$$H^+ + SO^-_{4_{ads}} = HSO_{4_{ads}}$$

$$4\,HSO^-_{4_{ads}} + PbO_2 + 2e = PbSO_{4_{ads}} + 3\,SO^{2-}_{4_{ads}} + 2\,H_2O$$

5. The effects (1)–(4) overshadow the differences between α- and β-PbO_2.

ACKNOWLEDGEMENTS

We thank the S.R.C. and Joseph Lucas, Ltd. for financial support to J. P. Carr. Professor R. F. Phillips is thanked for his interest.

SUMMARY

The impedance of α- and β-PbO_2 electrodes in aqueous sulphate electrolytes (0.0344 mol l^{-1}) has been measured as a function of the bias potential and pH. The results indicate that both SO_4^{2-} and HSO_4^- are adsorbed at the electrode. The reaction between adsorbed HSO_4^- and the lattice gives rise to a pseudocapacitance.

REFERENCES

1 J. P. CARR, N. A. HAMPSON AND R. TAYLOR, *J Electroanal. Chem.*, 27 (1970) 109.
2 B. N. KABANOV, I. G. KISELEVA AND D. I. LEIKIS, *Dokl. Akad. Nauk SSSR*, 99 (1954) 805.
3 G. A. KOKAREV, N. G. BAKHCHISARAITS'YAN AND V. V. PANTELEEVA, *Tr. Mosk. Khim. Tekhnol. Inst.*, 54 (1967) 161.
4 D. I. LEIKIS AND E. K. VENSTREM, *Proc. Acad. Sci. USSR, Phys. Chem. Sect. English Transl.*, 112 (1957) 7.
5 G. A. KOKAREV, N. G. BAKHCHISARAITS'YAN, A. N. SMIRNOVA AND G. I. MEDVEDEV, *Trans. Mosk. Tekhnol. Inst.*, 54 (1967) 169.
6 A. T. ANGSTADT, C. J. VENUTO AND P. RÜETCHI, *J. Electrochem. Soc.*, 109 (1962) 178.
7 B. N. KABANOV, *Proc. Electrochem. Conf., Warsaw*, 1955, p. 515.
8 I. G. KISELEVA AND B. N. KABANOV, *Dokl. Akad. Nauk SSSR*, 108 (1956) 864.
9 J. P. G. FARR AND N. A. HAMPSON, *Trans. Faraday Soc.*, 62 (1966) 3493.
10 B. E. CONWAY, *Theory and Principles of Electrode Processes*, Ronald Press, New York, 1965, chaps. 4 and 5.

ELECTROANALYTICAL CHEMISTRY AND INTERFACIAL ELECTROCHEMISTRY
Elsevier Sequoia S.A., Lausanne – Printed in The Netherlands

GENERATION–RECOMBINATION NOISE IN WEAK ELECTROLYTES

M. FLEISCHMANN AND J. W. OLDFIELD
Department of Chemistry, The University, Southampton (England)
(Received May 1st, 1970)

INTRODUCTION

Random fluctuations result from stochastic processes and as all chemical processes are, by their nature, stochastic, so they give rise to noise. Whether noise from a particular process is observable depends of course on its magnitude in relation to additional types of noise generated by the system.

In electrochemistry, where noise is conveniently measured as a fluctuating current or voltage, the minimum value of the noise generated by the system is the thermal or Johnson noise resulting from the random motion of electrons or ions within the system when it is in thermal equilibrium with its surroundings. An expression for the Johnson noise in terms of a fluctuating voltage was first derived by Nyquist[1] in 1928 and takes the form

$$\langle \Delta V^2 \rangle = 4kTZ\Delta f \tag{1}$$

where k is Boltzmann's constant, T the absolute temperature, Z the impedance of the system and Δf the frequency bandwidth within which the noise is measured. Clearly any noise that is to be studied must be detectable above the Johnson noise of the system.

This paper is concerned with the theoretical approach to homogeneous generation–recombination noise (henceforth referred to as G–R noise) in electrochemical systems and its possible use as a method of studying homogeneous reaction kinetics. G–R noise results when a system undergoes a small fluctuation from equilibrium; for example, by applying an electric field to a solution of a weak acid (smaller than the field required to induce high field dissociation) then the inherent fluctuation in the number of ionic particles present caused by the generation and recombination of the ions gives rise to a fluctuating current.

Previous work concerning electrochemical noise is limited. Barker[2] and Tyagai[3,4] have studied noise associated with electrode processes, the former from a theoretical standpoint, the latter studying the cathodic reduction of iodine on platinum. Both authors agree that studies of this kind give the number of electrons associated with the particular reaction and its exchange current, although Barker points out that these quantities can be readily obtained by more conventional methods. Green and Yafuso[5] have studied the noise spectra associated with transport through a membrane in an attempt to obtain information about the mechanism of ion exchange within the membrane. Their results indicate various distributions of relaxation times for the membranes used, implying contributions from several mechanisms.

In this work a brief resume of the theoretical treatment of noise resulting from stationary processes is first given, the noise spectrum being related to the current and

voltage spectra and to the Johnson noise of the system. This is followed by an outline of the derivation of the G–R noise spectrum for a multiple mixture of weak electrolytes; this general noise spectrum is then evaluated for single and bivariate systems. Finally computed values of the G–R noise spectra of various systems are given and discussed with a view to using G–R noise measurements for the determination of homogeneous reaction rate constants.

THEORETICAL TREATMENT OF NOISE

In the majority of chemical processes the probability distribution of the random variable about its mean is given by a Poisson distribution[6], *i.e.*

$$P_N(t) = \frac{(\lambda t)^N \mathrm{e}^{-\lambda t}}{N!} \tag{2}$$

where $P_N(t)$ is the probability that the random variable will have a value N at time t, λ being a constant and λt being the mean value of N at time t.

When considering a stationary process, defined as one whose mean value is independent of time, λt is replaced by $\langle N \rangle$, the expected value of N. The main feature of a Poisson distribution is that the mean value of the random variable is equal to its variance,

$$\langle N \rangle = \langle \Delta N^2 \rangle \tag{3}$$

thus when studying stationary processes the variance and standard deviation are automatically known provided the mean is known. From the point of view of studying noise however, we are interested in the short-term variation of N with time. The autocorrelation function, $\Phi(u)$, contains this variation and is defined by

$$\begin{aligned} \Phi(u) &= \langle \Delta N(t) \Delta N(t+u) \rangle \\ &= \langle \Delta N(0) \Delta N(u) \rangle \end{aligned} \tag{4}$$

for a stationary process where $\Delta N(t)$ is the value of ΔN at time t, and u is the time interval between the two values of ΔN. When u is large $\Phi(u) \rightarrow 0$ whereas when $u \rightarrow 0$, $\Phi(u) \rightarrow \langle \Delta N^2 \rangle$, the variance. The form of the decrease of $\Phi(u)$ from $\langle \Delta N^2 \rangle$ to zero contains information regarding the rates of the various processes giving rise to the noise. As it is inconvenient to work in the time domain we move into the frequency domain. This is done by Fourier transforming the autocorrelation function. The noise spectrum or power spectrum is then defined by[7]

$$G(\omega) = 4 \,\mathrm{Re} \int_0^\infty \Phi(u) \mathrm{e}^{j\omega u} \mathrm{d}u \tag{5}$$

where Re refers to the real part of the integral.

For convenience the noise spectrum for a multivariate process can be split into components such that

$$G(\omega) = \sum_{i,j=1}^{m} G_{ij} \tag{6}$$

where m is the number of independent variables in the system. Also as electrochemical

noise is conveniently measured as a fluctuating current or voltage it is desirable to relate noise spectra to their current and voltage spectra, $G_I(\omega)$ and $G_V(\omega)$ respectively. The relation is a simple one,

$$\frac{G_I(\omega)}{I} = \frac{G_V(\omega)}{V} = \frac{\left\{\sum_{ij} \mu_i \mu_j G_{ij} \Delta f\right\}^{\frac{1}{2}}}{v \sum_i \mu_i n_i} \tag{7}$$

where I and V are the current and voltage applied to the system, v is the volume of the system and μ_i is the mobility of species i.

If we make the simplifying assumptions that the mobility of each charged species is the same, the system has unit volume, and the bandwidth is unity, eqn. (7) becomes

$$\frac{G_I(\omega)}{I} = \frac{G_V(\omega)}{V} = \frac{[G(\omega)]^{\frac{1}{2}}}{\sum_i n_i} \tag{8}$$

which we define as G. This is in fact equal to the ratio of the r.m.s. number of fluctuating anions (or cations) to the total number of anions (or cations) in the system.

The current or voltage G–R noise of a system can be related to the Johnson noise in terms of the quantity G, bearing in mind that $G(\omega)$ is proportional to the volume of the system (see for example eqn. (27)). The G–R noise voltage can be written

$$\langle \Delta V^2_{\mathrm{G-R}} \rangle^{\frac{1}{2}} = \frac{VG\Delta f^{\frac{1}{2}}}{A^{\frac{1}{2}} l^{\frac{1}{2}}} \tag{9}$$

where A and l are the dimensions of the volume. The Johnson noise for the same system is given by

$$\langle \Delta V^2_{\mathrm{J}} \rangle^{\frac{1}{2}} = (4kT\rho)^{\frac{1}{2}} (l/A)^{\frac{1}{2}} \Delta f^{\frac{1}{2}} \tag{10}$$

where ρ is the specific resistance of the solution. Thus

$$\langle \Delta V^2_{\mathrm{G-R}} \rangle^{\frac{1}{2}} / \langle \Delta V^2_{\mathrm{J}} \rangle^{\frac{1}{2}} = G/[(4kT\rho)^{\frac{1}{2}}/E] \tag{11}$$

where $E = V/l$ is the applied field.

Equation (11) shows that the ratio of the G–R noise voltage to the Johnson noise is a function of the applied field (or current density) but that it is independent of the volume of the system. However it should be noted that in practice it may be necessary to use small volumes in order to increase both the G–R and Johnson noise levels above that of other types of noise, *e.g.* Flicker noise, generated by the system.

G–R NOISE IN WEAK ELECTROLYTES

We consider a system of the type

$$\begin{aligned} &\mathrm{HA}(1) \rightleftarrows \mathrm{H}^+ + \mathrm{A}(1)^- \\ &\mathrm{HA}(2) \rightleftarrows \mathrm{H}^+ + \mathrm{A}(2)^- \\ &\quad\vdots \qquad\quad \vdots \qquad\quad \vdots \\ &\mathrm{HA}(m) \rightleftarrows \mathrm{H}^+ + \mathrm{A}(m)^- \end{aligned} \tag{12}$$

This is an m variable stochastic process, the number of $A(i)^-$ ions, $i=1, 2, \ldots, m$, being independent variables and the number of H^+ ions being a dependent variable; it therefore gives rise to G–R noise when perturbed from equilibrium. Our aim is to predict the level of this noise and its frequency dependence.

In order to proceed it is necessary to assume that the overall reaction defined by eqn. (12) is a multivariate Markov process *i.e.* one in which the random variable Y_t, observed in the parameter space t obeys the following equality of conditional probabilities,

$$\begin{aligned} P\{Y_t = y_t | Y_0 = y_0,\ Y_1 = y_1 \ldots\ Y_{t-1} = y_{t-1}\} \\ = P\{Y_t = y_t | Y_{t-1} = y_{t-1}\} \end{aligned} \tag{13}$$

Clearly all stationary processes are Markovian and therefore since eqn. (12) refers to a stationary process it is also Markovian.

Equation (12) can be rewritten to define more clearly the random variables,

$$\begin{array}{llll} \mathrm{HA}(1) & -\mathrm{A}(1)^- & \underset{k_{s1}}{\overset{k_{1s}}{\rightleftharpoons}} & \mathrm{H}^+ \\ \mathrm{N}_1 - n_1 & n_1 & & n_s \\ \mathrm{HA}(2) & -\mathrm{A}(2)^- & \underset{k_{s2}}{\overset{k_{2s}}{\rightleftharpoons}} & \mathrm{H}^+ \\ N_2 - n_2 & n_2 & & n_s \\ \vdots & \vdots & & \vdots \\ \mathrm{HA}(m) & -\mathrm{A}(m)^- & \underset{k_{sm}}{\overset{k_{ms}}{\rightleftharpoons}} & \mathrm{H}^+ \\ N_m - n_m & n_m & & n_s \end{array} \tag{14}$$

where k_{is} (s^{-1}) and k_{si} (l molecule^{-1} s^{-1}) are rate constants and n_i, $i=1, 2, \ldots, m$, are the independent variables, equal to the number of $A(i)^-$ ions present per litre of solution. n_s is the dependent variable and corresponds to the number of H^+ ions per litre of solution while N_i, $i=1, 2, \ldots, m$, are constants corresponding to the total number of species i per litre.

In general reactions of the type

$$\begin{array}{llll} \mathrm{HA}(i) & -\mathrm{A}(i)^- & \underset{k_{ji}}{\overset{k_{ij}}{\rightleftharpoons}} & \mathrm{HA}(j) - \mathrm{A}(j)^- \\ N_i - n_i & n_i & & N_j - n_j \quad n_j \end{array} \tag{15}$$

must also be included with those given in eqn. (14).

We can now formulate the rates of formation of species j from i, species s from i and species i from s in a volume v

$$p_{ij} = k_{ij}(N_i - n_i)n_j v \tag{16}$$

$$p_{is} = k_{is}(N_i - n_i)v \tag{17a}$$

$$p_{si} = k_{si} n_i \sum_{j=1}^{m} n_j v \tag{17b}$$

It has been shown elsewhere[7] that the autocorrelation function for a reaction of the type described by eqns. (14) and (15) is given by

$$\Phi(t) = \phi(0)\mathrm{e}^{-Mt} \tag{18}$$

where M is the relaxation matrix defined by

$$M_{ij} = \frac{1}{v}\sum_{k=1}^{m}\left\{\frac{\partial p_{ik}}{\partial n_j} - \frac{\partial p_{ki}}{\partial n_j}\right\}_{n_i} \tag{19}$$

The eigen values of M give the inverse of the relaxation times of the noise spectrum.

The noise spectrum can be determined from the autocorrelation function. Again this has been shown elsewhere and will not be repeated here[7]. The result is

$$G(\omega) = \frac{2}{\omega^2}\,\mathrm{Re}\left\{I + \frac{M}{j\omega}\right\}^{-1} B \tag{20}$$

Where I is the unit matrix and B is a rate matrix defined by

$$B_{ii} \simeq 2\sum_{k=1}^{m} p_{ik} \qquad k \neq i \tag{21a}$$

$$B_{ji} = B_{ij} \simeq -2p_{ij} \tag{21b}$$

The noise spectrum will now be evaluated for single and bivariate systems.

THE SINGLE VARIABLE SYSTEM

Let us consider the single variable process

$$\mathrm{HA} \underset{k_2}{\overset{k_1}{\rightleftarrows}} \mathrm{A}^- + \mathrm{H}^+ \tag{22}$$

Using eqns. (17a) and (17b) we can write

$$p_{12} = k_1 n_{\mathrm{HA}} v \tag{23a}$$

$$p_{21} = k_2 n_{\mathrm{H}^+}^2 v = p_{12} \tag{23b}$$

Thus from eqn. (19)

$$M = -k_1 - 2k_2 n_{\mathrm{H}^+} \tag{24}$$

and the relaxation time is given by

$$\tau = 1/(2k_2 n_{\mathrm{H}^+} + k_1) \tag{25}$$

From eqns. (21a) and (21b)

$$B = 2p_{1s} = 2k_2 n_{\mathrm{H}^+}^2 v \tag{26}$$

Thus the noise spectrum is given by

$$\begin{aligned} G(\omega) &= 2\omega^{-2}\,\mathrm{Re}\{1 + (j/\omega\tau)\}^{-1} 2k_2 n_{\mathrm{H}^+}^2 v^- \\ &= (4k_2 n_{\mathrm{H}^+}^2 v\,\tau^2)/(1+\omega^2\tau^2) \end{aligned} \tag{27}$$

At low frequencies when $\omega^2\tau^2 \ll 1$ the denominator in eqn. (27) becomes unity. Under these conditions, substituting for τ, the noise spectrum becomes

$$G(\omega) = (4k_2 n_{H^+}^2 v)/(2k_2 n_{H^+} + k_1)^2 \tag{28}$$

If we now make the further assumption that HA is a weak acid such that $2k_2 n_{H^+} \gg k_1$ then the expression simplifies even further and the noise spectrum is simply given by

$$G(\omega) = v/k_2 \tag{29}$$

Thus it is possible to determine k_2, a fast recombination rate, simply by measuring the noise level resulting from the reaction defined in eqn. (22) at frequencies well below the relaxation frequency.

THE TWO-VARIABLE SYSTEM

Let us consider a two variable process; the various possible reactions are listed below,

$$\underset{N_1 - n_1}{HA(1)} \underset{k_{31}}{\overset{k_{13}}{\rightleftharpoons}} \underset{n_1}{A(1)^-} + \underset{n_3}{H^+} \tag{30a}$$

$$\underset{N_2 - n_2}{HA(2)} \underset{k_{32}}{\overset{k_{23}}{\rightleftharpoons}} \underset{n_2}{A(2)^-} + \underset{n_3}{H^+} \tag{30b}$$

$$\underset{N_1 - n_1 \quad n_2}{HA(1) + A(2)^-} \underset{k_{21}}{\overset{k_{12}}{\rightleftharpoons}} \underset{N_2 - n_2 \quad n_1}{HA(2) + A(1)^-} \tag{30c}$$

Using eqns. (16) and (17) we can define the various rates

$$p_{13} = k_{13}(N_1 - n_1)v \tag{31a}$$
$$p_{31} = k_{31} n_1 (n_1 + N_2)v \tag{31b}$$
$$p_{23} = k_{23}(N_2 - n_2)v \tag{31c}$$
$$p_{32} = k_{32} n_2 (n_1 + n_2)v \tag{31d}$$
$$p_{12} = k_{12}(N_1 - n_1)n_2 v \tag{31e}$$
$$p_{21} = k_{21}(N_2 - n_2)n_1 v \tag{31f}$$

With the aid of eqn. (19) we can now compute the elements of the M matrix,

$$M_{11} = k_{12} n_2 + k_{21}(N_2 - n_2) + k_{13} + k_{31}(2n_1 + n_2) \tag{32a}$$
$$M_{12} = k_{12}(N_1 - n_1) + k_{21} n_1 + k_{31} n_1 \tag{32b}$$
$$M_{21} = k_{21}(N_2 - n_2) + k_{12} n_2 + k_{32} n_2 \tag{32c}$$
$$M_{22} = k_{21} n_1 + k_{12}(N_1 - n_1) + k_{23} + k_{32}(2n_2 + n_1) \tag{32d}$$

The elements of the B matrix can be computed from eqns. (21a) and (21b),

$$B_{11} = 2v\{k_{12}(N_1 - n_1)n_2 + k_{13}(N_1 - n_1)\} \tag{33a}$$

$$B_{12} = -2vk_{12}(N_1 - n_1)n_2 \tag{33b}$$
$$= B_{21}$$
$$B_{22} = 2v\{k_{21}(N_2 - n_2)n_1 + k_{23}(N_2 - n_2)\} \tag{33c}$$

A two-variable process exhibits two relaxation times. These are the inverse of the eigen values of the M matrix and are therefore given by the equation

$$\begin{vmatrix} M_{11} - \frac{1}{\tau} & M_{12} \\ M_{21} & M_{22} - \frac{1}{\tau} \end{vmatrix} = 0 \tag{34}$$

Equation (20) can now be evaluated for the reactions in eqns. (30a–c) in the form

$$G(\omega) = G_{11} + G_{12} + G_{21} + G_{22} \tag{35}$$

where the individual components of the noise spectrum are given by the equations

$$G_{11} = 2\sum_{1,2} \frac{\tau_1\tau_2}{\tau_2 - \tau_1} \frac{\tau_1^2}{1+\omega^2\tau_1^2} \left\{\left(\frac{1}{\tau_1} - M_{22}\right) B_{11} + M_{12}B_{21}\right\} \tag{36a}$$

$$G_{22} = 2\sum_{1,2} \frac{\tau_1\tau_2}{\tau_2 - \tau_1} \frac{\tau_1^2}{1+\omega^2\tau_1^2} \left\{\left(\frac{1}{\tau_1} - M_{11}\right) B_{22} + M_{12}B_{12}\right\} \tag{36b}$$

$$G_{12} = 2\sum_{1,2} \frac{\tau_1\tau_2}{\tau_2 - \tau_1} \frac{\tau_1^2}{1+\omega^2\tau_1^2} \left\{\left(\frac{1}{\tau_1} - M_{22}\right) B_{12} + M_{12}B_{22}\right\} \tag{36c}$$

$$G_{21} = 2\sum_{1,2} \frac{\tau_1\tau_2}{\tau_2 - \tau_1} \frac{\tau_1^2}{1+\omega^2\tau_1^2} \left\{\left(\frac{1}{\tau_1} - M_{11}\right) B_{21} + M_{21}B_{11}\right\} \tag{36d}$$

where $G_{12} = G_{21}$ and where, as a consequence of microscopic reversibility

$$B_{12}(M_{22} - M_{11}) + M_{21}B_{11} - M_{12}B_{22} = 0 \tag{37}$$

The increase in complexity on going from the one variable to the two-variable case is enough to suggest that, at this stage, it would be of little use to study three and more variable systems. In fact the two-variable case described by eqns. (30)–(37) is difficult to manage; in order to simplify it we now consider the situation that arises when reaction (30c) does not take place to any significant extent, *i.e.*

$$p_{12} = p_{21} = 0 \tag{38a}$$
$$k_{12} = k_{21} = 0 \tag{38b}$$

Under these conditions the total noise spectrum can be written in the form

$$G(\omega) = \frac{2\tau_1\tau_2}{\tau_1 - \tau_2}\left[B_{11}\left\{\frac{\tau_2}{1+\omega^2\tau_2^2}(1-\tau_2M_{22}) - \frac{\tau_1}{1+\omega^2\tau_1^2}(1-\tau_1M_{22})\right\}\right.$$
$$+B_{22}\left\{\frac{\tau_2}{1+\omega^2\tau_2^2}(1-\tau_2M_{11}) - \frac{\tau_1}{1+\omega^2\tau_1^2}(1-\tau_1M_{11})\right\}$$
$$\left.+2M_{12}B_{22}\left\{\frac{\tau_2^2}{1+\omega^2\tau_2^2} - \frac{\tau_1^2}{1+\omega^2\tau_1^2}\right\}\right] \tag{39}$$

At frequencies well below τ_1^{-1} and τ_2^{-1} this simplifies further to

$$G(\omega) = \frac{2\tau_1\tau_2}{\tau_1-\tau_2}[B_{11}\{M_{22}(\tau_1^2-\tau_2^2)-(\tau_1-\tau_2)\} + B_{22}\{M_{11}(\tau_1^2-\tau_2^2)-(\tau_1-\tau_2)\}+2M_{12}B_{22}(\tau_2^2-\tau_1^2)] \quad (40)$$

It is clear that by varying the concentrations of the different species it is possible to determine the rate constants of the two reactions by measuring the noise spectrum at frequencies below the relaxation frequencies. However this is by no means a simple operation if eqn. (40) cannot be simplified further.

We now consider two possible assumptions that may be applicable to eqn. (40)

(i) $\tau_1 \gg \tau_2$

This condition will frequently apply, resulting in the following expression for the noise spectrum,

$$G(\omega) = 2\tau_2\tau_1\{B_{11}(M_{22}\tau_1-1)+B_{22}(M_{11}\tau_1-1)-2M_{12}B_{22}\tau_1\} \quad (41)$$

where, using eqn. (34), τ_1 and τ_2 can be written

$$\tau_1 = (M_{11}+M_{22})/(M_{11}M_{22}-M_{12}M_{21}) \quad (42)$$

$$\tau_2 = 1/(M_{11}+M_{22}) \quad (43)$$

(ii) $\tau_1 \gg \tau_2$, $M_{11}M_{22} \gg M_{12}M_{21}$

Again these two conditions will frequently be applicable. Substituting for τ_1 and τ_2 in eqn. (41) results in the much simplified equation

$$G(\omega) = 2\left\{\frac{B_{11}}{M_{11}^2}+\frac{B_{22}}{M_{22}^2}\right\} \quad (44)$$

These are just two examples of assumptions that make eqn. (40) more manageable. Clearly there are other approximations one could make to suit particular systems; however, the two mentioned above will be the most common.

THEORETICALLY COMPUTED NOISE SPECTRA

As mentioned in the introduction it is of prime importance that the G–R noise to be studied should be detectable above the Johnson noise of the system. In order to determine the type of system in which this condition holds various noise spectra have been computed, using rate constants obtained from the literature.

In all, three systems have been studied, firstly a one-variable system, namely water. This was chosen since it could be a suitable starting point for experimental investigations. The second system chosen was the two-variable water–acetic acid mixture, acetic acid being a typical weak acid with a diffusion controlled recombination rate and a fast dissociation rate. Finally, the noise spectrum of the water–barbituric acid system was computed, barbituric acid having both slow dissociation and recombination rate constants.

The results are plotted in terms of the function G, defined by eqn. (8), against the logarithm of the angular frequency, ω. With the use of eqn. (11) and values of the

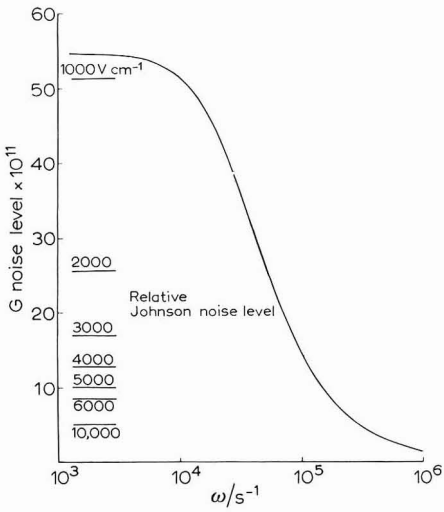

Fig. 1. Computed G–R noise spectrum for 1 cm^3 water with relative values of the Johnson noise at various applied field strengths indicated. (---)$\omega = 1/\tau$.

specific resistance of the solution the values of the Johnson noise relative to the G–R noise voltage at various field strengths have been calculated. Each system will now be considered in detail.

(*i*) *Water*

We assume that the dissociation of water occurs in the form

$$H_2O \underset{k_2}{\overset{k_1}{\rightleftarrows}} H^+ + OH^- \tag{45}$$

Using values[8] of $k_1 = 2.5 \times 10^{-5}\ s^{-1}$ and $k_2 = 2.34 \times 10^{-13}$ l molecule^{-1} s^{-1}, the noise spectrum was computed from eqns. (27) and (8) and is shown in Fig. 1. A value[9] of $\rho = 1.67 \times 10^7\ \Omega$ cm was used to determine relative values of the Johnson noise.

The absolute value of the G–R noise voltage can be found for a particular set of parameters from eqn. (9), the value of G being taken from Fig. 1. For example if the system is a 1 mm cube with 100 V applied across it, the noise being measured in 100 Hz bandwith, then the low frequency value of the G–R noise is 17.3 μV and of the Johnson noise 16.2 μV. As the two types of noise are uncorrelated the total noise is 23.7 μV.

From Fig. 1 we can conclude that for any experimental attempt at measuring the G–R noise voltage in water, fields of the order of 1000 V cm^{-1} are a minimum requirement. Also it would be desirable to measure the noise at frequencies below 10 kHz, its level falling off rapidly above this value.

(*ii*) *Water–acetic acid*

In this case we assume the system consists of the following reactions

$$H_2O \underset{k_{31}}{\overset{k_{13}}{\rightleftharpoons}} OH^- + H^+ \tag{46a}$$

$$HAc \underset{k_{32}}{\overset{k_{23}}{\rightleftharpoons}} Ac^- + H^+ \tag{46b}$$

where[8] $k_{23} = 7.8 \times 10^5$ s^{-1} and $k_{32} = 7.5 \times 10^{-14}$ l molecule^{-1} s^{-1}. It is assumed that the reaction

$$H_2O + Ac^- \rightleftarrows HAc + OH^- \tag{46c}$$

does not take place. The noise spectrum is then given by eqn. (39). Values of G as a function of log ω for three values of acetic acid concentration are shown in Fig. 2. For each concentration the relative value of the Johnson noise to the G–R noise is given for an applied field of 5×10^4 V cm^{-1}. A value[9] of $\lambda = 390\ \Omega^{-1}$ cm^2 equiv.$^{-1}$ was used for the equivalent conductivity of acetic acid in order to determine these values.

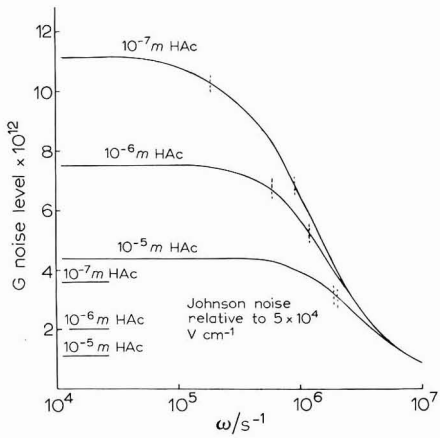

Fig. 2. Computed G–R noise spectra for 1 cm^3 water containing various acetic acid concns. (HAc) as shown. The relative values of the Johnson noise correspond to an applied field of 5×10^4 V cm^{-1}. (---)$\omega = 1/\tau_{1,2}$.

It is clear from the values of G in Fig. 2 that the G–R noise level is less than in pure water, fields of 5×10^4 V cm^{-1} being necessary to obtain a value of the G–R noise greater than the Johnson noise. In fact, if we consider the same parameters as were considered for pure water, *i.e.* 1 mm cube volume, 100 V applied and a 100 Hz bandwidth, then the G–R noise voltage in 10^{-5} M acetic acid is 0.14 μV against a Johnson noise of approximately 1.5 μV, the G–R noise thus being swamped.

Although the G–R to Johnson noise ratio can only be increased by increasing the field, the actual noise levels can be increased in this instance by measuring in a wider bandwidth. This is made possible by the fact that the relaxation times are high in 10^{-5} M acetic acid solution and it would be possible to use a bandwidth of at least 1000 Hz.

We can conclude however that experimentally it would be difficult to observe G–R noise in water–acetic acid mixtures.

(*iii*) *Water–barbituric acid*

We assume this system consists of the reactions

$$H_2O \underset{k_{31}}{\overset{k_{13}}{\rightleftharpoons}} OH^- + H^+ \tag{47a}$$

$$C_4H_4O_3N_2 \underset{k_{32}}{\overset{k_{23}}{\rightleftharpoons}} C_4H_3O_3N_2^- + H^+ \tag{47b}$$

where[8] $k_{23} = 10\ s^{-1}$ and $k_{32} = 1.67 \times 10^{-19}$ l molecule^{-1} s^{-1}. Again the reaction

$$H_2O + C_4H_3O_3N_2^- \rightleftarrows OH^- + C_4H_4O_3N_2 \tag{47c}$$

is neglected, and as in the previous case the noise spectrum is given by eqn. (39).

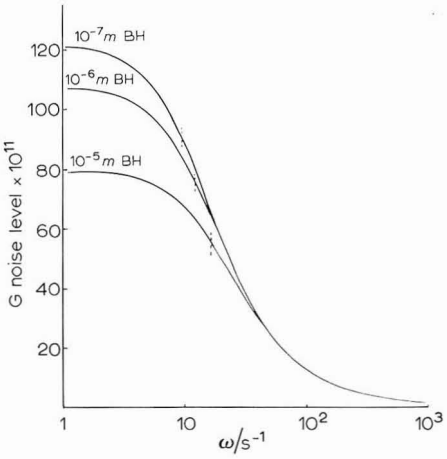

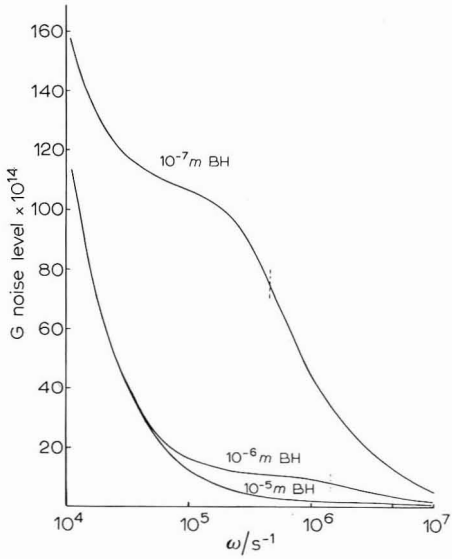

Fig. 3. Computed G–R noise spectra for 1 cm^3 water containing various barbituric acid (BH) concns. as shown. (---)$\omega = 1/\tau_1$.

Fig. 4. A continuation of the spectra in Fig. 3 to higher frequencies. (---)$\omega = 1/\tau_2$.

Values of G as a function of log ω are shown in Figs. 3 and 4 for three concentrations of barbituric acid. In all cases the relaxation times are far apart and the low frequency noise level in terms of G is higher than for pure water. Also although no reliable value of λ for barbituric acid is known it will obviously be greater than for pure water and therefore the G–R to Johnson noise ratio will be greater than for pure water at the same value of the applied field.

From Fig. 3 we see that to take full advantage of the high value of G the noise must be measured at around 10 Hz. At this frequency a bandwidth of the order of 1 Hz would have to be used; with this bandwidth the G–R noise in a 1 mm cube of a 10^{-5} M barbituric acid solution with 100 V applied across it is 2.5 μV, the Johnson noise being significantly lower (< 1 μV).

Thus this particular system looks attractive from an experimental point of view provided the dissociation of barbituric acid can be considered in the simple manner expressed in eqn. (47b).

DISCUSSION

From the quantitative treatment of homogeneous G–R noise set down in this paper we can conclude that the determination of rate constants from noise measurements is feasible under certain conditions. The main reason for this is the fact that the noise level at frequencies well below the relaxation frequencies contains information concerning the rate constants; for example for a single variable process the noise level in this frequency range is given by eqn. (28). Values of $G(\omega)$ at two concentrations of n_{H^+} are enough to determine both k_1 and k_2. For a two-variable system such that eqn. (44) is applicable the noise level at four different concentrations will suffice to determine k_{13}, k_{31}, k_{23}, and k_{32}. In principle one could determine k_{12}, k_{21}, k_{23}, k_{32}, k_{13} and k_{31} from six measurements of $G(\omega)$ when $G(\omega)$ for the two-variable process is given by eqns. (35) and (36); however in this situation the calculation of the rate constants from measured values of $G(\omega)$ would be extremely complicated.

Thus the complexity of $G(\omega)$ puts one limit on the use of this method for determining rate constants. Another limit is whether or not the G–R noise is measurable. This was discussed in the previous section and we can conclude that, in aqueous solutions the noise is greater the slower the dissociation and recombination rates and the smaller the equilibrium constant and that in a number of cases it should be measurable.

With these restrictions the measurement of G–R noise could well become a useful method for studying homogeneous reaction kinetics.

SUMMARY

A quantitative treatment of generation–recombination noise in mixtures of weak electrolytes is given; the noise spectra are derived in detail for one- and two-variable processes. A number of noise spectra are computed and these are discussed with a view to using generation–recombination noise as a method of studying homogeneous reaction kinetics.

REFERENCES

1 H. NYQUIST, *Phys. Rev.*, 32 (1928) 110.
2 G. C. BARKER, *J. Electroanal. Chem.*, 21 (1969) 127.
3 V. A. TYAGAI AND N. B. LUK'YANCHIKOVA, *Elektrokhimiya*, 3 (1967) 316.
4 V. A. TYAGAI, *Elektrokhimiya*, 3 (1967) 1331.
5 M. E. GREEN AND MASAO YAFUSO, *J. Phys. Chem.*, 72 (1968) 4072.
6 D. A. MCQUARRIE, *Stochastic Approach to Chemical Kinetics*, review series in Applied Probability, Vol. 8, Methuen, London, 1967.
7 K. M. VAN VLIET AND J. R. FASSETT, in R. E. BURGESS (Ed.), *Fluctuation Phenomena in Solids*, Academic Press Inc., New York, 1965, chap. 7.
8 M. EIGEN, W. KRUSE, G. MAASS AND L. DE MAEYER, in G. PORTER (Ed.), *Progress in Reaction Kinetics*, Vol. II, Pergamon Press, Oxford, 1964, chap. 6.
9 G. W. C. KAYE AND T. H. LABY, *Tables of Physical and Chemical Constants*, Longmans, London, 1958.

ELECTROANALYTICAL CHEMISTRY AND INTERFACIAL ELECTROCHEMISTRY
Elsevier Sequoia S.A., Lausanne – Printed in The Netherlands

THE ELECTROREDUCTION OF PEROXYDISULPHATE ANION IN FORMAMIDE

W. R. FAWCETT AND M. D. MACKEY
Department of Chemistry, University of Guelph, Guelph, Ontario (Canada)
(Received March 3rd, 1970)

INTRODUCTION

In an attempt to elucidate further the effects of interfacial structure on heterogeneous electron transfer processes, the electroreduction of peroxydisulphate anion has been studied at a dropping mercury electrode in formamide. This reaction has been investigated extensively in aqueous systems by Frumkin, Nikolaeva-Fedorovich, and co-workers[1-4] who found that reaction rates at potentials cathodic of the working electrode's point of zero charge were markedly dependent on the nature and concentration of the base electrolyte. They attributed their observations to a double layer effect, namely changes in the potential distribution in the solution adjacent to the electrode with electrolyte composition. An interesting feature of the above results was the marked dependence of the reaction rate on the nature of the base electrolyte cation. Several explanations have been offered for the cation effect, including cation specific adsorption[5], interaction between the reacting anion and cations in the double layer[6], and differences in the distances of closest approach to the electrode for these species[7].

Obviously, the structure of the mercury–solution interface in water and formamide will differ because of differences in the size of the solvent molecules and their orientation with respect to the electrode, and in the mechanism of ionic solvation. From differential capacity studies[8,9], it has been concluded that the inner layer thickness in the two solvents is about the same (4–5 Å). Consequently, the number of solvent molecules per unit area in the inner layer is less in the case of formamide, and probably, ionic solvation is more important in determining molecular orientation and dielectric properties adjacent to the electrode. It has been observed that the inner layer capacity for solutions of the alkali metal chlorides at far cathodic potentials increases in the order $Li^+ < Na^+ < K^+ < Cs^+$ in water[10], whereas in formamide[11,12] the order is $K^+ < Na^+ < Li^+ < Cs^+$. These changes could be ascribed to changes in both inner layer thickness and effective dielectric constant with the predominant ion at the outer Helmholtz plane (OHP). A further conclusion of the capacity studies[9] is that formamide is strongly adsorbed on mercury with the negative end of its dipole orientated towards the metal such that reorientation of the solvent molecules at the interface does not occur until the charge density of mercury is about $-7\ \mu C\ cm^{-2}$. In contrast, the same reorientation at the mercury–water interface occurs close to the point of zero charge[13].

The differences in double layer structure outlined above are pertinent to the

proposed explanations of the cation effect in that they might result in differences in the effect which would help clarify its nature. In the present paper, the results of a study of the cation effect for peroxydisulphate reduction in formamide are reported and compared with those in water.

EXPERIMENTAL

The apparatus and experimental procedure for measurement of the current–potential data have been described previously[14]. The experiments were carried out in a dry box in which the atmosphere was purified dried nitrogen. The temperature in the dry box was maintained at $25.0 \pm 0.2°$ C by means of a simple off–on temperature regulator with a thermistor sensor.

B.D.H. formamide was purified by double distillation under reduced pressure and once purified was stored in the dry box. The resulting solvent had no polarographically detectable impurities, the dropping mercury electrode having the same polarizable range as observed previously[15]. Alkali metal perchlorates used as base electrolytes were purified by recrystallization from their aqueous solutions and dried at 250° C (185° C in the case of $LiClO_4$) under vacuum for 1–2 h[16]. The depolarizer, AnalaR-grade potassium peroxydisulphate, was used without further purification. Mercury was purified by double distillation after having been washed by passing it in a fine stream through 1 m columns of dilute nitric acid and distilled water.

The dropping mercury electrode was prepared by drawing a fine capillary from 1 mm borosilicate capillary tubing. The resulting capillaries had a fine tip (diameter less than 1 mm) and a flow rate between 0.2 and 0.3 mg s^{-1} for a mercury column height of 70 cm. The drop times in formamide were in the range 7–11 s. Siliconizing the capillaries did not improve their behaviour. The counter electrode was a coil of platinum wire. An aqueous saturated calomel electrode was used as a reference electrode, the junction between it and the non-aqueous solution being made in a ground glass joint. The reference electrode was immersed in pure formamide 1 h before being introduced into the dry box, in order to avoid contamination by excess water in the joint. The potential of the electrocapillary maximum (e.c.m.) in the various alkali metal perchlorate–formamide solutions was measured by the streaming electrode method as described by Grahame[17]. This potential with respect to the above reference was reproducible to better than 1 mV.

The concentration of the base electrolyte used in the experiments was in the range 0.01–0.1 M, while that of the depolarizer was 5×10^{-4} M. The reproducibility of the kinetic data, expressed in terms of $(\ln k)/f$ where k is the rate of reaction and $f = F/RT$, was ± 2 mV for a given base electrolyte concentration and electrode potential.

METHOD OF DATA ANALYSIS

The rate of charge transfer was calculated from the measured currents and drop times at 50 mV intervals using Koutecký's theory with corrections for electrode sphericity[14]. The diffusion current i_d could not be determined in all cases, especially when the concentration of base electrolyte was low. In these cases, i_d was calculated from the measured flow rate, drop times, depolarizer concentration, and the average

value of the diffusion coefficient as determined from experiments where i_d was observable.

Double layer data for the alkali metal perchlorates in formamide were not available; it was assumed that they could be calculated from data for a system where anion adsorption is not significant at cathodic potentials. Perchlorate anion in aqueous solution is adsorbed to a small extent on negatively charged mercury[18]. However, the adsorption is probably attributable to the structure-breaking properties of this ion in water rather than specific interaction between it and mercury[19]. Since formamide itself is strongly adsorbed on mercury at low cathodic potentials, it is likely that perchlorate anion is not significantly adsorbed from formamide solutions in the same potential range. The potentials of the e.c.m. in these solutions in the concentration range 0.01–0.1 *M* with respect to an aqueous SCE were almost constant (-0.449 ± 0.0015 V). Although these potential differences include an indeterminate liquid junction potential and, therefore, are not completely valid evidence for the absence of specific adsorption, they would probably vary significantly with base electrolyte concentration if an ion were specifically adsorbed at the e.c.m.

Double layer data were calculated by combining the capacity data of Dutkiewicz and Parsons[9] for KF and of Nancollas *et al.*[12] for the alkali metal chlorides in formamide. The first authors showed that specific adsorption was negligible in KF at cathodic potentials. Differential inner layer capacities for KF and KCl calculated from the above data assuming that specific adsorption is negligible and that the diffuse layer capacity is given by the Gouy–Chapman theory are shown in Fig. 1.

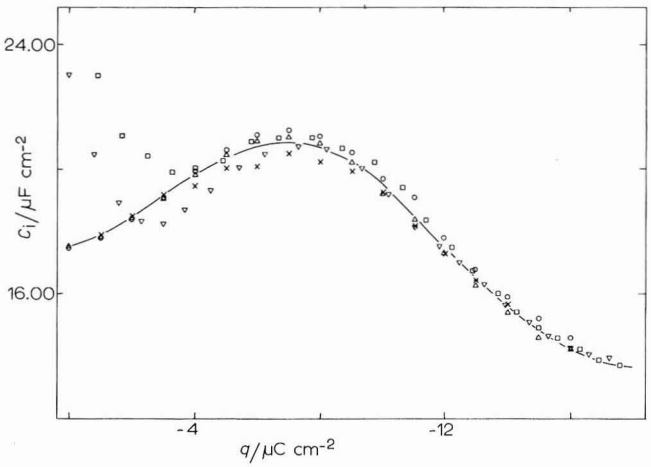

Fig. 1. Differential capacity of the inner layer, C_i for KF[9] and KCl[12] in formamide calcd. with the assumption that there is no specific adsorption and plotted as a function of electrode charge density, q: (×) 0.01 *M*, (○) 0.1 *M*, (△) 0.3 *M* KF (Dutkiewicz and Parsons); (▽) 0.05 *M*, (□) 0.1 *M* KCl (Nancollas *et al.*).

It is obvious that in concentrations less than 0.1 *M* chloride ion is specifically adsorbed at charge densities greater than $-4\ \mu C\ cm^{-2}$. Inner layer capacity data for the other alkali metal chlorides were calculated as above for charge densities less than $-4\ \mu C\ cm^{-2}$. At lower charge densities the differential inner layer capacity C_i was assumed to be the same as that in KF (negligible cation effect). The values of C_i used to calculate

TABLE 1

DIFFERENTIAL CAPACITY OF THE INNER LAYER C_i AS A FUNCTION OF ELECTRODE CHARGE DENSITY FOR THE ALKALI METAL CHLORIDES IN FORMAMIDE

The data have been corrected for chloride ion specific adsorption

Electrode charge density $q/\mu C\ cm^{-2}$	*Differential capacity of inner layer* $C_i/\mu F\ cm^{-2}$			
	LiCl	*NaCl*	*KCl*	*CsCl*
0	17.57	17.57	17.57	17.57
− 1	17.86	17.86	17.86	17.86
− 2	18.44	18.44	18.44	18.44
− 3	19.15	19.17	19.17	19.17
− 4	19.33	19.60	19.82	19.87
− 5	19.58	19.96	20.25	20.32
− 6	19.90	20.46	20.67	20.85
− 7	20.03	20.71	20.94	20.94
− 8	19.96	20.78	20.74	20.81
− 9	19.63	20.56	20.31	20.45
−10	19.02	20.02	19.53	19.88
−11	18.14	18.89	18.51	19.16
−12	17.45	17.81	17.52	18.28
−13	16.71	16.97	16.56	17.24
−14	15.89	15.91	15.64	16.50
−15	15.29	14.97	14.91	15.93
−16	14.80	14.42	14.35	15.60
−17	14.42		13.86	15.62
−18	14.41		13.71	15.94

tables of differential capacity, electrode charge density, and OHP potential as functions of electrode potential and electrolyte concentration are given in Table 1.

RESULTS AND DISCUSSION

Typical current–potential data obtained in this study are shown in Fig. 2. At potentials cathodic of the e.c.m., the current decreased from its diffusion limited value i_d, the magnitude of the depression depending on the base electrolyte cation in the order $Li^+ > Na^+ > K^+ > Cs^+$. The general characteristics of the current minima were similar to those reported for the aqueous system by Frumkin and Nikolaeva-Fedorovich[2]. However, for a given base electrolyte concentration and electrode potential on the rational scale, the current ratio i/i_d and its change from the Cs^+ to the Li^+ system were considerably less in formamide.

Because of the limited polarizable range of mercury in formamide, the current was not observed to return to its diffusion limited value at higher cathodic potentials for base electrolyte concentrations less than 0.1 *M*. In addition, the diffusion limited current at potentials anodic of the e.c.m. was obscured by polarographic maxima of the first kind at low base electrolyte concentrations (0.01 and 0.02 *M*). From experiments where i_d was observable, the average value of the diffusion coefficient for $S_2O_8^{2-}$ was $(2.08 \pm 0.09) \times 10^{-6}$ cm^2 s^{-1} compared with a value of $(8.67 \pm 0.18) \times 10^{-6}$ cm^2 s^{-1} for aqueous systems in the same range of ionic strengths. The correspond-

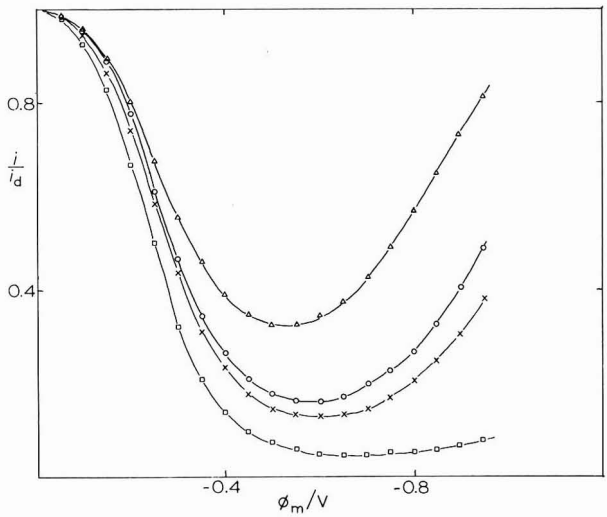

Fig. 2. Ratio of the current to the diffusion current i/i_d *vs.* the electrode potential with respect to that at the e.c.m. ϕ_m for the electroreduction of $S_2O_8^{2-}$ at mercury with 0.02 *M* alkali metal perchlorate as base electrolyte in formamide: (□) $LiClO_4$, (×) $NaClO_4$, (○) $KClO_4$, (△) $CsClO_4$.

ing Stoke's law radii are 3.13 and 2.82 Å respectively. This result follows the trend observed by Notley and Spiro[20] whereby ionic radii calculated from transport properties are larger in formamide than in water.

The charge on the reacting species was determined by the finite difference method described earlier[14]. Assuming that electron transfer is the rate determining step in the electrode reaction, then, according to the Frumkin equation,

$$\Delta[(\ln k)/f]/\Delta(\phi_2 - \phi_m) = \beta - z\Delta\phi_2/\Delta(\phi_2 - \phi_m) \quad (1)$$

where ϕ_m is the electrode potential on the rational scale, ϕ_2 the potential at the OHP, β the Tafel slope, z the charge on the reacting species, and Δ an operator indicating a small but finite increment in the given function. Typical plots for finite differences taken at 50 mV intervals are shown in Fig. 3. The characteristics of these plots were as follows: (1) the plots were not linear as would be expected from eqn. (1) but were curved, the amount of curvature increasing with increase in ϕ_m in the cathodic direction; (2) in the limit of low ϕ_m, the plots were approximately linear with a slope of two; (3) the intercept on the ordinate axis obtained for straight lines drawn through the linear portion with a slope of two varied with the base electrolyte cation, increasing with increase in the cation's atomic number. It was concluded that the charge on the reacting particle was -2. The same conclusion was reached on applying the method of Frumkin *et al.*[5] to data at higher cathodic potentials. The above results parallel those obtained for the aqueous system[7]. Accordingly, they can be qualitatively rationalized in terms of a model in which the reacting particle is in the inner layer in the transition state, its distance from the OHP depending on the specific cation at that plane and on the potential drop across the inner layer. In this case the Tafel slope is $\alpha n - \lambda(\alpha n - z)$ where α is the transfer coefficient, n the number of electrons transferred in the rate determining step, and $1 - \lambda = x_r/x_2$, the ratio of the distance of closest

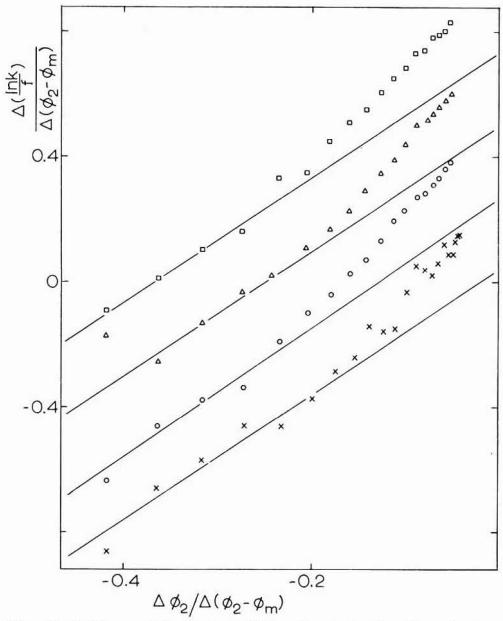

Fig. 3. Differential plots of kinetic data for the electroreduction of $S_2O_8^{2-}$ with 0.02 M base electrolyte concn. in formamide: (×) $LiClO_4$, (○) $NaClO_4$, (△) $KClO_4$, (□) $CsClO_4$. The ordinate scale is correct for $LiClO_4$ but has been shifted vertically by 0.2, 0.4, and 0.6 units for $NaClO_4$, $KClO_4$ and $CsClO_4$, respectively.

approach of the reacting particle to the electrode to that of the predominant double layer cation. The change in the Tafel slope with base electrolyte cation is such that the thickness of the inner layer x_2 increases in the order $x_2(Cs^+) < x_2(K^+) < x_2(Na^+) < x_2(Li^+)$. The change with potential indicates that x_2 decreases with increase in $|\phi_m - \phi_2|$ in accordance with Macdonald and Barlow's model of the inner layer[21].

Corrected Tafel plots (CTP) for the kinetic data were constructed with the charge on the reacting particle set equal to -2. According to the Frumkin equation

$$(\ln k)/f + z\phi_2 = (\ln k_0)/f + \beta(\phi_2 - \phi_m) \qquad (2)$$

where k_0 is the rate constant at the e.c.m. Typical results for a base electrolyte concentration of 0.02 M are shown in Fig. 4. In summary, it was found that: (1) the corrected rate of reaction for a given value of $\phi_2 - \phi_m$ increased with increase in the atomic number of the cation at the OHP; (2) the slope of the CTP varied with $\phi_2 - \phi_m$; (3) the curvature of the CTP increased with increase in cation atomic number; (4) for low values of $\phi_2 - \phi_m$ the slope of the CTP increased with increase in cation atomic number; (5) at high values of $\phi_2 - \phi_m$ the slope of the CTP approached an approximately constant value of 0.28 ± 0.01 except for the Li^+ system. According to the model outlined above, the non-superimposability of the CTP for a given value of $\phi_2 - \phi_m$ is attributed to a change in the average potential at the reaction plane with the specific cation at the OHP because of a corresponding change in the inner layer thickness. The curvature is associated with a decrease in the thickness of the inner layer with increase in the potential drop across it. At higher values of $\phi_2 - \phi_m$, the average potential at the reaction plane does not vary with increase in $\phi_2 - \phi_m$.

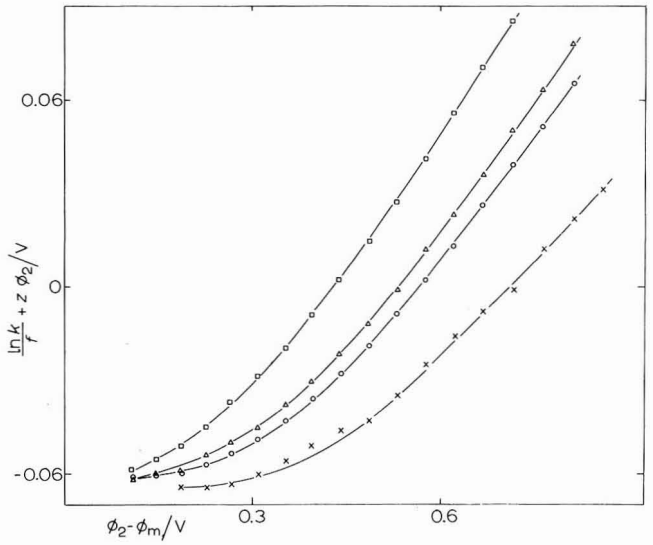

Fig. 4. Corrected Tafel plots of kinetic data for the electroreduction of $S_2O_8^{2-}$ with 0.02 *M* base electrolyte concn. in formamide: (×) $LiClO_4$, (○) $NaClO_4$, (△) $KClO_4$and (□) $CsClO_4$.

Apparently, this condition is not achieved for the Li^+ system within the polarizable range of mercury in formamide.

CTP for different concentrations of the base electrolyte $KClO_4$ in the range 0.01–0.1 *M* are shown in Fig. 5. The results for the Li^+, Na^+, and Cs^+ systems were similar. These plots were not superimposable as predicted by the simple model but instead the corrected reaction rate for a given value of $\phi_2 - \phi_m$ decreased as the base electrolyte concentration increased. A similar observation was made by Frumkin

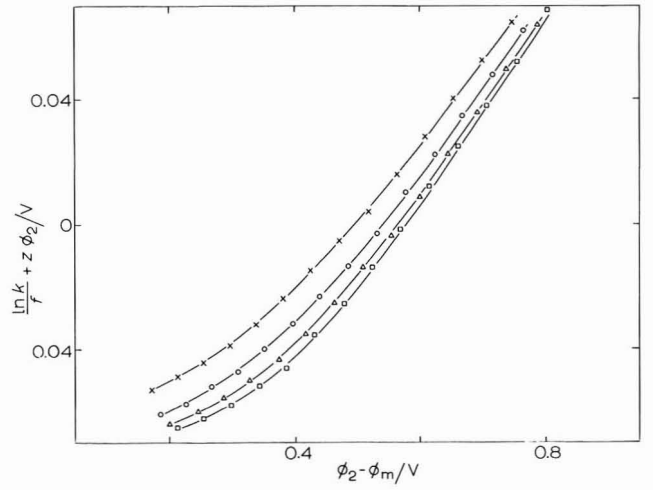

Fig. 5. Corrected Tafel plots of kinetic data for the electroreduction of $S_2O_8^{2-}$ with varying concns. of $KClO_4$ as base electrolyte in formamide: (×) 0.01 *M*, (○) 0.02 *M*, (△) 0.05 *M*, (□) 0.1 *M*.

et al.[5] for aqueous systems with the same range of base electrolyte concentrations. The non-coincidence of the CTP can be partially attributed to a failure to account for variations in k_0 with ionic strength. For constant concentration of the reacting ion, k_0 will decrease with increase in ionic strength due to a decrease in the activity of the ion in the bulk of the solution. The magnitude of this effect may be estimated from the limiting form of the Debye–Hückel equation whereby $(\ln \gamma)/f = -0.0182\, z^2 \sqrt{\mu}$ for formamide solutions at 25°C. γ is the single ion activity coefficient and μ the ionic strength. Accordingly, for a change in μ from 0.0115 to 0.1015, $(\ln \gamma)/f$ for $S_2O_8^{2-}$ changes from -0.0078 to -0.0232. Keeping in mind that the change in $(\ln \gamma)/f$ is overestimated when the simple Debye–Hückel theory is used, this correction is somewhat less than that required to bring the CTP into coincidence within experimental error (see Fig. 5). The remainder of the effect could be due to defects in the Gouy–Chapman model used to estimate the OHP potential[22,23]. The qualitative effect of an error in ϕ_2 can be discussed in terms of a correction to the CTP. If ϕ_2 is the actual value of the average potential at the OHP, and ϕ_2^{GC}, that estimated by the Gouy–Chapman model, then eqn. (2) may be written.

$$(\ln k)/f + z\phi_2^{GC} + (\alpha n - z)(\phi_2^{GC} - \phi_2) = (\ln k_0)/f + \alpha n(\phi_2^{GC} - \phi_m) \qquad (3)$$

According to the calculations of Hurwitz *et al.*[22] when dielectric saturation, ionic size and electrostriction, and other discrete effects are considered, the absolute value of ϕ_2 is greater than that determined by the simple model, the magnitude of the difference increasing with charge density and ionic strength. As can be seen from eqn. (3), this correction is also in a direction which would improve coincidence of the CTP. However, the above calculations did not include a consideration of the change in the activity coefficient of ions at the interface with respect to that in the bulk of the solution. According to Bell and Levine[23], this correction is of the same magnitude as the others. Further discussion of errors in the CTP due to errors in ϕ_2 must await the development of a modified theory of the diffuse layer which is valid at higher concentrations and electrode charge densities. In conclusion, it should be emphasized that the concentration effect not accounted for by change in the bulk activity of the reacting ion was small.

From capacity studies in formamide, it has been concluded that Cs^+ is weakly adsorbed on mercury at cathodic potentials but that adsorption of the other alkali metal cations is probably negligible[24]. The effects of ionic specific adsorption on the kinetics of simple electron transfer reactions have been considered recently by Parsons[25]. Firstly, the potential distribution in the inner layer and the potential at the OHP are altered. In the present case, failure to consider cation specific adsorption would result in high estimates of $|\phi_2|$ and thus, of corrected reaction rates. The amount of cation specific adsorption would increase with cation bulk concentration at constant electrode potential. Thus, from eqn. (3), CTP constructed with ϕ_2 estimated without consideration of specific adsorption would lie above one another in the order of increasing base electrolyte concentration. This is opposite to what was found experimentally. The second effect is related to lateral interactions between the reacting anion and the adsorbed cations. To a first approximation these would consist of attractive electrostatic forces and could be estimated from the surface excess of adsorbed cations and the second virial coefficient for cation–cation interaction[25]. The order of this effect is the same as the first, the increase in reaction rate increasing

with increase in specific adsorption, that is, base electrolyte concentration. The final effect to be considered is coverage of the electrode surface with adsorbed ions. This would result in a decrease in reaction rate with coverage. In the present case, coverage is small and could probably be neglected with respect to the first two effects. The order of the concentration effect on the CTP and the observation that its magnitude did not vary significantly with cation indicate that cation specific adsorption is not an important consideration in the system studied. In the case of the Cs^+ system there was some indication that the Tafel slope was higher than 0.28 for $\phi_2 - \phi_m > 0.8$ V ($|q| > 15\ \mu C\ cm^{-2}$). This increase is in the direction expected from the above considerations and occurs in the potential range where adsorption of Cs^+ becomes significant.

The present results differed from those obtained in the corresponding aqueous systems in several aspects (Fig. 6). The change in the corrected rate of reaction from the Li^+ to the Cs^+ system was considerably less in formamide. In addition, the change in curvature of the CTP with base electrolyte cation was opposite to that observed in aqueous systems. In other aspects, the results for the two solvents were qualitatively similar. It was especially interesting to note that the order of the cation effect in the CTP was the same for water and formamide whereas for capacity data at high cathodic potentials it differed. If it is accepted that the thickness of the inner layer increases with increase in solvated cation radius, then the capacity effect can be attributed to changes in the inner layer dielectric constant with the nature of the cation at the OHP. The orientation of solvent dipoles in the inner layer will be a function of both the field due to the charge on the electrode and the field of the individual ions. Strongly solvated ions such as Li^+ will tend to keep more solvent molecules out of alignment with a given electrode field than more weakly solvated ions. Thus, the order of the dielectric constant in the inner layer would be $Li^+ > Na^+ > K^+ > Cs^+$. The relative values of the dielectric constant and inner layer thickness would be such that the ratio of the dielectric constant to the thickness (*i.e.* the capacity) increases in the order $K^+ < Na^+ < Li^+ < Cs^+$. The position of Cs^+ in this series could well be different

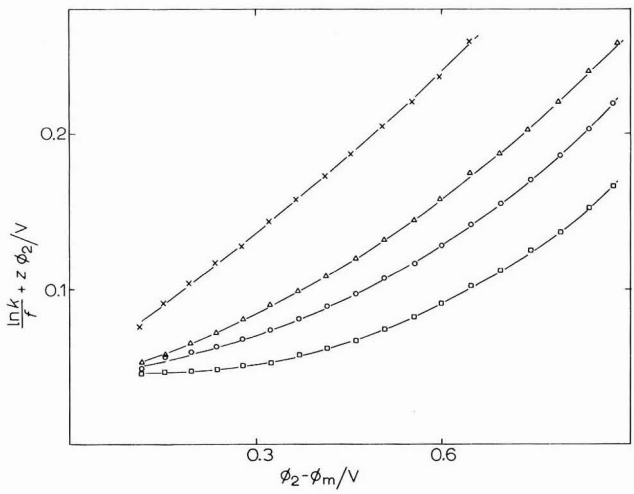

Fig. 6. Corrected Tafel plots of kinetic data for the electroreduction of $S_2O_8^{2-}$ with 0.01 *M* alkali metal fluorides as base electrolytes in water: (□) LiF, (○) NaF, (△) KF, (×) CsF.

if it were not specifically adsorbed. The values of the inner layer capacity in the region of the capacity maximum give further evidence of the correctness of the order of the thickness. In the vicinity of the maximum, the solvent dipoles are reorienting so that the dielectric constant of the inner layer should be a maximum and less characteristic of the nature of the ion at the OHP. In this region the order of the inner layer capacity is $Cs^+ > K^+ > Na^+ > Li^+$ (see Table 1).

According to a model proposed earlier[7], the curvature of the CTP can be related to the change in inner layer thickness with electrostrictive pressure. If the distance of the reacting particle in the transition state from the electrode is constant, then for small changes in inner layer thickness, the Tafel slope for the case that the reacting particle is in the inner layer is given by the following equation:

$$\beta = \alpha n - \lambda_0(\alpha n - z) - \sigma(\alpha n - z)q(\phi_2 - \phi_m) \tag{4}$$

λ_0 is the value of λ at the e.c.m. and $\sigma = \kappa x_r / 2x_{20}^2$ where κ is the compressibility constant for the inner layer, and x_{20} is the thickness of the inner layer at the e.c.m. On combining eqns. (2) and (4), the following relationship between first differences is obtained:

$$\Delta[(\ln k)/f + z\phi_2]/\Delta(\phi_2 - \phi_m) = [\alpha n - \lambda_0(\alpha n - z)] + \sigma(\alpha n - z)\Delta[q(\phi_2 - \phi_m)^2]/\Delta(\phi_m - \phi_2) \tag{5}$$

Typical plots of the change in Tafel slope *versus* the change in electrostrictive pressure are shown in Fig. 7. No significant difference was observed in these plots with change

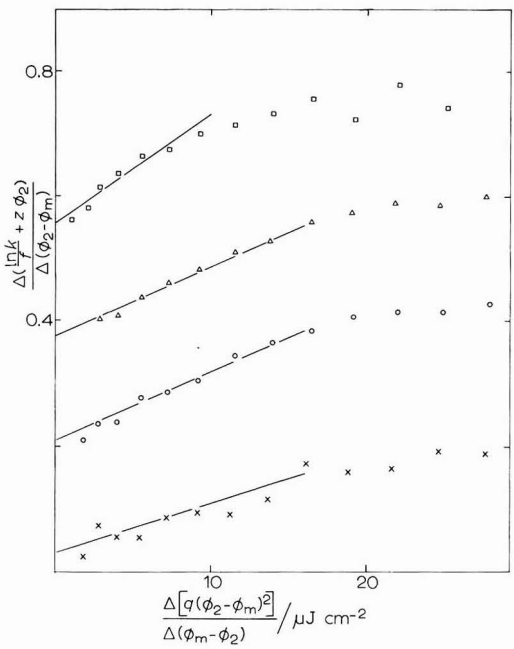

Fig. 7. Plot of change in Tafel slope *vs.* change in electrostrictive pressure in the inner layer for peroxydisulphate kinetic data with 0.05 *M* alkali metal perchlorates as base electrolytes in formamide: (×) $LiClO_4$, (○) $NaClO_4$, (△) $KClO_4$, (□) $CsClO_4$. The ordinate scale is correct for $LiClO_4$ but has been shifted vertically by 1.5, 3.0 and 4.5 units for $NaClO_4$, $KClO_4$, and $CsClO_4$, respectively.

in base electrolyte concentration. Their slope was approximately constant for values of the abscissa variable less than 16($|q| < 10$ μC cm^{-2}) with Li^+, Na^+, and K^+ systems, and for values less than 8($|q| < 8$ μC cm^{-2}) with Cs^+ systems. The average values of $\alpha n - \lambda_0(\alpha n - z)$ and $\sigma(\alpha n - z)$ together with the corresponding values of x_{20}/x_r and κ/x_r are recorded in Table 2 for both formamide and water systems.

TABLE 2

LIMITING TAFEL SLOPE AND CURVATURE PARAMETERS FOR REDUCTION OF $S_2O_8^{2-}$ IN FORMAMIDE AND WATER

Double layer cation	$\alpha n - \lambda_0(\alpha n - z)$	$\sigma(\alpha n - z) \cdot 10^3/cm^2\ \mu J^{-1}$	x_{20}/x_r	$(\kappa/x_r) \cdot 10^3/cm^2\ \mu J^{-1}$
Formamide				
Li^+	0.031 ± 0.009	7.7 ± 0.8	1.12	8.5
Na^+	0.060 ± 0.009	11.2 ± 0.6	1.11	12.0
K^+	0.077 ± 0.009	11.2 ± 0.6	1.10	11.8
Cs^+	0.110 ± 0.010	16.3 ± 1.6	1.08	16.7
		$\alpha n = 0.28$, $z = -2$		
Water				
Li^+	0.011 ± 0.007	9.1 ± 0.3	1.16	10.5
Na^+	0.077 ± 0.008	8.3 ± 0.1	1.13	9.0
K^+	0.140 ± 0.010	6.2 ± 0.3	1.09	6.3
Cs^+	0.34 ± 0.02	–	1.0	–
		$\alpha n = 0.34$, $z = -2$		

It is undoubtedly true that the above model, if it is indeed a correct qualitative explanation of the curvature of the CTP, oversimplifies the real situation. In the case of formamide, one would expect the compressibility constant of the inner layer to change with potential on the cathodic side of the e.c.m. During desorption of the solvent molecules whose dipoles are oriented with the negative end towards the metal, solvated cations should easily be able to move closer to the electrode since solvent molecules on the side of the solvation sheath towards the metal are oriented in the correct fashion. Once reorientation is complete further compression of the inner layer depends on more efficient packing of similarly oriented dipoles and is probably more difficult. The compressibility constants calculable from the data reported in Table 2 are more characteristic of the first process since they were obtained in the potential region of the capacity maximum. Furthermore, a weakly solvated cation such as Cs^+ would be able to accommodate itself to the preferred orientation of the free solvent molecules more readily than a strongly solvated ion such as Li^+. Thus, the trend for κ is to increase in the order $Li^+ < Na^+ < K^+ < Cs^+$. If the inner layer contains two regions, one of low dielectric constant adjacent to the electrode, and one of higher dielectric constant adjacent to the OHP, then the potential in the latter region will be approximately constant and equal to ϕ_2. Once the reacting particle is in this region, the CTP have a constant slope and the effects of compressibility are not observed. In water, the compressibility constants are characteristic of the second process described above, namely packing of similarly oriented dipoles. Since the inner layer is only a few angstroms thick, its compressibility will be a function of the number of

solvent molecules contained therein. The order of κ in this case ($Li^+ > Na^+ > K^+ > Cs^+$) probably reflects a corresponding change in total number of water molecules.

The observed curvature of the CTP could also be attributed to defects in the Gouy–Chapman theory. If the true value of ϕ_2 is greater than that calculated by the simple model, then according to eqn. (3), the corrected reaction rate will be high by an amount $(\alpha n - z)(\phi_2 - \phi_2^{GC})$ when CTP are constructed using ϕ_2^{GC}. If the error in ϕ_2 increases with electrode charge density, then the shape of the CTP is qualitatively accounted for by such an error. However, the constancy of the slope of the CTP constructed with ϕ_2^{GC} requires that the difference $\phi_2 - \phi_2^{GC}$ is constant at higher electrode charge densities. As pointed out above, no calculations with an extended version of the Gouy–Chapman model are available for these conditions, but such a result would seem fortuitous. In the limit of small electrode charge density, $\phi_2 - \phi_2^{GC}$ is zero. The dependence of the Tafel slope on the nature of the double layer cation in this limit is unequivocal evidence that the cation effect cannot be entirely attributed to errors in estimation of ϕ_2. Finally, it is noted that, in a recent experimental test of the simple diffuse layer model[26], it was concluded that errors in it are small.

ACKNOWLEDGEMENTS

The authors thank Drs. R. Parsons and D. S. Reid for supplying the double layer data used in this paper. Financial assistance was received from the National Research Council and Defence Research Board of Canada, and from the Department of University Affairs (Ontario) through award of a scholarship to M.D.M.

SUMMARY

The results of a polarographic study of the effect of the double layer on the kinetics of electroreduction of peroxydisulphate anion at a mercury electrode in formamide are presented. As was observed previously with aqueous systems, the reaction rate was markedly dependent on the nature of the cation in the double layer. The results in the two solvents are compared and several explanations for the cation effect discussed.

REFERENCES

1 G. M. Florianovich and A. N. Frumkin, *Zh. Fiz. Khim.*, 29 (1955) 1827.
2 A. N. Frumkin and N. V. Nikolaeva-Fedorovich, *Vestn. Mosk. Univ., Ser. II Khim.*, (1957) 169.
3 N. V. Nikolaeva-Fedorovich, B. B. Damaskin and O. A. Petry, *Collection Czech. Chem. Commun.*, 25 (1960) 2982.
4 V. K. Venkatesyan, B. B. Damaskin and N. V. Nikolaeva-Fedorovich, *Zh. Fiz. Khim.*, 39 (1965) 129.
5 A. N. Frumkin, O. A. Petry and N. V. Nikolaeva-Fedorovich, *Electrochim. Acta*, 8 (1963) 177.
6 L. Gierst, L. Vandenbergen, E. Nicolas and A. Fraboni, *J. Electrochem. Soc.*, 113 (1966) 1025.
7 W. R. Fawcett, *J. Electroanal. Chem.*, 22 (1969) 19.
8 J. R. Macdonald and C. A. Barlow, *Proceedings First Australian Conference on Electrochemistry, Sydney, February 1963*, Pergamon Press, London, 1964, p. 199.
9 E. Dutkiewicz and R. Parsons, *J. Electroanal. Chem.*, 11 (1966) 196.
10 D. C. Grahame, *J. Electrochem. Soc.*, 98 (1951) 343.
11 B. B. Damaskin, R. V. Ivanova and A. A. Survila, *Elektrokhimiya*, 1 (1965) 767.

12 G. H. NANCOLLAS, D. S. REID AND C. A. VINCENT, *J. Phys. Chem.*, 70 (1966) 3300.
13 R. PARSONS, *Ann. Rep. Chem. Soc. (London)*, 61 (1964) 80.
14 W. R. FAWCETT, J. E. KENT AND Y. C. KUO LEE, *J. Electroanal. Chem.*, 20 (1969) 357.
15 R. PAYNE, *J. Chem. Phys.*, 42 (1965) 3371.
16 V. GUTMANN, M. MICHELMAYR AND G. PEYCHAL HEILING, *Anal. Chem.*, 40 (1968) 619.
17 D. C. GRAHAME, E. M. COFFIN, J. I. CUMMINGS AND M. A. POTH, *J. Am. Chem. Soc.*, 74 (1952) 1207.
18 R. PAYNE, *J. Phys. Chem.*, 70 (1966) 204.
19 R. PARSONS, *Rev. Pure Appl. Chem.*, 18 (1968) 91.
20 J. M. NOTLEY AND M. SPIRO, *J. Phys. Chem.*, 70 (1966) 1502.
21 J. R. MACDONALD AND C. A. BARLOW, *J. Chem. Phys.*, 36 (1962) 3062.
22 H. D. HURWITZ, A. SANFELD AND A. STEINCHEN-SANFELD, *Electrochim. Acta*, 9 (1964) 929.
23 G. M. BELL AND S. LEVINE, in B. E. CONWAY AND R. G. BARRADAS (Ed.), *Chemical Physics of Ionic Solutions*, Wiley, New York, 1966, p. 409.
24 R. PAYNE, *J. Phys. Chem.*, 73 (1969) 3598.
25 R. PARSONS, *J. Electroanal. Chem.*, 21 (1969) 35.
26 R. PARSONS AND S. TRASATTI, *Trans. Faraday Soc.*, 65 (1969) 3314.

ELECTROANALYTICAL CHEMISTRY AND INTERFACIAL ELECTROCHEMISTRY
Elsevier Sequoia S.A., Lausanne – Printed in The Netherlands

REDUCTION CHIMIQUE ET ELECTROCHIMIQUE DES IONS SILICO-MOLYBDATE DANS LE DICHLORO-1,2 ETHANE

R. KOLLAR*, V. PLICHON ET J. SAULNIER

Laboratoire de Chimie Analytique Générale associé au C.N.R.S., ESPCI, 10 rue Vauquelin, Paris (France)

(Reçu le 7 février, 1970)

INTRODUCTION

La réduction des complexes silicimolybdiques en dérivés bleus est utilisée pour doser par spectrophotométrie cet hétéropolyacide. Mais, selon les conditions opératoires et les méthodes de réduction, de nombreux dérivés peuvent être obtenus, tous colorés en bleu. En particulier, Massart[2] a montré l'existence de plusieurs étapes de réduction électrochimique, fonction des conditions de pH, et différentes pour les isomères α et β. La réduction chimique conduit à d'autres espèces, par suite de la formation de complexes entre les produits de la réaction[3].

A la suite de notre travail[1] concernant l'extraction des complexes silicimolybdiques par le nitrate de triiso-octylamine en solution dans le dichloro-1,2 éthane, nous avons étudié leur réduction chimique et électrochimique dans ce solvant.

Après avoir précisé les trois premières étapes de la réduction électrochimique, nous avons comparé les produits obtenus par différents réducteurs chimiques aux dérivés préparés par électrochimie. Il s'est avéré que la réduction chimique n'est jamais simple, par suite de la formation de complexes ou de la précipitation des dérivés réduits.

Mais avant l'étude électrochimique proprement dite, nous avons dû préciser quelques propriétés électrochimiques générales du dichloro-1,2 éthane, ce solvant ne semblant pas, à notre connaissance, avoir été utilisé en électrochimie.

PARTIE EXPÉRIMENTALE

Solvant

Pour la purification du solvant, il faut considérer le milieu complet, c'est-à-dire le solvant contenant l'électrolyte indifférent $(hept)_4NClO_4$ 10^{-1} M et l'acide R_3NHClO_4 4×10^{-2} M (R = triiso-octyle) servant à fixer le pH. En effet, en présence d'air et de lumière, on observe une oxydation de ce milieu, qui se traduit par la présence de produits colorés et électroréductibles. Cette oxydation, très importante en milieu nitrate, reste limitée en milieu perchlorate.

Le milieu est purifié par réduction par un amalgame de zinc et extraction simultanée par la soude molaire des produits de la réaction, simplement en agitant

* Ce mémoire recouvrira en partie la thèse de Docteur-Ingénieur de M. R. Kollar.

les trois phases en présence (solvant, amalgame, soude). Par évaporation sous vide, on élimine dans la fraction de tête une partie de l'eau contenue dans le solvant : il en reste moins de 2000 p.p.m.

Réactifs

Les silicomolybdates α et β ont été préparés selon la méthode de Massart[2], le dérivé β étant extrait par R_3NHNO_3 en milieu dichloroéthane, puis purifié par agitation de la phase organique avec une solution 1 *M*, puis 0.1 *M* d'acide perchlorique.

Bromure de tétraheptylammonium : Eastman Kodak.

Perchlorate et chlorure de tétraheptylammonium sont préparés en solution dans le dichloroéthane, en agitant une solution dans ce solvant de bromure de tétraheptylammonium dans le premier cas, de perchlorate dans le second, avec une solution aqueuse de perchlorate d'argent ou de chlorure de potassium. Le chlorure d'argent ou le perchlorate de potassium se séparent par précipitation.

TABLEAU 1

Amalgame	Bi	Pb	Sn	In	Tl	Cd
Sel	nitrate	nitrate	chlorure	chlorure	sulfate	nitrate
Milieu	acide tartrique pH = 4.5	$HClO_4$ 1 *M*	NaBr 3 *M* HCl 0.3 *M*	HCl	HCl 1 *M*	$HClO_4$ 1 *M*
E/V (ECS)	−0.35	−0.48	−0.70	−0.60	−0.56	−0.67

Amalgames. Sauf l'amalgame de zinc (dissolution du zinc dans le mercure chaud), les amalgames 0.5 *M* sont préparés par électrolyse à potentiel contrôlé *E*, d'une solution concentrée d'un sel du métal (Tableau 1).

Techniques électrochimiques

Il n'est pas possible d'utiliser une électrode au calomel saturé en milieux aqueux, par suite de la précipitation de KCl à la jonction eau–solvant. Nous avons utilisé une électrode de comparaison $Ag(s)/AgClO_4(s)$, sans cependant en faire l'étude théorique. Préparée toujours dans les mêmes conditions (oxydation anodique d'un fil d'argent pendant 15 min, sous 4 mA) l'électrode prend un potentiel d'équilibre reproductible à ± 7 mV. Sa dérive est inférieure à 10 mV en trois semaines.

La contre-électrode est un fil de platine, situé dans un compartiment séparé par un double fritté No. 3 du reste de la solution. L'appareillage est un montage classique à 3 électrodes.

Les solutions sont dégazées par de l'azote U saturé en solvant parce que l'oxygène est électroactif ($E_{\frac{1}{2}} = -1.4$ et -1.65 V).

CARACTÉRISTIQUES ÉLECTROCHIMIQUES DU DICHLORO-1,2 ÉTHANE

Les composés minéraux peuvent être mis en solution dans le dichloro-1,2 éthane lorsqu'ils forment une paire d'ions avec un cation ammonium quaternaire à longue chaîne. Généralement, le cation tétraheptylammonium est suffisant. Nous

avons pu ainsi mettre en solution, par extraction, les ions nitrate, perchlorate, halogénure, les complexes chlorés de l'étain(II), etc.

De nombreuses constantes de dissociation de paires d'ions ont été déterminées par conductimétrie (les références sont rassemblées dans réf. 4). Le perchlorate de tétraheptylammonium est suffisamment soluble et conducteur pour permettre le tracé des courbes intensité–potentiel.

Nous n'avons pas trouvé dans la littérature d'étude générale concernant les réactions acides–bases et la notion d'acidité dans le dichloroéthane pur: on connaît seulement des constantes de dimérisation d'acides organiques[7], des potentiels de neutralisation d'amines par un acide, mais en présence d'un tiers solvant basique, eau ou dioxanne[8], et des différences de pK d'acide entre l'eau et le solvant, mais obtenues par le calcul[9]. Ne connaissant ni l'origine de l'échelle de pH, ni de valeur de pK de tampons dans le solvant pur, nous avons fixé l'acidité du milieu à l'aide de l'acide R_3NH^+ (sous forme de R_3NHClO_4) en concentration 4×10^{-2} M (R = triiso-octyle).

TABLEAU 2

DOMAINES D'ÉLECTROACTIVITÉ

Potentiels en volts (électrode de comparaison Ag(s)/$AgClO_4$(s)) pour lesquels $i = 0.1$ mA cm^{-2}. Electrolyte indifférent: $(hept)_4NClO_4$ 10^{-1} M. Milieu acide: (R_3NHClO_4) 4×10^{-2} M, R = triiso-octyle. Milieu halogénure: halogénure de tétraheptylammonium en milieu R_3NHClO_4.

Electrode	*Milieu*	*Limite anodique/V*	*Limite cathodique/V*	*Etendue totale/V*
Pt poli	neutre	+1.1	−2.8	3.9
Pt poli	acide	+1.1	−2.4	3.5
C vitreux	neutre	+1.0	−3.0	4.0
C vitreux	acide	+1.0	−2.4	3.4
Hg	neutre	+0.1	−2.9	3.0
Hg	acide	+0.1	−2.5	2.5
Hg	chlorure	−1.05	−2.5	1.5
Hg	bromure	−1.2	−2.5	1.3
Hg	iodure	−1.35	apparition d'iode	
Pt poli	ferrocène	$E_{\frac{1}{2}} = -0.27$		

Le domaine d'électroactivité du dichloro-1,2 éthane dépend de l'électrode et du milieu choisis (Tableau 2). Comparé à d'autres solvants, le dichloroéthane semble particulièrement intéressant dans le cas de l'électrode de mercure en milieu non complexant (perchlorate). Cela provient sans doute du potentiel élevé d'oxydation du mercure, puisque cette oxydation n'interfère pas avec la réduction des ions silicomolybdique, contrairement à ce qu'on observe dans l'eau.

Le ferrocène est oxydable à une électrode de platine poli ($E_{\frac{1}{2}} = -0.275$ V), mais la forme de la vague ne correspond pas parfaitement à celle d'un système rapide ($E_{\frac{3}{4}} - E_{\frac{1}{4}} = 75$ mV). Cela pourrait provenir d'une compensation imparfaite de la chute ohmique, malgré l'utilisation d'un montage à trois électrodes, le milieu étant relativement résistant ($\varepsilon = 10$).

RÉDUCTION ÉLECTROCHIMIQUE

A l'inverse de l'eau[2], on peut observer dans le dichloro-1,2 éthane les vagues de réduction des ions silicomolybdate à une électrode à gouttes de mercure, en milieu non complexant (ClO_4^-). En effet, le mercure est relativement plus difficile à oxyder que dans l'eau en milieu perchlorate. Il n'est évidemment pas question d'utiliser un halogénure comme électrolyte. En revanche, les essais tentés à une électrode de platine poli ou de carbone vitreux ont conduit à des courbes peu exploitables en milieu neutre comme en milieu acide.

En milieu neutre non tamponné, les isomères α et β sont réductibles à une électrode à gouttes de mercure, mais les vagues sont très mal définies. Au contraire, en

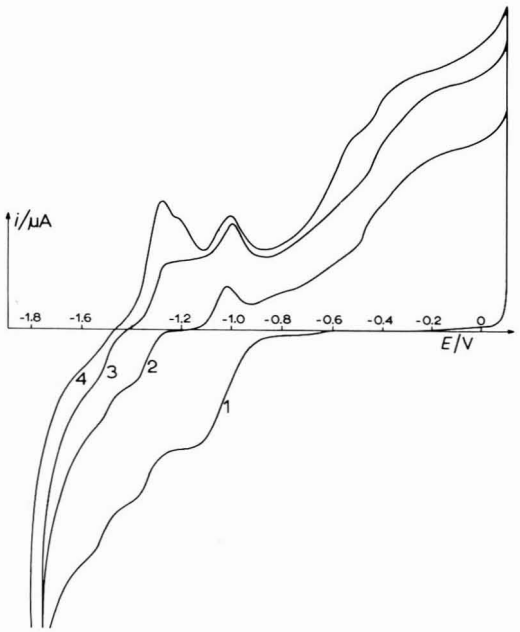

Fig. 1. Courbe intensité–potentiel à une électrode à gouttes de mercure de (1) 0α, (2) IVα, (3) VIα, (4) après électrolyse à -1.55 V. Concentration 10^{-3} M en 0α.

milieu acide, les polarogrammes comprennent trois vagues bien définies suivies d'une série de maximums que nous n'avons pas étudiés (Fig. 1). Mais à l'inverse de ce que Massart a observé dans l'eau, les isomères α et β sont réduits à des potentiels de demi-vague trop proches, compte tenu de la précision de leur détermination, pour qu'on puisse les distinguer par électrochimie.

—isomère α: -1.05 ± 0.03 V $\quad -1.30 \pm 0.03$ V $\quad -1.50 \pm 0.05$ V
—isomère β: -1.10 ± 0.03 V $\quad -1.30 \pm 0.03$ V $\quad -1.50 \pm 0.05$ V

Dans la suite de cette étude, nous avons considéré exclusivement l'isomère α.

La première vague, qui a une hauteur double de celle des deux suivantes, débute par un maximum de première espèce que ni la gélatine, ni le rouge de méthyle, ni le dodécylsulfonate de sodium (Teepol), ne suppriment.

Le maximum n'apparaît pas si le solvant a été préalablement très soigneusement purifié par réduction chimique.

Les trois vagues sont des vagues de diffusion pure. En effet, leur hauteur est proportionnelle à la racine carrée de la hauteur de la colonne de mercure et à la concentration en silicomolybdate dans le domaine 5×10^{-4} à 10^{-2} M. Le coefficient de température est $+1.6\%$ par degré.

Première étape de réduction

Une électrolyse à potentiel contrôlé (-1.20 V) indique un échange de 4 ± 0.07 électrons par molécule. Selon la terminologie adoptée par Massart[2], on obtient donc directement l'espèce IVα et non le dérivé IIα comme dans l'eau. IVα est assez stable à

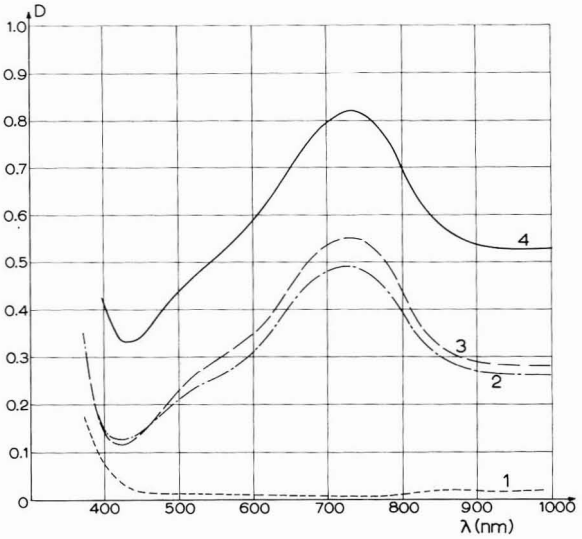

Fig. 2. Spectre de (1) 0α, (2) IVα, (3) VIα, (4) après électrolyse à -1.55 V.

l'air (3% de disparition en 4 h) et son spectre (Fig. 2) ressemble au spectre obtenu par Massart pour IVα dans l'eau.

Le polarogramme de IVα est représenté Fig. 1. On observe toujours les deux étapes ultérieures de réduction ($E_{\frac{1}{2}} = -1.35$ et -1.51 V). En revanche, la vague d'oxydation de IVα en 0α ne comporte qu'une suite de maximums de faible intensité.

La réoxydation de IVα en 0α à potentiel contrôlé est difficile, par suite des très faibles courants d'électrolyse. Pratiquement, pour faire complètement disparaître la coloration bleue de IVα, nous avons dû imposer un potentiel de -0.1 V. Une certaine quantité de mercure a été oxydée simultanément, comme l'indique une analyse qualitative, ce qui a empêché la détermination du nombre d'électrons échangés par molécule de IVα. Quant à l'espèce obtenue lors de cette réoxydation, le polarogramme représenté Fig. 3, indique que ce n'est plus 0α: on distingue en particulier une prévague située vers -0.75 V.

Deuxième étape de réduction

Une électrolyse à potentiel contrôlé (-1.40 V) indique un échange de 2 ± 0.01

électrons par molécule. IVα est donc réduit en VIα. Son spectre est très voisin de celui de IVα (Fig. 2).

Le polarogramme de VIα (Fig. 1) comprend, en réduction une vague ($E_{\frac{1}{2}} = -1.52$ V) et en oxydation la vague d'oxydation de VIα en IVα ($E_{\frac{1}{2}} = -1.32$ V) suivie de la série de maximums précédemment observés pour IVα. La comparaison des

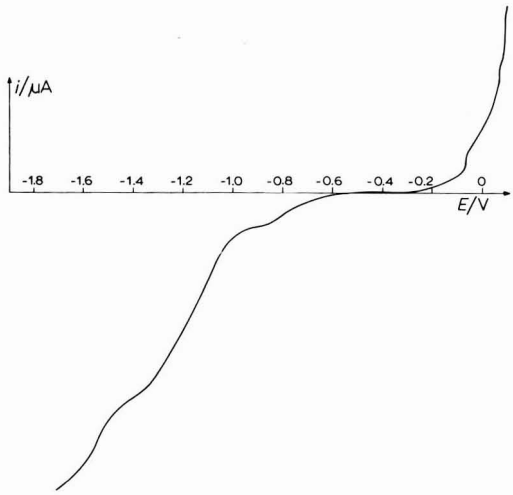

Fig. 3. Courbe intensité–potentiel à une électrode à gouttes de mercure de l'espèce obtenue par oxydation de IVα à 0.1 V.

potentiels de demi-vague anodique et cathodique du système IVα/VIα indique la réversibilité de ce système à une électrode de mercure. Chimiquement, des traces d'oxygène suffisent pour réoxyder très rapidement VIα en IVα.

Troisième étape de réduction

La hauteur de la vague de diffusion laisse prévoir une réduction à deux électrons conduisant à VIIIα. En fait, une électrolyse à potentiel contrôlé à -1.55 V n'a pas conduit à des résultats significatifs.

Malgré le passage d'une importante quantité d'électricité, la troisième vague ne diminue que de 30 %, tandis que la partie anodique du polarogramme ne se déforme que faiblement. Il est vraisemblable que VIIIα se dismute en milieu acide, comme cela se produit dans l'eau.

Pour résumer, le dérivé α est réductible à une électrode à gouttes de mercure en trois étapes, mais seules les deux premières conduisent à des dérivés stables en milieu acide. A l'inverse de ce qui a lieu dans l'eau, le dérivé IIα n'est pas stable dans le dichloro-1,2 éthane, en milieu acide.

$$0\alpha \xrightarrow{+4e} IV\alpha \underset{}{\overset{+2e}{\rightleftharpoons}} VI\alpha \xrightarrow{+2e} VIII\alpha \longrightarrow \text{dismutation?}$$

$$0\alpha \xrightarrow{-ne} ?$$

RÉDUCTION CHIMIQUE

L'isomère α est donc réductible, en milieu acide, en au moins deux dérivés stables, semblables par leur spectre d'absorption, mais distincts par leur polarogramme. Les réducteurs chimiques étant d'un emploi plus simple, nous avons cherché à comparer les dérivés obtenus par réduction chimique à IVα et VIα, en nous appuyant sur les prévisions déduites de la position relative des potentiels de réduction $E_{\frac{1}{2}}$ (cat.) de l'isomère α et des potentiels d'oxydation $E_{\frac{1}{2}}$ (an.) des réducteurs chimiques.

En effet, en supposant les systèmes rapides, si $E_{\frac{1}{2}}$ (an.) est moins négatif que $E_{\frac{1}{2}}$ (cat.), on peut prévoir l'absence de réaction chimique. Si $E_{\frac{1}{2}}$ (an.) est voisin ou un peu plus négatif que $E_{\frac{1}{2}}$ (cat.), la réduction chimique est possible, mais vraisemblablement lente. Si $E_{\frac{1}{2}}$ (an.) est très inférieur à $E_{\frac{1}{2}}$ (cat.), la réduction chimique est alors rapide.

(1) *Mercure en milieu halogénure*

En milieu complexant, le mercure est plus facile à oxyder et devient susceptible de réduire l'isomère α. D'après les potentiels d'oxydation du mercure en milieu halogénure (Tableau 2), on peut supposer que la réduction en milieu chlorure conduit lentement et incomplètement au dérivé IVα, mais est totale en milieu bromure.

En agitant une solution d'isomère α au contact d'une nappe de mercure, on constate une réduction lente et incomplète en milieu chlorure (30%) comme en milieu bromure (50%). Les polarogrammes des mélanges obtenus ne permettent pas de conclure à une réduction en IVα. Cette méthode n'a donc pas d'application analytique.

(2) *Amalgames*

Les potentiels d'oxydation de divers amalgames dans le dichloro-1,2 éthane sont indiqués dans le Tableau 3. Nous avons ajouté leur potentiel d'oxydation dans

TABLEAU 3

POTENTIELS[a] D'OXYDATION D'AMALGAMES

	Hg	*Bi(Hg)*	*Sn(Hg)*	*Pb(Hg)*	*In(Hg)*	*Cd(Hg)*	*Tl(Hg)*	*Zn(Hg)*
DCE, E/V (milieu acide)	+0.05	−0.30	−0.78	−0.81	−0.90	−1.01	−1.11	−1.38
H_2O[b], E/V ($HClO_4$ = 1 *M*)	+0.50	+0.10	−0.37	−0.34	−0.44	−0.54	−0.48	−0.96

[a] *E* pour $i = 1$ μA à une électrode à gouttes d'amalgame 0.5 *M* (Ref. Ag(s)/$AgClO_4$(s)). [b] D'après ref. 5. *E* en volts par rapport à l'électrode au calomel saturé.

l'eau, bien que les réactions ne soient pas directement comparables : en milieux $HClO_4$ aqueux, les ions provenant de l'oxydation des métaux restent en solution, alors qu'ils sont vraisemblablement insolubles dans le dichloroéthane. On constate que l'ordre des pouvoirs réducteurs est conservé, mis à part une inversion entre l'étain et le plomb, au demeurant très voisins. Seul le thallium fait vraiment exception, puisqu'il devient beaucoup plus réducteur.

Les prévisions que l'on peut faire à partir de la simple comparaison des potentiels d'oxydation des amalgames et de réduction de l'ion silicomolybdate, ne

sont absolument pas vérifiées expérimentalement. En effet, on peut prévoir que les amalgames de bismuth, d'étain et de plomb ne réduisent pas l'ion silicomolybdate, les amalgames de cadmium et peut-être l'indium, conduisent au dérivé IVα, et ceux de zinc et peut-être de thallium, au dérivé VIα.

Expérimentalement, on constate que tous les amalgames réduisent l'ion silicomolybdate, mais jamais sous forme de IVα ni VIα. Bi(Hg) agit lentement, Sn(Hg) rapidement. L'un et l'autre conduisent à des dérivés bleus solubles, mais dont les spectres diffèrent l'un de l'autre et de ceux de IVα et VIα (Fig. 4).

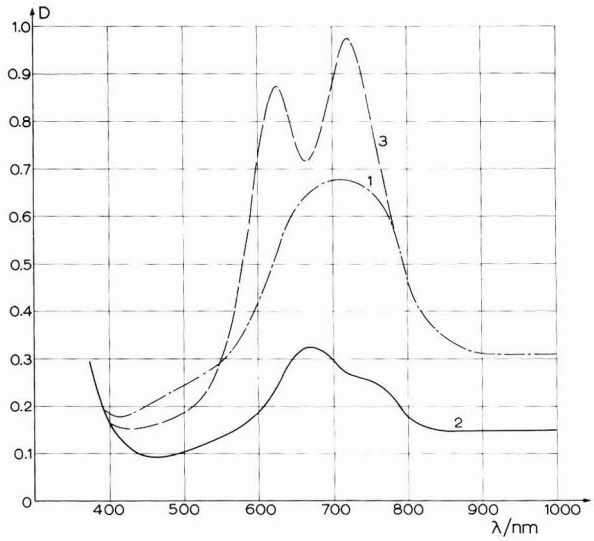

Fig. 4. Spectre du produit de réduction de 0α par: (1) Bi(Hg), (2) Sn(Hg), (3) Sn(II).

Quant aux autres amalgames, ils réduisent dans un premier temps l'isomère α en dérivés bleus, plus ou moins rapidement selon leur pouvoir réducteur. Rapidement ensuite, la solution se décolore totalement et l'hétéropolyanion précipite.

Il est surprenant de constater que les amalgames de bismuth, d'étain et de plomb réduisent l'ion silicomolybdate. Si l'on utilise une grande sensibilité en courant pour tracer le polarogramme de l'ion silicomolybdate à une électrode à gouttes tombantes de ces amalgames, on observe, aux potentiels inférieurs à -1.0 V, un courant d'oxydation faible, mais nettement supérieur au courant résiduel. Le courant d'échange au potentiel d'équilibre est donc loin d'être négligeable, ce qui est compatible avec l'existence de la réduction chimique.

Pour expliquer le fait que les amalgames sont oxydés plus facilement en présence d'ions silicomolybdate, on peut envisager la formation de complexes entre les ions provenant du métal et les produits de réduction de l'hétéropolyanion. De tels complexes sont déjà connus, en particulier dans le cas de l'étain[2]. Ces complexes auraient des spectres d'absorption différents de ceux de IVα ou VIα s'ils sont solubles. Mais dans la plupart des cas, ils seraient insolubles dans le dichloroéthane, peut-être parce que n'étant pas chargés, ils ne forment pas de paires d'ions avec les amines à longue chaîne.

Quoiqu'il en soit, la réduction par les amalgames ne conduit pas aux dérivés obtenus par électrolyse et, seul le complexe obtenu à partir de l'amalgame d'étain pourrait présenter un intérêt analytique: il est stable en fonction du temps, et son coefficient d'absorption molaire est de 8800 l mol^{-1} cm^{-1} à 720 nm.

(3) *Autres réducteurs*

Parmi les réducteurs classiquement utilisés pour réduire les hétéropolyacides, nous avons choisi l'acide ascorbique et l'étain(II).

L'acide ascorbique n'est pas soluble dans le dichloro-1,2 éthane, mais l'ascorbate de triiso-octylamine l'est suffisamment. Il est oxydable à une électrode de mercure à partir de -0.95 V. On peut donc espérer réduire chimiquement l'isomère 0α en IVα. En pratique, la réduction en IVα est lente et non quantitative, et ne peut être utilisée en analyse.

L'étain(II) est mis en solution dans le dichloroéthane par extraction par la triiso-octylamine, de ses complexes chlorure qui sont sous forme d'anions en milieu acide chlorhydrique 0.6 *M*. Il réduit l'isomère α en un composé bleu de spectre caractéristique (Fig. 4). Ce spectre est différent de celui du dérivé obtenu par réduction par l'amalgame d'étain en l'absence de chlorure. On serait donc en présence d'un complexe chloro–silico–stanni–molybdique, dont l'existence est indiquée par Massart[2].

Ce complexe est stable en fonction du temps, et son coefficient d'absorption molaire est élevé: $\varepsilon = 11300$ l mol^{-1} cm^{-1} à 725 nm.

Nous avons cherché à l'utiliser pour le dosage du silicium. Mais on n'obtient pas une meilleure sensibilité (2×10^{-6} moles de Si par litre de solution aqueuse) que par détermination directe dans l'ultra-violet de l'hétéropolyacide non réduit en solution dans le dichloroéthane, méthode évidemment plus simple[1]. Le seul avantage réside dans le fait que la transformation isomérique $\beta \rightarrow \alpha$ ne gêne pas, car les complexes provenant de la réduction de ces deux isomères, bien qu'ayant des spectres différents, présentent tous deux à 725 nm un maximum avec un coefficient d'extinction molaire identique.

CONCLUSION

Bien qu'il n'ait pas été utilisé, à notre connaissance, comme solvant en électrochimie, le dichloro-1,2 éthane semble avoir des caractéristiques suffisamment intéressantes pour justifier son emploi lorsque l'on désire oxyder ou réduire électrochimiquement une espèce dans un milieu non miscible à l'eau. L'exemple des complexes silicimolybdiques prouve que la réduction électrochimique de ces hétéropolyanions conduit à des dérivés plus simples que ceux qui sont obtenus à partir de réducteurs chimiques classiques, puisqu'on évite ainsi la formation de complexes, souvent insolubles, entre les produits de la réaction. En revanche, l'inconvénient présenté par un tel solvant provient de la nécessité de lier, sous forme de paires d'ions par exemple, les espèces hydrophiles à des groupements hydrophobes, si on veut les maintenir en solution.

RÉSUMÉ

Les domaines d'électroactivité du dichloro-1,2 éthane aux électrodes de platine, mercure et carbone, déterminés par rapport au potentiel de demi-vague du

ferrocène, indiquent que ce solvant présente des caractéristiques électrochimiques intéressantes.

La réduction chimique et électrochimique de l'ion silicomolybdate α est étudiée dans ce solvant à une électrode à gouttes de mercure. Des trois premières étapes (4,2,2 électrons), seules les deux premières conduisent à des dérivés stables en milieu acide. La réduction par des agents chimiques conduit à des dérivés différents de ceux qu'on obtient par voie électrochimique.

SUMMARY

The accessible potential ranges in 1,2-dichloroethane at several working electrodes (Pt, Hg, C) and with different background electrolytes have been determined (reference system: half-wave potential of ferrocene).

At a dropping mercury electrode, electrochemical reduction of α-molybdosilicic acid takes place through three successive steps (2, 2, and 4 electrons respectively). Only the first two steps result in stable products in acid medium. Chemical reduction leads to different species, generally insoluble, whose nature depends on the nature of the reducing agent.

BIBLIOGRAPHIE

1 R. KOLLAR, V. PLICHON ET J. SAULNIER, sous presse.
2 R. MASSART, *Thèse*, Paris, 1967; *Ann. Chim. (Paris)*, 3 (1968) 507.
3 R. MASSART ET G. HERVE, *Rev. Chim. Miner.*, 5 (1968) 501.
4 V. PLICHON, *Bull. Soc. Chim. France*, (1969) 3369.
5 M. BRÉANT ET J. C. MERLIN, *Bull. Soc. Chim. France*, (1963) 2225.
6 B. P. SEN ET S. N. CHATTERJEE, *Anal. Chem.*, 38 (1966) 536.
7 J. F. COETZEE ET R. MEI-SHUN-LOK, *J. Phys. Chem.*, 69 (1965) 2690.
8 H. K. HALL JR., *J. Phys. Chem.*, 60 (1956) 63.
9 N. A. IZMAILOV ET L. L. SPIVAK, *Zh. Fiz. Khim.*, 36 (1962) 757.

ELECTROANALYTICAL CHEMISTRY AND INTERFACIAL ELECTROCHEMISTRY
Elsevier Sequoia S.A., Lausanne – Printed in The Netherlands

CATALYTIC POLAROGRAPHIC WAVE OF NICKEL(II) IN AQUEOUS THIOCYANATE SOLUTIONS CONTAINING TETRAETHYLAMMONIUM IONS

EIKI ITABASHI AND SHIGERO IKEDA
Department of Chemistry, Faculty of Science, Osaka University, Toyonaka, Osaka (Japan)
(Received February 28th, 1970)

The reduction wave of nickel(II) at the dropping mercury electrode is irreversible and drawn-out in sodium nitrate or sodium perchlorate solutions. When pyridine[1-4], *o*-phenylenediamine[5-9], ethylenediamine[10], thiourea[11], chloride ion[12,13], thiocyanate ion[14-16], etc. are present in aqueous solutions, nickel(II) exhibits a catalytic polarographic wave which arises at less negative potentials than those for the usual hydrated nickel(II) reduction wave.

Nickel(II) in aqueous thiocyanate solution produces a well-defined reduction wave in the potential region between -0.6 and -1.1 V *vs.* SCE. The polarographic behavior of the nickel(II)–thiocyanate system is unusual; on the direct current (d.c.) polarogram of the system a minimum appears at relatively negative potentials, and on the alternating current (a.c.) polarogram a negative admittance is observed in the potential region where the minimum appears on the d.c. polarogram[17,18].

The present authors found that nickel(II) in aqueous thiocyanate solutions containing quaternary ammonium salts gave a new catalytic polarographic wave having the shape of a "maximum". This catalytic wave, which is not due to stirring and also does not have the characteristics of the Brdička catalytic wave, occurs in the potential region where the reduction wave of nickel(II) obtained in thiocyanate solution reaches its limiting plateau. Of the many quaternary ammonium salts investigated, tetraethylammonium perchlorate was the most suitable. In the present paper, the characteristics of this maximum wave and the conditions for its occurrence are reported. The most plausible mechanism to explain the catalytic effect is proposed.

EXPERIMENTAL

$Ni(H_2O)_2(ClO_4)_2$ and tetraethylammonium perchlorate (Et_4NClO_4) were prepared using the same procedures as given in a previous paper[19]. All the other chemicals were of analytical reagent grade. Redistilled water was used and all solutions were deaerated with high-purity nitrogen.

D.c. polarograms and current–time (*i–t*) curves of individual drops at constant potential were obtained with the potentiostat previously described[20] and made from operational amplifiers. Polarograms were recorded with a Yokogawa X-Y recorder, PRO-11A type and *i–t* curves with a Riken Denshi SP-G2 type recorder. In the following section and in the figures, "current" means the maximum current observed at the drop time. A.c. polarograms were obtained with a pen-recording Yanagimoto

polarograph, PA-102. The controlled potential electrolysis was carried out with a Shimazu potentiostat, PS-1. The working electrode for the controlled potential electrolysis was a mercury pool whose surface area was approximately 12 cm^2. The counter electrode was a platinum spiral electrode which was connected to the electrolytic solution through a sintered glass. The cell equipment for the polarographic measurements was the same as previously reported[20].

The potential of the DME was measured against a saturated calomel electrode (SCE).

Two capillaries were used throughout this work. The rate of flow of mercury (m) and the drop time (t) of capillary I were 1.35 mg s^{-1} and 5.15 s, respectively, measured in 0.5 M $NaClO_4$ solution under an applied pressure of 60 cm of mercury at open circuit. Capillary II had the characteristics $m=1.22$ mg s^{-1} and $t=5.83$ s, in 0.1 M $NaClO_4$ solution under an applied pressure of 60 cm of mercury at open circuit. Capillary II was employed for the measurements of the electrocapillary curves and the a.c. polarograms. All the other experiments were carried out with capillary I.

Measurements were made at $25.0\pm0.1°C$, unless otherwise stated. The pH of the solution was measured with a Hitachi-Horiba pH meter, F-5.

RESULTS

Effect of the concentration of NaSCN, Et_4NClO_4 and nickel(II)

The effect of thiocyanate concentration over the range 0–5 M on the polarograms of 0.5 mM nickel(II) in 0.1 M Et_4NClO_4 solution is shown in Figs. 1 and 2. The ionic strength was not adjusted because of the relative in solubility of Et_4NClO_4 in water. The pH of the solution was 6.8 ± 0.2.

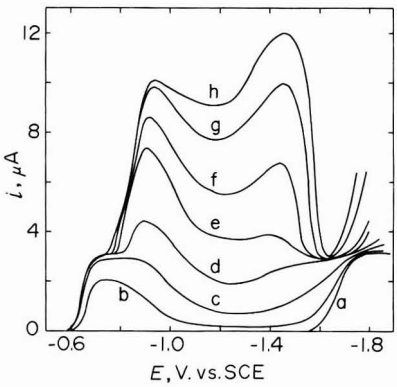

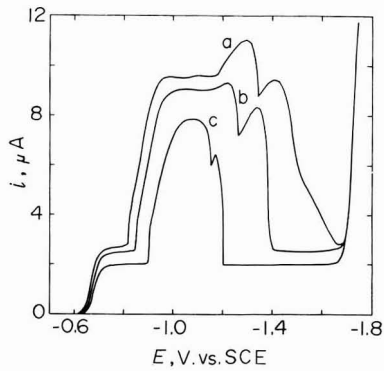

Fig. 1. Polarograms of 0.5 mM nickel(II) in 0.1 M Et_4NClO_4 solutions containing various concns. of NaSCN: (a) 0, (b) 0.02 M, (c) 0.05 M, (d) 0.1 M, (e) 0.2 M, (f) 0.3 M, (g) 0.5 M, (h) 1.0 M.

Fig. 2. Polarograms of 0.5 mM nickel(II) in 0.1 M Et_4NClO_4 solutions containing various concns. of NaSCN: (a) 2.0 M, (b) 3.0 M, (c) 5.0 M.

Nickel(II) in 0.1 M Et_4NClO_4 gave an irreversible wave with a half-wave potential of -1.67 V *vs.* SCE.

Thiocyanate ions displace the nickel(II) reduction wave to considerably less negative potentials. At low concentrations of NaSCN, nickel(II) exhibits a flat maxi-

mum followed by a shallow minimum (curve b, Fig. 1). With increasing NaSCN concentration, the amplitude of the flat maximum increases and eventually reaches the diffusion current (curve c, Fig. 1). With further addition of NaSCN above 0.1 *M*, a characteristic reduction wave with two maxima is observed in the potential region between −0.8 and −1.6 V *vs.* SCE (curves e–h, Fig. 1). For convenience this extended reduction wave can be divided into four sections; the pre-wave (−0.6 to −0.8 V), the maximum A (−0.8 to −1.2 V), the maximum B (−1.2 to −1.6 V) and the post-wave which is observed at potentials more negative than −1.6 V *vs.* SCE.

When the concentration of NaSCN is increased up to about 1.0 *M*, the heights of the pre- and post-wave remain almost unchanged, while the maxima A and B increase in height.

However, when the concentration of NaSCN exceeds 2 *M*, the opposite effect is observed, as shown in Fig. 2. The pre-wave shifts back towards cathodic potentials and the entire wave decreases in height. The region of the maximum becomes considerably deformed, with maximum A shifted towards more negative potentials, and maximum B towards less negative potentials. A single round maximum wave was observed in 5 *M* NaSCN solution.

Figure 3 shows the polarograms of 0.5 m*M* nickel(II) in 0.5 *M* NaSCN solu-

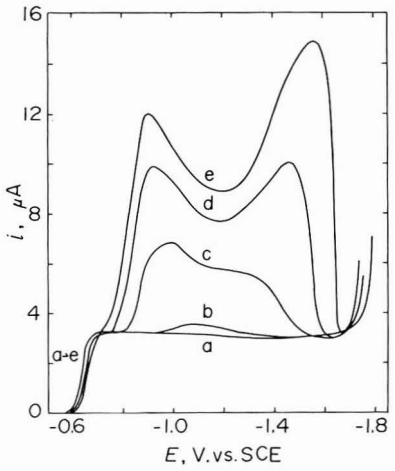

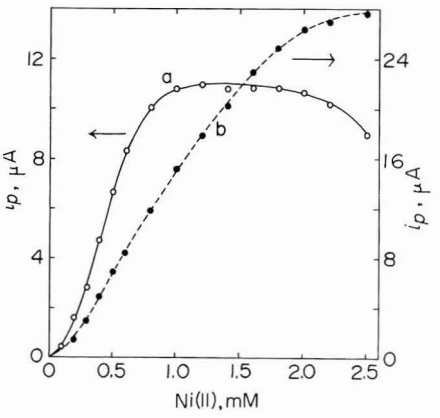

Fig. 3. Polarograms of 0.5 m*M* nickel(II) in 0.5 *M* NaSCN solutions containing various concns. of Et_4NClO_4: (a) 0, (b) 0.02 *M*, (c) 0.05 *M*, (d) 0.1 *M*, (e) 0.2 *M*.

Fig. 4. Variation of peak height of (a) maximum A, and (b) maximum B with concn. of nickel(II) in 0.5 *M* NaSCN and 0.1 *M* Et_4NClO_4.

tion with varying concentrations of Et_4NClO_4.

Nickel(II) in 0.5 *M* NaSCN solution gave a minimum at relatively negative potentials. With 0.02 *M* Et_4NClO_4 present, nickel(II) exhibited a small maximum at about −1.1 V *vs.* SCE. With increasing concentration of Et_4NClO_4, the maximum increased in height and also developed to appreciable potentials, and finally separated into the two maxima A and B. The half-wave potential of the pre-wave shifted slightly towards more negative potentials with the concentration of Et_4NClO_4.

Figure 4 presents the relationships between the peak currents of maxima A and B and the nickel(II) concentration in 0.5 *M* NaSCN and 0.1 *M* Et_4NClO_4 solution. The increment i_p is defined by:

$$i_p = i_t - i_l$$

where i_t is the total height of the maximum wave and i_l the limiting current obtained in the absence of Et_4NClO_4. At constant concentrations of NaSCN and Et_4NClO_4, the peak potentials of maxima A and B remained virtually unchanged.

The heights of the peak currents do not vary linearly with the concentration of nickel(II). When the nickel(II) concentration was below 0.5 m*M*, maxima A and B were nearly equal in height. When the nickel(II) concentration exceeded 1 m*M*, maximum A reached a limited value, while maximum B increased in height with increase in concentration of nickel(II) up to about 2 m*M*. With further increase of nickel(II) above 2 m*M*, maximum A appeared merely as a shoulder of maximum B.

The i–t curves, effects of drop time and stirring

The *i–t* curves of individual drops at various potentials and the effects of drop time and stirring were investigated to determine if the electrode process of the double maxima was diffusion- or kinetically-controlled. Figure 5 shows typical *i–t* curves corresponding to the peaks of maxima A and B, and to the minimum. In the potential region of the maximum wave, the *i–t* curves exhibited slight irregularities which appeared as sudden increase or decrease of current at some time after the birth of the drop. The slopes of log *i*–log *t* plots for curves a, b and c in Fig. 5 had values of 0.64 ± 0.04, 0.65 ± 0.02 and 0.67 ± 0.02, respectively. These values are close to the value of 0.67 expected for a pure kinetically-controlled electrode mechanism. On the other hand, the *i–t* curves of the pre- and post-waves obtained in NaSCN and Et_4NClO_4 solutions showed a well-defined shape and the slopes of log *i*–log *t* plots were close to the value of 0.17 expected for a diffusion-controlled mechanism.

Under the conditions where the concentrations of NaSCN and Et_4NClO_4 exceeded 0.5 *M* and 0.1 *M*, respectively, it was found that the peak currents of the double maxima were independent of the height of the mercury reservoir from 30 to 80 cm, while the limiting currents of the pre- and post-waves were proportional to the square root of mercury height.

The effect of stirring on the maximum wave was also investigated by using 0.5 m*M* nickel(II) and 0.5 *M* NaSCN solution both in the presence and the absence of 0.1 *M* Et_4NClO_4. The stirring was accomplished by means of a magnetic stirrer. In the absence of Et_4NClO_4, it was found that the stirring increased the limiting current about twofold. With 0.1 *M* Et_4NClO_4 present, the increases in the heights of maxima A and B were 10–15% and 5–8%, respectively. This result suggests that the double maxima are not caused by the stirring, but are controlled by another process and that the electrode mechanism does not involve the local formation of a concentration gradient of some reactive species.

Effect of temperature

Measurements of the wave height were carried out at 5, 15, 20, 25, 30 and 35°C, using the solution containing 0.5 m*M* nickel(II), 0.5 *M* NaSCN and 0.1 *M* Et_4NClO_4. The resultant temperature coefficients at the peak potentials of maxima A and B were

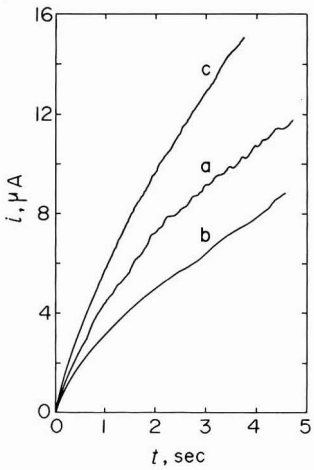

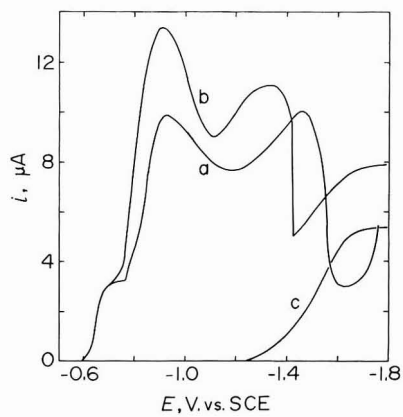

Fig. 5. Current–time curves for the reduction wave of 0.5 m*M* nickel(II) in 0.5 *M* NaSCN and 0.2 *M* Et_4NClO_4. The electrode potential is set up at (a) −0.94 V, (b) −1.20 V, (c) −1.56 V *vs.* SCE.

Fig. 6. Polarograms of 0.5 m*M* nickel(II) in 0.5 *M* NaSCN and 0.1 *M* Et_4NClO_4 solutions without (a) and with 0.45 m*M* (b) of $HClO_4$, and of 0.45 m*M* $HClO_4$ in the same electrolyte solution (c).

8.0 and 8.2% per degree, respectively. The temperature coefficient of the minimum current observed at −1.20 V *vs.* SCE was 9.2% per degree. On the other hand, the temperature coefficients of the pre- and post-waves were only 1.6 and 2.1% per degree, respectively.

The fact that maxima A and B exhibit the same temperature coefficient seems to indicate that maxima A and B might be attributed to the same reaction mechanism.

Effect of pH

The pH of the solution was changed from 4.0 to 5.9 by varying the ratio of acetic acid to sodium acetate, and from 2.5 to 3.5 by adding perchloric acid. The total acetate concentration was kept constant at 0.05 *M*. In the acetate buffer solutions, the peak potential of maximum A remained virtually unchanged, while that of maximum B shifted towards less negative potentials with decreasing pH of the solution. The effect of perchloric acid is given in Fig. 6, which shows the polarograms of nickel(II) in 0.5 *M* NaSCN and 0.1 *M* Et_4NClO_4 solution in the presence and absence of 0.45 m*M* $HClO_4$. Maxima A and B increased in height with increasing concentration of $HClO_4$. The *i*–*t* curves obtained in acidified solutions showed a well-defined profile without any irregularities, and the slopes of the log *i*–log *t* plots for maxima A and B had the value expected for a kinetically controlled electrode mechanism.

With increase in concentration of $HClO_4$, the pre-wave increased in height and the rising potential of the maximum wave A shifted towards less negative values. The pre-wave and the rising portion of maximum A observed in acidified solution have a mixed adsorption–kinetic character.

The slopes of log *i*–log *t* plots for the *i*–*t* curves obtained at −0.75 and −0.85 V *vs.* SCE in 0.5 *M* NaSCN and 0.1 *M* Et_4NClO_4 solution containing 0.5 m*M* nickel(II) and 2.34 m*M* $HClO_4$ were found to be 0.92 and 0.77, respectively.

It is known that cobalt(II) in ammoniacal solutions in the presence of some sulfur-containing organic compounds exhibits a Brdička catalytic wave[21-24], which is attributed to catalytic hydrogen evolution. To compare the present system with the Brdička mechanism, some experiments were performed with ammoniacal solutions containing ammonium hydroxide and ammonium thiocyanate. Nickel(II) in 0.5 *M* NH_4SCN solution gave an ill-defined reduction wave with a flat maximum followed by a minimum. After addition of ammonia, the reduction wave shifted towards more negative potentials as a result of the formation of nickel(II)–ammine complexes, and at the same time two maxima were observed, the first at the potential of the rising portion of the reduction wave and the second about −1.2 V *vs.* SCE (Fig. 7). With increasing pH, the height of the second maximum remained unchanged, while that of the first increased. The more positive maximum was of convective origin as shown by the stirring effect, while the more negative one was not affected by stirring. The *i–t* curves for the more negative maximum showed some irregularities towards the end of the drop life. This irregularity is due to the formation of an insoluble compound at the electrode surface. The characteristics of the second maximum are quite different from those of Brdička waves. This second maximum is observed at considerably less negative potentials than those of the Brdička waves.

Effect of surfactants

The maximum wave observed in NaSCN and Et_4NClO_4 solutions is not suppressed by the presence of small amounts of other quaternary ammonium salts such as tetra-n-butylammonium perchlorate and cetyltrimethylammonium perchlorate, but is easily suppressed by gelatin. In the presence of gelatin, not only did the heights of maxima A and B decrease, but also the corresponding *i–t* curves showed consider-

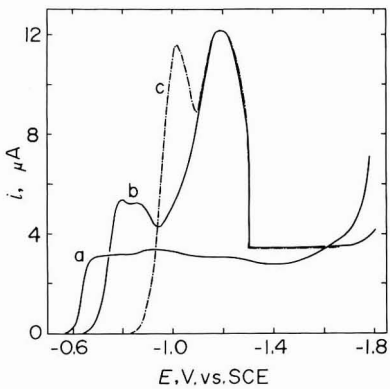

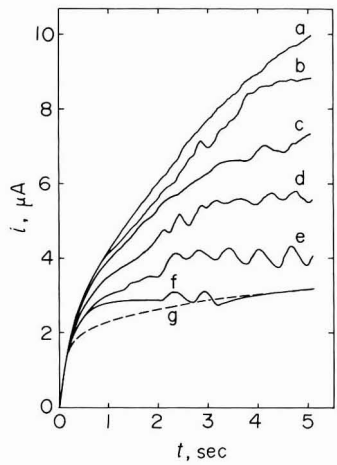

Fig. 7. Variation of the polarogram of 0.5 m*M* nickel(II) in 0.5 *M* NH_4SCN with pH: (a) 7.05, (b) 8.40, (c) 9.53.

Fig. 8. Current–time curves for the reduction wave of 0.5 m*M* nickel(II) in 0.5 *M* NaSCN and 0.1 *M* Et_4NClO_4 solutions containing various concns. of gelatin: (a) 0, (b) 0.4×10^{-3}, (c) 0.8×10^{-3}, (d) 1.2×10^{-3}, (e) 2×10^{-3}, (f) 4×10^{-3}, (g) 1×10^{-2}%. The electrode potential is set up at −0.94 V *vs.* SCE.

able irregularities which appeared as sudden increase or decrease of the current, as shown in Fig. 8, which presents the *i–t* curves for maximum A obtained in 0.5 m*M* nickel(II), 0.5 *M* NaSCN and 0.1 *M* Et_4NClO_4 solution containing various concentrations of gelatin. With further addition of gelatin above 5×10^{-3}%, the double maxima were completely eliminated and hence nickel(II) in 0.5 *M* NaSCN and 0.1 *M* Et_4NClO_4 solution exhibited a well-defined reduction wave with a small current minimum at potentials more negative than −1.0 V *vs.* SCE.

Drop time curves

Both thiocyanate ions[25,26] and tetraethylammonium ions[27] are capillary active species. In order to investigate the form of the electrocapillary curve, drop time measurements were made for 0.5 *M* NaSCN solution with and without Et_4NClO_4 present. The resultant curves are shown in Fig. 9. Tetraethylammonium ions in a 0.5 *M* NaSCN solution displaced the e.c.m. towards less negative potentials and adsorbed on the mercury surface to appreciable potentials. The complete desorption of tetraethylammonium ions in 0.5 *M* NaSCN solution occurred at −0.15 and −1.80 V *vs.* SCE, from which the drop time curves observed in the presence and absence of 0.1 *M* Et_4NClO_4 coincided. The drop time curve for a 0.1 *M* Et_4NClO_4 solution was also plotted in the same Figure. The e.c.m. in 0.1 *M* Et_4NClO_4 solution was observed at −0.38 V *vs.* SCE. The solution containing NaSCN and Et_4NClO_4 decreased the drop time to appreciable extent in the potential region of the e.c.m. and also tetraethylammonium ions were adsorbed preferentially at mercury at potentials more negative than the e.c.m.

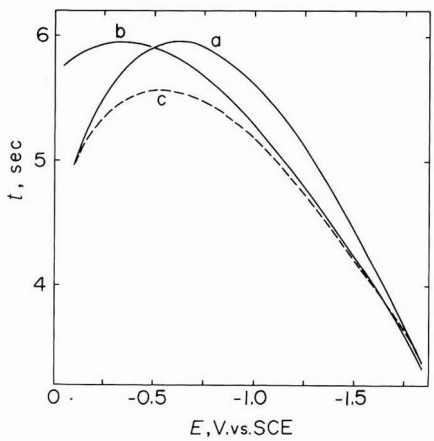

Fig. 9. Drop time curve in (a) 0.5 *M* NaSCN, (b) 0.1 *M* Et_4NClO_4, (c) 0.5 *M* NaSCN and 0.1 *M* Et_4NClO_4.

The adsorption of some metal ions from an aqueous thiocyanate solution at mercury has been observed by several investigators[28–31]. Although specific adsorption of nickel(II) was not observed in thiocyanate solution, as pointed out by O'Dom and Murray[30], nickel(II) in thiocyanate solutions containing Et_4NClO_4 was adsorbed at mercury. It was found that nickel(II) was adsorbed from thiocyanate solution containing tetraethylammonium ions at potentials less negative than about −0.6 V *vs.* SCE. The adsorption of nickel(II) from NaSCN and Et_4NClO_4 solution was also

supported by the a.c. polarographic measurements.

Apparently, maxima A and B are observed in the potential region where tetraethylammonium ions are preferentially adsorbed at mercury.

A.c. polarography

It is known that the a.c. polarogram of nickel(II) in thiocyanate solution exhibits a negative admittance in the potential region where the minimum appears on the d.c. polarogram[17,18]. Figure 10 shows the a.c. polarogram of nickel(II) in 0.5 *M* NaSCN and 0.1 *M* Et_4NClO_4 solution.

Tetraethylammonium ions in 0.5 *M* NaSCN solution exhibited a negative tensammetric wave with a peak potential at −1.81 V *vs.* SCE. In the absence of thiocyanate ions, the solution of 0.1 *M* Et_4NClO_4 did not exhibit a tensammetric wave. When nickel(II) was present in 0.5 *M* NaSCN and 0.1 *M* Et_4NClO_4 solution, a capacity peak was also observed at about −0.40 V *vs.* SCE. With increase in concentration of nickel(II), the capacity peak gradually increased in height and the peak potential shifted slightly towards more negative values. This means that the capacity peak is due to the specific adsorption of nickel(II)–thiocyanate complexes. The negative and positive faradaic admittances were observed at potentials more negative than the half-wave potential of the corresponding d.c. polarogram. With increase in concentration of Et_4NClO_4, the peak potential of the negative admittance shifted anodically, while that of the positive admittance shifted cathodically and coincided with the peak potential of maximum B of the corresponding d.c. polarogram. The negative admittance was observed in the potential region where the current of maximum A began to decrease; however, the current was large compared to the diffusion current of nickel(II). The negative admittance followed by the positive admittance reflects the unique mechanism of the electrode reaction of nickel(II) at the electrode surface in NaSCN and Et_4NClO_4 solution.

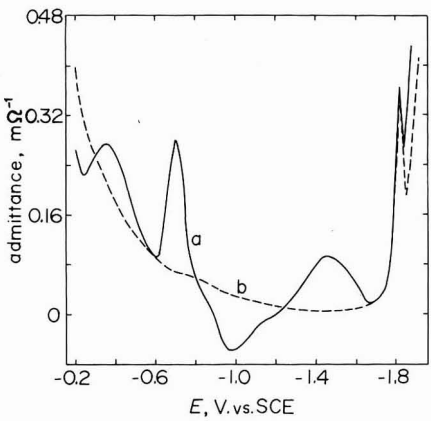

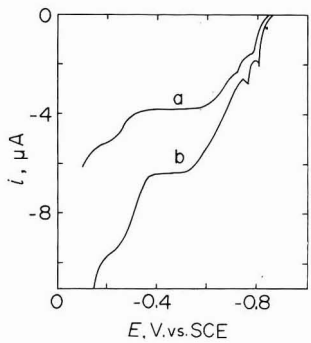

Fig. 10. Alternating current polarogram of (a) 1 m*M* nickel(II) in 0.5 *M* NaSCN and 0.1 *M* Et_4NClO_4, and (b) 0.5 *M* NaSCN and 0.1 *M* Et_4NClO_4.

Fig. 11. Polarograms in 0.5 *M* NaOH solutions containing (a) gases obtained by the controlled potential electrolysis, and (b) 0.6 m*M* Na_2S and 0.6 m*M* NaCN.

Controlled potential electrolysis

Controlled potential electrolysis with a mercury pool electrode as working electrode was used in order to identify the reaction products for the electrode reaction of nickel(II) in thiocyanate solutions with and without Et_4NClO_4 present. Electrolysis was performed with the solution containing 2.5 m*M* nickel(II), 0.5 *M* NaSCN and 0.1 *M* Et_4NClO_4. With electrode potential controlled at -0.90, -1.20 or -1.45 V *vs.* SCE, respectively, the surface of the mercury pool was covered with a black compound. However, no bubbles of gas could be seen during the course of the electrolysis. The black compound was washed several times with water and then with ethanol. When the compound was dissolved into a 5 *M* H_2SO_4 solution, bubbles of gas were observed. The qualitative analysis of the gas was carried out polarographically by dissolving the gas in 0.5 *M* NaOH solution. The solution gave an ill-defined anodic wave with a half-wave potential of about -0.78 V *vs.* SCE. Sulphide ions in 0.5 *M* NaOH solution exhibit an anodic wave with the half-wave potential of -0.75 V *vs.* SCE. Evaporation of the sulfuric acid solution gave a residue which was blue and turned red on treatment with a solution of dimethylglyoxime. Hence, it follows that the black compound is nickel sulphide.

When controlled potential electrolysis was performed with an acid solution containing 2.5 m*M* nickel(II), 0.5 *M* NaSCN, 0.1 *M* Et_4NClO_4 and 10 m*M* $HClO_4$ at -0.90 V *vs.* SCE, bubbles of gas appeared during the electrolysis, and nickel sulphide was not produced. These bubbles which were dissolved in 0.5 *M* NaOH solution exhibited a double anodic wave, as shown by curve a in Fig. 11. Curve b in the same Figure shows the anodic wave for the solution containing NaCN and Na_2S at equal concentrations.

The first and second waves are thus caused by reactions (1) and (2), respectively.

$$Hg + S^{2-} \rightleftharpoons HgS + 2\,e \quad (1)$$

$$Hg + 2\,CN^- \rightleftharpoons Hg(CN)_2 + 2\,e \quad (2)$$

Consequently, it follows that the bubbles of gas obtained from acidified solution are hydrogen sulphide and hydrogen cyanide.

Electrolysis was also performed with a solution containing 2.5 m*M* nickel(II) and 0.5 *M* NaSCN. At -0.80, -1.20 or -1.50 V *vs.* SCE, respectively, the mercury surface was covered with small amounts of nickel sulphide.

Shirai[32] has also shown that nickel sulphide is formed by electrolyzing a thiocyanate solution of nickel(II) at a hanging mercury electrode.

In the absence of Et_4NClO_4, nickel sulphide can be produced under certain conditions. This has been observed, for example, with large nickel(II) concentrations and relatively long periods of electrolysis. The above results suggest that maxima A and B observed in NaSCN and Et_4NClO_4 solutions are not due to hydrogen evolution, but are related to the reduction of thiocyanate ions.

DISCUSSION

Hydrated nickel(II) in 0.1 *M* Et_4NClO_4 solution is reduced with a much greater overvoltage than in sodium perchlorate at the same concentration. This effect can be explained by a double layer effect since tetraethylammonium ions are adsorbed on mercury, as shown in Fig. 9.

When thiocyanate ions are present, nickel(II) forms complexes with them which are reduced at a much smaller overvoltage. When the thiocyanate concentration exceeds 0.1 *M*, nickel(II) yields three thiocyanate complexes, $NiNCS^+$, $Ni(NCS)_2$ and $Ni(NCS)_3^-$.

Galus and Jeftic[16] have reported that at low thiocyanate concentrations nickel(II) exhibits three waves corresponding to the reduction of $Ni(NCS)_3^-$, $NiNCS^+$ and the hydrated nickel(II). They proposed that the first wave observed at the most positive potential was due to the reduction of $Ni(NCS)_3^-$.

Nickel(II) in thiocyanate solution containing tetraethylammonium ions exhibits a characteristic maximum wave in the potential region where the nickel(II) reduction wave obtained in thiocyanate solution reaches its limiting plateau.

The peak potential and the peak current of the maximum wave are dependent on the concentrations of nickel(II), NaSCN and Et_4NClO_4. Usually, the maximum wave separates into two maxima denoted as the maxima A and B, from positive to negative potentials.

Under conditions for which the maxima A and B are large compared to the nickel(II) reduction wave obtained in thiocyanate solution without Et_4NClO_4, the investigation of the *i–t* curves and of the effect of height of mercury column on maxima A and B indicates that the mechanism of the double maxima is kinetic in nature and involves a chemical reaction which follows the electron transfer step. The temperature coefficients of the peak currents suggest also the kinetic nature of the maximum wave. The peak morphology of the catalytic current could be the result of a slight convective maximum, or it could indicate that the electrode mechanism involves some adsorbed species. Mairanovskii[22] has shown that catalytic reactions involving adsorbed species may exhibit a peak current.

Although the profile of maxima A and B resembles that of a Brdička catalytic wave, the catalytic wave of nickel(II) obtained in NaSCN and Et_4NClO_4 solution is not caused by catalytic hydrogen evolution.

Controlled potential electrolysis shows that nickel sulphide is precipitated in a neutral thiocyanate solution, and that hydrogen sulphide and hydrogen cyanide are formed in acid solutions. These results suggest that in the presence of nickel(II) and Et_4NClO_4 thiocyanate ion is reduced to cyanide and sulphide ions. The catalytic maximum wave is observed at potentials at which the reduction of nickel(II)–thiocyanate complexes already occurs. It is reasonable to assume that the primary product of the electrode reaction is metallic nickel or a zerovalent nickel compound, $Ni(NCS)_n^{n-}$, which is unstable and quickly decomposes to metallic nickel and thiocyanate ions. At the same time, the metallic nickel is also unstable and quickly amalgamates.

It is known that the amalgamation of the deposited iron-group metals is inhibited under certain conditions.

Such a behavior has been observed on the reduction of divalent iron-group metal ions in concentrated chloride solution containing small amounts of tetra-n-butylammonium ions[33], on the reduction of cobalt(II) in thiocyanate solutions with[34] and without[35] several surface-active substances, and on the reduction of cobalt(II) in acid solution containing cysteine-like compounds[36]. These metal ions in the above-stated solutions exhibit a catalytic maximum wave, which has been explained by the catalytic reduction of hydrogen ions or water molecules on the deposited metal since the hydrogen overvoltage on the metal is much less than on mercury.

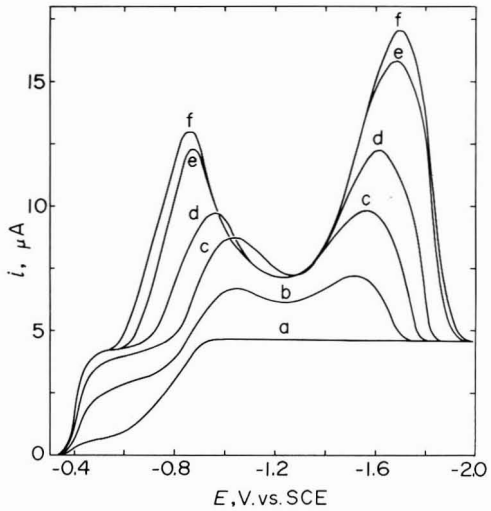

Fig. 12. Polarograms of 0.5 mM nickel(II) in acetonitrile solutions containing 0.1 M Et_4NClO_4 and various concns. of LiSCN: (a) 0, (b) 0.05 mM, (c) 0.1 mM, (d) 0.2 mM, (e) 0.5 mM (f) 1.0 mM.

In the present system, the neutral thiocyanate solution of nickel(II) did not give any bubbles of gas during the electrolysis time at a mercury pool electrode. One would expect that the catalytic maximum wave is not due to the catalytic hydrogen evolution, but to the catalytic reduction of thiocyanate ions. If the catalytic wave corresponds to the reduction of thiocyanate ions, a similar catalytic wave would be observed in some aprotic non-aqueous solvents. Some experiments were carried out in an acetonitrile medium. Figure 12 shows the d.c. polarograms of nickel(II) in acetonitrile solution containing 0.1 M Et_4NClO_4 and various amounts of LiSCN. In the absence of LiSCN, nickel(II) in a 0.1 M Et_4NClO_4 solution exhibits a two-step reduction wave[19]. With small amounts of LiSCN present, both waves increased in height with increase in concentration of LiSCN, and at the same time two maxima were observed. With further addition of LiSCN above 0.2 mM, the more positive maximum wave shifted anodically, while the more negative maximum wave shifted cathodically, and two maxima increased in height with the thiocyanate concentration up to about 1 mM. When the thiocyanate concentration exceeded 0.5 mM, the peak currents of the double maxima were independent of the height of the mercury column, and the slope of the log i–log t plot for the peak currents had a value of 0.65 ± 0.02. This implies that the reaction mechanism of the double maxima obtained in acetonitrile is kinetic in nature.

The catalytic maximum wave of nickel(II) is observed in the acetonitrile medium as well as in other nitrile solvents[37]. These findings can be accounted for using the following sequence of reactions.

$$\mathrm{Ni(II)} + n\ \mathrm{NCS^-} \underset{\text{rapid}}{\overset{K_{st}}{\rightleftharpoons}} \{\mathrm{Ni(NCS)}_n^{(2-n)+}\}_{\text{bulk}} \underset{\text{rapid}}{\overset{K_{ads}}{\rightleftharpoons}} \{\mathrm{Ni(NCS)}_n^{(2-n)+}\}_{\text{ads}}$$

$$\{\mathrm{Ni(NCS)}_n^{(2-n)+}\}_{\text{ads}} + 2\,e \xrightarrow[\text{fast}]{} \mathrm{Ni(0)metal} + n\ \mathrm{NCS^-_{ads}}$$

$$\mathrm{Ni(0)metal} + \mathrm{NCS^-_{ads}} \xrightarrow[\text{slow}]{k} \mathrm{Ni(II)} + \mathrm{CN^-} + \mathrm{S^{2-}} \tag{5}$$

where k is the rate constant for the reaction of the deposited metallic nickel with the adsorbed thiocyanate ion, K_{st} the effective stability constant of the nickel(II)–thiocyanate complex in the bulk of solution, and K_{ads} the adsorption equilibrium constant of the complex. The cyclic regeneration of nickel(II) accounts for the catalytic process. The kinetic property of the maximum wave observed in aqueous solution where the concentration of thiocyanate ion is in large excess compared to that of nickel(II) might be explained by considering the decomposition reaction as reaction (6) instead of reaction (5),

$$\mathrm{NCS^-_{ads}} + 2\,e \rightarrow \mathrm{CN^-} + \mathrm{S^{2-}} \tag{6}$$

Reaction (6) means that adsorbed thiocyanate ion is reduced at the deposited nickel acting as the working electrode. However, reaction (6) may not be applicable to the catalytic maximum wave observed in acetonitrile solution. It should be noted that the height of the maximum wave of nickel(II) observed in acetonitrile solution is larger than the diffusion controlled current to be expected if thiocyanate ion is 100% associated in a 1 : 1 ratio with nickel(II) and is reduced at the deposited metallic nickel. Hence, it is reasonable to assume that nickel(II) is regenerated by reaction (5).

The drop time curves and a.c. polarograms suggest the adsorption of nickel(II)–thiocyanate complexes at mercury in NaSCN and Et_4NClO_4 solution. The i–t curves for the pre-wave and the rising portion of maximum A observed in acidified thiocyanate solution show that the exponents of the i–t curves are well beyond the value of 0.67 expected for a purely kinetically-controlled electrode mechanism. This result also provides evidence of the adsorption of thiocyanate complexes.

The adsorption of tetraethylammonium ions at mercury seems to play an essential role on the catalytic wave of nickel(II) in thiocyanate solution. The catalytic wave is observed in the potential region where tetraethylammonium ions are strongly adsorbed at the mercury electrode.

It is plausible to assume that the overall reduction process of nickel(II)–thiocyanate complexes consists of two simultaneous parallel reactions, one of which proceeds at the naked part of the electrode and the other at the part of the electrode covered with adsorbed tetraethylammonium ions. When the reduction of thiocyanate complexes takes place on the covered surface, the amalgamation of the electroreduced metallic nickel is inhibited and the deposit remains on the surface of the mercury electrode. If the electroreduced metallic nickel is an active species, it could react with thiocyanate ion. At potentials more negative than the peak potential of maximum B, the catalytic current decreases as a result of decreasing adsorption of tetraethylammonium ions and hence of decreasing concentration of the active superficial metallic nickel.

The catalytic reaction is enhanced by the adsorption of tetraethylammonium ions, but is retarded by the presence of gelatin, which is less surface active than tetraethylammonium ions. Inhibition of the catalytic reaction was also observed in the presence of oxygen. With a trace of oxygen present, not only did the height of the maximum wave decrease, but also the i–t curves for the maximum wave exhibited irregularities similar to those observed in the presence of gelatin.This retardation by

gelatin and oxygen could be the result of a deactivation of the active nickel deposit.

Nickel(II) regenerated by reaction (5) or diffusing to the electrode may react with the reduction products of the thiocyanate ion. The irregularities of the *i–t* curves for the catalytic maximum wave obtained in both neutral and ammoniacal thiocyanate solutions suggest that the formation of insoluble nickel sulphide occurs at the electrode surface. The formation of nickel sulphide tends to decrease the height of the catalytic wave. With decreasing pH, the catalytic maximum wave increases and also the *i–t* curves exhibit a well-defined shape without any irregularities. This means that nickel sulphide is not formed at the electrode surface in acid solutions.

On the other hand, if $Ni(CN)_4^{2-}$ ions are formed in the vicinity of the electrode, they are reduced at potentials more negative than -1.4 V *vs.* SCE, in 0.5 *M* NaSCN and 0.1 *M* Et_4NClO_4 solution. When the mole ratio of cyanide ion to nickel(II) exceeded four in 0.5 *M* NaSCN and 0.1 *M* Et_4NClO_4 solution, the catalytic maximum wave disappeared completely and nickel(II) gave an irreversible wave corresponding to the reduction of cyanide complex with a half-wave potential of about -1.50 V *vs.* SCE. It is known[38–40] that nickel(II) in cyanide solution forms the stable complex, $Ni(CN)_4^{2-}$, which is essentially the only complex present even when the total concentration of cyanide ions is lower than its stoichiometric value. Kolski and Margerum[41] have shown that intermediate species such as $NiCN^+$, $Ni(CN)_2$, and $Ni(CN)_3^-$ are not involved in the kinetics of formation and dissociation of $Ni(CN)_4^{2-}$ ions. If intermediate species of cyanide complexes were formed in the vicinity of the electrode, they should be reduced at potentials less negative than -1.4 V *vs.* SCE.

No attempt has been made to discuss separately the reaction mechanism of the two catalytic maxima A and B , although the peak potentials and peak heights of maxima A and B are dependent on the concentrations of NaSCN and Et_4NClO_4.

These results may be related qualitatively to the fact that the surface coverage of thiocyanate and tetraethylammonium ions, the activity of the electroreduced metallic nickel, the electroactive species of nickel(II) regenerated by reaction (5), etc. are dependent on the electrode potential.

This aspect of the problem remains to be investigated in more detail.

ACKNOWLEDGEMENT

The authors thank the Ministry of Education for the financial support.

SUMMARY

In aqueous thiocyanate solution containing tetraethylammonium ions nickel(II) gave a catalytic polarographic current which appears as a maximum wave in the potential region where the reduction wave of nickel(II) in thiocyanate solution reaches its limiting plateau. The characteristics of this catalytic wave have been investigated by d.c. polarography,*i–t* curve analysis, a.c. polarography and controlled potential electrolysis method. The catalytic current has been studied as a function of concentration of nickel(II), NaSCN, and Et_4NClO_4. The effect of mercury height, stirring, pH, surfactant, and temperature on the catalytic wave has been described. The controlled potential electrolysis for the nickel(II)–thiocyanate system indicated that the thiocyanate ion is reduced to cyanide and sulphide ions. A mechanism which involves

a rapid adsorption equilibrium between the bulk and adsorbed nickel(II)–thiocyanate complexes and the catalytic reduction of thiocyanate ion with the electroreduced active metallic nickel has been proposed. The role of tetraethylammonium ions on the catalytic wave is also discussed.

REFERENCES

1 YA. I. TUR'YAN AND G. F. SEROVA, *Zh. Fiz. Khim.*, 31 (1957) 1976, 2200.
2 H. B. MARK, JR. AND C. N. REILLEY, *Anal. Chem.*, 35 (1963) 195; *J. Electroanal. Chem.*, 4 (1962) 189.
3 W. KEMULA, LJ. JEFTIC AND Z. GALUS, *J. Electroanal. Chem.*, 10 (1965) 387.
4 YA. I. TUR'YAN AND O. N. MALYAVINSKAYA, *J. Electroanal. Chem.*, 23 (1969) 69.
5 H. B. MARK, JR., *J. Electroanal. Chem.*, 7 (1964) 276.
6 H. B. MARK, JR. AND L. R. MCCOY, *Rev. Polarog. (Kyoto)*, 14 (1967) 122.
7 H. B. MARK, JR., L. R. MCCOY, E. KIROWA-EISNER AND H. C. MACDONALD, JR., *J. Phys. Chem.*, 72 (1968) 1083.
8 L. R. MCCOY, H. B. MARK, JR. AND L. GIERST, *J. Phys. Chem.*, 72 (1968) 4637.
9 L. R. MCCOY AND H. B. MARK, JR., *J. Phys. Chem.*, 73 (1969) 953, 2764.
10 H. B. MARK, JR., *J. Electroanal. Chem.*, 8 (1964) 253.
11 YA. I. TUR'YAN AND O. E. RUVINSKII, *J. Electroanal. Chem.*, 23 (1969) 61.
12 A. A. VLČEK, *Z. Elektrochem.*, 61 (1957) 1014.
13 N. TANAKA, R. TAMAMUSHI AND M. KODAMA, *Bull. Chem. Soc. Japan*, 33 (1960) 14.
14 YA. I. TUR'YAN AND G. F. SEROVA, *Zh. Fiz. Khim.*, 34 (1960) 1009.
15 YA. I. TUR'YAN, *Dokl. Akad. Nauk SSSR*, 140 (1961) 416.
16 Z. GALUS AND LJ. JEFTIC, *J. Electroanal. Chem.*, 14 (1967) 415.
17 H. SHIRAI, *J. Chem. Soc. Japan, Pure Chem. Sect. (Nippon Kagaku Zasshi)*, 81 (1960) 1248.
18 R. TAMAMUSHI AND K. MATSUDA, *J. Electroanal. Chem.*, 12 (1966) 436.
19 E. ITABASHI AND S. IKEDA, *J. Electroanal. Chem.*, in press.
20 E. ITABASHI AND S. IKEDA, *Bull. Chem. Soc. Japan*, 42 (1969) 1901.
21 R. BŘEZINA AND P. ZUMAN, *Polarography in Medicine, Biochemistry and Pharmacy*, Interscience, New York, 1958, p. 585.
22 S. G. MAIRANOVSKII, *J. Electroanal. Chem.*, 6 (1963) 77.
23 R. BRDIČKA, M. BŘEZINA AND V. KALOUS, *Talanta*, 12 (1965) 1149.
24 A. CĂLUSARU, *J. Electroanal. Chem.*, 15 (1967) 269.
25 N. TANAKA, T. TAKEUCHI AND R. TAMAMUSHI, *J. Chem. Soc. Japan, Pure Chem. Sect. (Nippon Kagaku Zasshi)*, 85 (1964) 846.
26 S. MINC AND J. ANDRZEJCZAK, *J. Electroanal. Chem.*, 17 (1968) 101.
27 M. A. V. DEVANATHAN AND M. J. FERNANDO, *Trans. Faraday Soc.*, 58 (1962) 368.
28 E. D. MOORHEAD, *Anal. Chem.*, 38 (1966) 1796.
29 F. C. ANSON AND D. J. BARCLAY, *Anal. Chem.*, 40 (1968) 1791.
30 G. W. O'DOM AND R. W. MURRAY, *J. Electroanal. Chem.*, 16 (1968) 327.
31 G. LAUER AND R. A. OSTERYOUNG, *Anal. Chem.*, 41 (1969) 1882.
32 H. SHIRAI, *J. Chem. Soc. Japan, Pure Chem. Sect. (Nippon Kagaku Zasshi)*, 85 (1964) 322.
33 V. F. IVANOV AND Z. A. IOFA, *Russ. J. Phys. Chem. English Transl.*, 36 (1962) 571; 38 (1964) 1026.
34 M. SHINAGAWA, H. NEZU, H. SUNAHARA, F. NAKASHIMA, H. OKASHITA AND T. YAMADA, *Advances in Polarography*, Vol. 3, Pergamon Press, Oxford, 1960, p. 1142.
35 S. P. PERONE AND W. F. GUTKNECHT, *Anal. Chem.*, 39 (1967) 892.
36 I. M. KOLTHOFF AND P. MADER, *Anal. Chem.*, 41 (1969) 924.
37 E. ITABASHI, *Doctoral Thesis*, Osaka University, 1969.
38 A. A. VLČEK, *Collection Czech. Chem. Commun.*, 22 (1957) 948.
39 H. FREUND AND C. R. SCHNEIDER, *J. Am. Chem. Soc.*, 81 (1959) 4780.
40 A. L. VAN GEET AND D. N. HUME, *Inorg. Chem.*, 3 (1964) 523.
41 G. B. KOLSKI AND D. W. MARGERUM, *Inorg. Chem.*, 7 (1968) 2239.

ELECTROANALYTICAL CHEMISTRY AND INTERFACIAL ELECTROCHEMISTRY
Elsevier Sequoia S.A., Lausanne – Printed in The Netherlands

ADSORPTION OF POTENTIAL-DETERMINING IONS AT THE ALUMINIUM OXIDE–AQUEOUS INTERFACE AND THE POINT OF ZERO CHARGE

H. SADEK, A. K. HELMY*, V. M. SABET AND TH. F. TADROS
Faculty of Science, Alexandria University, Alexandria (U.A.R.)
(Received December 13th, 1969; in revised form April 10th, 1970)

Insoluble oxide particles immersed in aqueous electrolytes usually develop surface charges by adsorption or desorption of potential-determining ions[1]. Within certain pH limits that depend on the oxide, H^+ and OH^- ions could be considered as the only potential-determining ions present in the system. The surface reactions which are involved in the establishment of the surface charge may be represented by schemes (a) and (b):

$$M(OH)_z(\text{surface}) + zH_3O^+ = M(OH)_z^+ + zH_2O \quad (a)$$

$$M(OH)_z(\text{surface}) + zH_2O = M(O_2)_{z/2}^{z-} + zH_3O^+ \quad (b)$$

By definition, the potential-determining ions are the ionic species constituting the lattice of the oxide (M^{z+} and O^{2-}), and H^+ and OH^- ions which are in equilibrium with them at a given pH.

Independent of the particular oxide to be used, the special role played by H^+ and OH^- ions can be readily observed by direct measurements using the potentiometric technique. This procedure was successfully applied by Parks and de Bruyn[1] and Quirk and coworkers[2] in the case of Fe_2O_3. Similar determinations were reported for Al_2O_3 by Yopps and Fuerstenau[3].

The experimental measurement of the oxide surface charge is obtained through titration of the oxide in the presence of an indifferent supporting electrolyte. In this case, the adsorbed potential-determining ions are assigned to the solid side of the interface[1], *i.e.*, the only counterions present in the system are those from the indifferent electrolyte.

Under these conditions σ is given by de Bruyn and Agar[4]

$$\sigma = (F/A)(\Gamma_{H^+} - \Gamma_{OH^-}) \quad (1)$$

where σ is a surface excess charge/cm^2, F is the Faraday constant and A is the surface area in cm^2/g. The excess of one species over the other can be directly determined as the difference between the total acid added (or base) and the equilibrium H^+ (or OH^-) ion concentration. It must, however, be clear that actually not all H^+ or OH^- are adsorbed or desorbed. This is simply because adsorption of H^+ ion or desorption of OH^- ion leaves the surface with an excess of a positive charge, and *vice versa*, for a negatively charged surface.

* Faculty of agriculture, Alexandria University.

The point of zero charge (p.z.c.) can, thus, be evaluated from the adsorption isotherms when the net surface charge density attains a zero value at a characteristic pH.

The potential difference, ψ, across the ionic double layer at the oxide–electrolyte interface, can be related to the concentration (or activity) of potential-determining ions by the equation:

$$\psi = (RT/F)\ln(a_{H^+}/a^0_{H^+}) \tag{2}$$

where a_{H^+} and $a^0_{H^+}$ refer to the ion activity of the solution and of the p.z.c., respectively.

The differential capacity, defined by the relation

$$C = d\sigma/d\psi \tag{3}$$

gives more information on the structure of the ionic double layer. In this expression the Nernst equation (eqn. (2)) relating the double layer potential to the activity of the potential-determining ions in the solution phase is assumed to be valid.

In the present paper, potentiometric titrations of aluminium oxide are reported to yield information on the p.z.c. and the surface reactions involved. The electrical conductance and migration of Al_2O_3 particles in several electrolytes are also reported.

EXPERIMENTAL MATERIALS AND METHODS

Al_2O_3 for chromatography (Veb Lab. Apolda), was not subjected to any further treatment. Microscopic examination shows that the diameter of the particles ranges from 2 to 5 μ. The surface area from the BET measurement was found to be 67.3 $m^2\ g^{-1}$.

The method used to determine the adsorption densities Γ_{H^+} and Γ_{OH^-} was essentially that of Parks and de Bruyn[1]. Titration data were obtained using a Pye pH meter with glass and silver–silver chloride electrodes. Two grams each, of Al_2O_3 in 200 ml of KCl solution were stirred with a magnetic stirrer and titrated with 0.1 *N* HNO_3 or 0.1 *N* KOH. Potassium chloride from 1 to 0.0001 *M* was used as the supporting electrolyte. Blank titrations were carried out similarly using 200 ml of the appropriate KCl solution. Loss of H^+ or OH^- ions by the oxide at $25° \pm 2°C$ was found by taking the difference in concentration of potential-determining ion between test suspension and blank titration. Addition of titrant did not exceed 4 ml in the pH range 3–10, so that the ionic strengths were assumed to be constant except at low ionic strengths. After each addition of the titrant, the solutions were left to equilibrate for 30 min with continuous stirring, and the pH and the e.m.f. were recorded. The uncertainty in pH measurements was ± 0.05 unit, although absolute errors were greater at extreme pH values. Attainment of equilibrium in reactions at hydrated solid surfaces is often difficult to establish. After the initially rapid adsorption (H^+ or OH^- ions) the oxide surface may continue to adsorb ions very slowly. The slow H^+ transfer has been attributed by Onoda and de Bruyn[5] to extension of the proton-excess charge into hydrated surface layers of the oxide, and by Quirk *et al.*[2] to the structural rearrangement of the surface. The slow H^+ transfer may involve reactions different in nature from the initial rapid H^+ transfer occurring when the pH is changed, and accordingly only the initial fast reaction at the phase boundary is considered in this study.

A Pye conductance bridge (model 11700) was used to measure the conductance

of the solutions at 3000 Hz. All measurements were carried in an air thermostat at $30° \pm 0.1°C$.

The cell constant of the dipping cell was measured using A.R. KCl solutions whose conductance was given by Shedlovsky *et al.*[6]. The cell constant was found to be 0.529 ± 0.002 cm^{-1}.

To each 1 g Al_2O_3, 100 ml of HCl, NaOH, NaCl or K_2SO_4 solutions of concentrations varying from 0.15 to 0.001 N were added. The mixtures were stirred and left for 72 h before the conductance was determined for the suspensions and the equilibrium solutions free from oxide particles.

For the determination of electrophoretic mobility a modified Burton tube was used[7]. The main feature of the apparatus is a Pyrex U-tube of 1 cm diameter. The electrodes are made of carbon and dipped in saturated KCl and connected to the side arms through agar gel links. The potential electrodes are small platinum wires fixed just below the connections to the side arms. A known potential (70 V) from an accumulator was applied across the platinum electrodes and the potential in the tubes was adjusted to be equal to this by varying the voltage between the carbon electrodes. The potential across the side arms had to be adjusted every 3 min to keep the potential gradient constant across the main tube. One hour experiments were made. The ζ-potential of particles in the different solutions was calculated at 20°C using the equation:

$$\zeta = 6\pi\eta u/HD = 21592\, u/H$$

where $\eta = 0.01$ P, $D = 78.6$, u is the migration velocity (cm s^{-1}) and H is the potential difference.

RESULTS AND DISCUSSION

I. Potentiometric measurements

The titration curves of Al_2O_3 are shown in Fig. 1. They may be regarded as adsorption isotherms for H^+ and OH^- ions by the use of the approximations

$$\sigma A = F(\Gamma_{H^+} - \Gamma_{OH^-}) \simeq F\Gamma_{H^+} \quad \text{(on the acid side of the p.z.c.)}$$

$$\sigma A = F(\Gamma_{OH^-} - \Gamma_{H^+}) \simeq F\Gamma_{OH^-} \quad \text{(on the alkaline side of the p.z.c.)}$$

Positive charges on the surface are thus considered to be due entirely to excess of adsorbed H^+ ions with respect to the p.z.c. Negative charges are considered to arise entirely from the removal of positive charges from the surface. At the p.z.c. the net charge is zero.

From Fig. 1, one can conclude that H^+ and OH^- ions are potential-determining ions for Al_2O_3 and that KCl acts as an indifferent electrolyte. The best value of the p.z.c. as determined by the intersection of the adsorption curves is at pH 8.9. A small shift in the intersection of the curves was observed towards the alkaline side at higher ionic strengths, and towards the acid side at lower ionic strengths. The maximum spread observed in each case did not exceed 0.3 pH unit. A similar behaviour was observed in the case of Fe_2O_3[1].

For the acid side of the p.z.c., using the double layer model, Quirk *et al.*[2] derived the equation:

$$\log \Gamma_H + \tfrac{1}{2}\,\mathrm{pH} = \log k_H V_H + \tfrac{1}{2} \log [\mathrm{Cl}] - K_1 \Gamma_H / 2.303 \qquad (4)$$

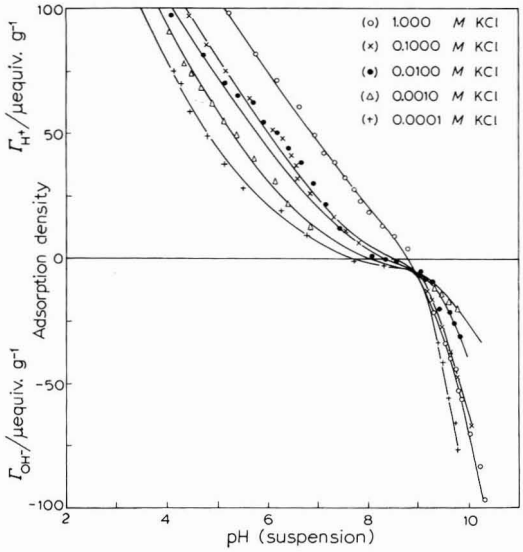

Fig. 1. Adsorption isotherms.

For the alkaline side of the p.z.c. they derived the equation

$$\log \Gamma_{OH} - \tfrac{1}{2}\,\mathrm{pH} = \tfrac{1}{2}\log K_w - \log k_{OH} V_{OH} \quad \tfrac{1}{2}\log [K] - K_2 \Gamma_{OH}/2.303 \qquad (5)$$

where $k_H = \exp\{-(\Delta\mu_H + \Delta\mu_{Cl})/2\,RT\}$, μ is the chemical potential, V_H the maximum number of sites available for H^+ ion, and K_1 and K_2 are interaction constants.

Equations (4) and (5) are tested in Figs. 2 and 3. The slopes of the plots of the left-hand side against Γ_H (eqn. (4)) or Γ_{OH} are 0.022 and 0.0037 μ equiv. g^{-1} respectively. Assuming a constant capacity of the electric double layer they obtained the relation:

$$K_1 = 4\pi F\delta/2\,RTD'A = 2.16 \times 10^5 \delta/D'A \qquad (6)$$

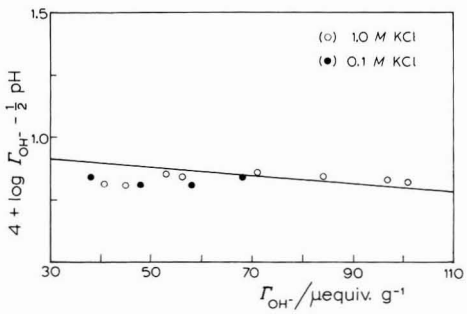

Fig. 2. Test of eqn. (4).

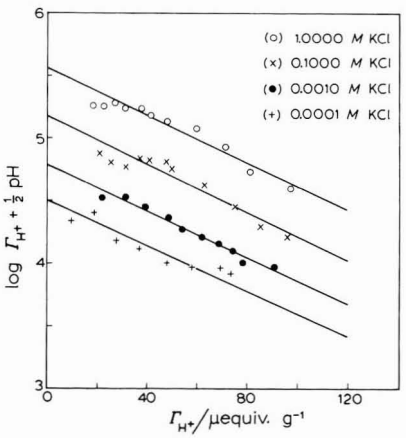

Fig. 3. Test of eqn. (5).

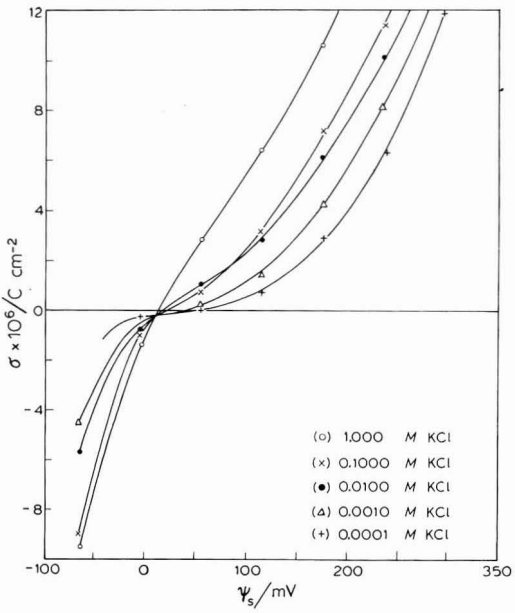

Fig. 4. Charge density–surface potential relationship.

where A is the surface area in $cm^2\ g^{-1}$ and δ, (in Å) is the average distance in the direction normal to the surface plane between the plane of the surface charge and the plane of average approach of the centers of solvated counterions. Since the values of δ and D' are not known, they were assumed to be $\delta = 0.5$ Å and $D' = 6$ for water at dielectric saturation. Thus $K_1 = 0.026$ for Al_2O_3 which is in fair agreement with the experimental value 0.022.

The chosen value of δ is probably too small and should not be considered constant, since the double layer capacity, as will be shown below, is a function of the electrolyte concentration, as is evident from the gradual change of the slopes of the lines in Fig. 4 with change in pH.

1. *The surface potential and capacity.* For any oxide surface, H^+ ion is potential-determining and it may be assumed that the potential with respect to the p.z.c. is given by eqn. (2). This assumes that the χ-potential does not change when the composition of the solution is not changed too drastically.

Figure 4 shows the plot of σ *vs.* ψ and Fig. 5 the differential capacity of the double layer plots *vs.* ψ. The differential capacity of the double layer has a minimum value around +60 mV and a maximum displaced towards the negative side of the p.z.c. Both the minimum and the maximum are indications of the presence of a diffuse double layer at these points, and high capacities are usually interpreted as indications of a Gouy double layer.

The capacity is much greater on the negative than on the positive side of the p.z.c. This indicates that on the positive side there is specific adsorption of chloride, but no specific adsorption of K^+ ion could take place at the negative side. Also specific adsorption of chloride is higher the higher the Cl^- ion concentration, as indicated by the fact that the maximum capacity is lower at lower Cl^- ion concentrations. General-

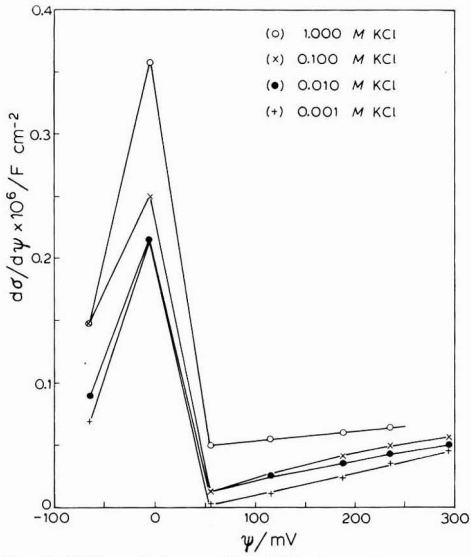

Fig. 5. Differential capacity of Al_2O_3 surface.

ly, the capacity is found to increase with increase in electrolyte concentration. This is normal behaviour according to any model of the double layer theory.

There are many similarities between the capacity of Al_2O_3 double layer and that of mercury in KCl solutions[9]. In mercury the maximum capacity occurs around the i.e.p.; this is not explained by the Stern theory but may be explained by the Bikerman theory[10] which at lower potentials gives an effect similar to a diffuse model of the double layer. Also here, as in mercury, the maximum is higher the higher the concentration of indifferent electrolyte and is also displaced to the negative side of the i.e.p. indicating the preference of the surface to primary adsorption of anions.

Figure 6 represents the plot of Δ e.m.f., the difference between the e.m.f. of the suspension and that of the blank, *versus* the equilibrium e.m.f. of the suspension. It can be seen that the shift along the x-axis depends on the difference in the initial pH (e.m.f.) of the KCl solutions, being higher the lower the concentration. The shift along the y-axis is due to the reasons given above, and that adsorption of H^+ ion is more favoured the higher the KCl concentration (potential barrier), while the formation of negative sites is favoured at lower KCl concentrations (*i.e.*, competition between Cl^- and OH^- ion). The constant distance arises from the experimental procedure in which increments of acid or base were added progressively. Now if $CE = ED$ this means that $\sigma_+ = \sigma_-$ which is correct according to the association–dissociation mechanism:

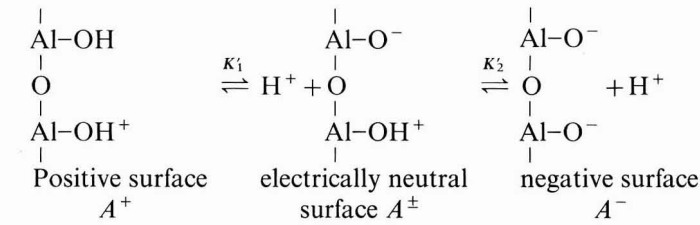

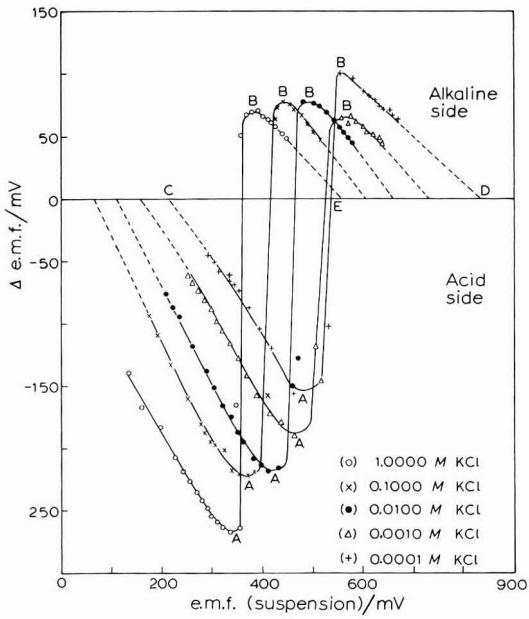

Fig. 6. Potentiometric titration of suspensions.

2. *Calculation of* pK'_1 *and* pK'_2. Various investigators[11,12] working with γ-alumina have suggested that the possible sites on the surface include hydroxyls, oxide ions, exposed aluminium ions and protonated vacancies. Infrared study[13] has shown that molecular CO_2 can be strongly held by a few sites ("α-sites") on dry γ-alumina. These α-sites normally contain reactive oxide ions in close proximity to an exposed cation. Also, adsorption of HCl at room temperature on dry γ-alumina creates new hydroxyl groups and H_2O[13].

It is more reasonable and in accord with capacity data to assume the presence of equal amounts of positive and negative charges on the surface at the p.z.c. Starting from this idea and the surface structure given above, the apparent ionization constants are given by:

$$K'_1 = [A^{\mp}][H^+]/[A^+] \quad \text{and} \quad K'_2 = [A^-][H^+]/[A^{\mp}] .$$

In order to calculate the pK', use is made of the Henderson relation. When the acid is half neutralized then pH = pK'. To calculate the amount of surface acid titrated, a plot is made of $(\Delta^2 \text{ e.m.f.}/(\Delta V)^2)$ *vs.* the volume V of the titrant. The difference in volume between the two inflection points (at zero value on the curves) amounting to about 2 ml of the titrant, corresponds to the equivalents of the surface groups titrated. The pH of the Al_2O_3–KCl system when half of this amount of titrant was added, corresponds to pK'. In Table 1, pK'_1, and pK'_2 are given for 1 and 0.1 M KCl solutions, where the buffer action permits reliable pH calculations. The mean values could be used as a further check on the p.z.c.

Therefore, p.z.c. $= \frac{1}{2}(7.68 + 9.38) = 8.53$, which is fairly close to 8.9 obtained from Fig. 1.

TABLE 1

VALUES OF pK'_1 AND pK'_2 FOR Al_2O_3

	1 *M KCl*	0.1 *M KCl*	*Mean value*
pK'_1	7.83	7.52	7.68
pK'_2	9.36	9.39	9.38

II. Conductance

Figure 7 shows the relative conductance as a function of electrolyte concentration. It can be readily seen that the isoconductance value of 0.10 was obtained for the oxide suspensions in the various electrolytes. This value in HCl solutions corresponds to a cation exchange capacity of 3.2 mequiv. g^{-1}, which is in good agreement with 3.3 mequiv. g^{-1} obtained from charge density determination (Fig. 8a). It was also found that the specific conductance of the original electrolyte may be higher or lower than that after equilibrium. This behaviour is attributed to the type of adsorption. When positive adsorption of the electrolyte takes place the conductance is less than the original. However, for negative adsorption the reverse is true. For HCl and NaOH suspensions, positive adsorption takes place and therefore this fact may be used for the location of the p.z.c., when the difference in the specific conductance $\Delta\kappa$ between the equilibrium and the original solutions becomes zero; Fig. 8b shows a plot of $\Delta\kappa$ *vs.* pH. The p.z.c. is found to be at pH 9, which is in good agreement with that obtained from adsorption of potential-determining ions (*cf.* Fig. 8a).

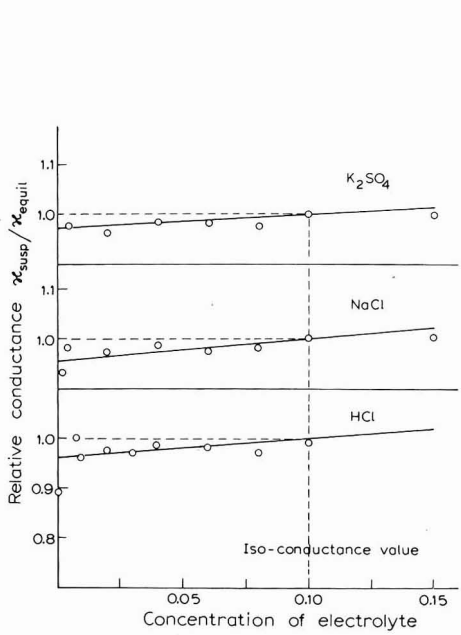

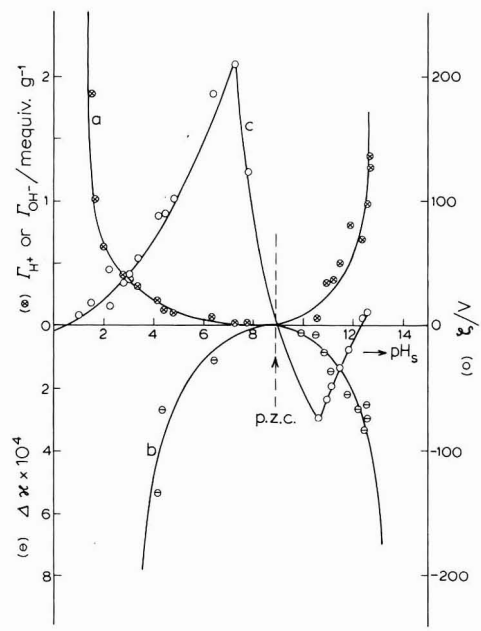

Fig. 7. Isoconductance value of Al_2O_3 suspensions in different electrolytes.
Fig. 8. The p.z.c. by (a) charge density, (b) conductance, (c) ζ-potential according to eqn. (11).

It has been shown earlier[14] that the specific conductance of a kaolin suspension L_t is related to that of the equilibrium solution L_s and the specific conductance of particles L_p by the relation:

$$L_t = aL_s + (1-a)L_p \tag{10}$$

where a is a constant. Figure 9 shows the linear plots of L_p *vs.* c the electrolyte concentration, they were obtained only when a is equal to 0.6. This behaviour is similar to the clay-electrolyte system[15].

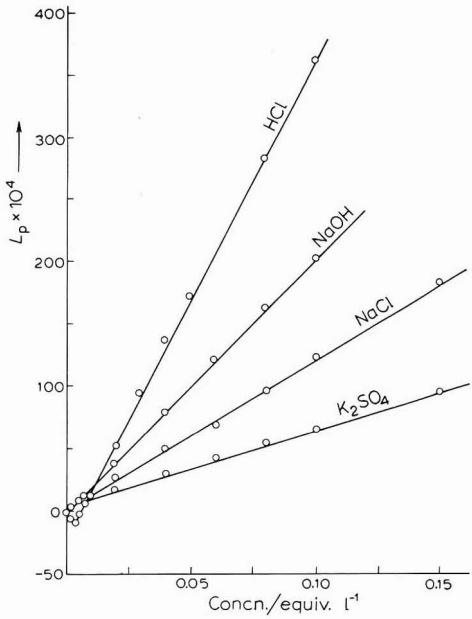

Fig. 9. Test of eqn. (10).

III. Electrophoresis

In Table 2 are given the ζ-potential and the mobility of Al_2O_3 particles. These results shows that the particles are positively charged in all electrolytes and within the concentration ranges studied. The charge carried by the particles is higher in HCl than in the other electrolytes because of the low pH and the adsorption of

TABLE 2

THE ζ POTENTIAL OF Al_2O_3 PARTICLES IN DIFFERENT ELECTROLYTES

Original electrolyte	pH_s *susp.*	$10^4 \times$ *Migration velocity* $u/cm\ s^{-1}$	$10^4 \times$ *Mobility* $(u/H)/cm^2\ s^{-1}\ V^{-1}$	*Electrophoretic mobility* ζ/mV
0.001 *N* HCl	4.80	7.45	5.77	125
0.0005 *N* HCl	6.40	7.64	6.77	146
0.001 *N* NaCl	7.90	2.88	2.55	55
0.0005 *N* NaCl	8.00	2.50	2.215	48
0.0005 *N* K_2SO_4	8.70	0.595	3.69	8

potential-determining H^+ ion as already observed. This is in agreement with the conductance values reported earlier.

The values obtained for electrophoresis may be compared with those calculated by using the Nernst equation as described. Knowing that 0.001 *N* and 0.0005 *N* HCl give equilibrium pH values of 4.8 and 6.4 respectively; this method gives 246 and 150 mV for the surface potentials of Al_2O_3 in HCl at pH 4.8 and 6.4 respectively. The last value of 150 mV is in good agreement with 146 mV obtained experimentally.

The electrostatic free energy difference corresponding to the change in the pH can be calculated by the theory of Hartley and Roe[16]. If some acidic groups are situated on the surface of particles, the potential near the surface is greater than the average for the whole solution by the amount ζ. The H^+ ion concentration near the surface will be $\exp(-\zeta/kT)$ times the H^+-ion concentration in the bulk. Therefore, it is possible to write

$$pH_s = pH_b + \zeta/60 \tag{11}$$

where s and b denote surface and bulk quantities *i.e.* equilibrium and initial pH values. Values of ζ are plotted *vs.* pH_s in Fig. 8c. Judging from Fig. 8c the p.z.c. obtained by this method is in good agreement with that obtained from conductance and adsorption methods.

SUMMARY

Adsorption of the potential-determining H^+ and OH^- ions at the Al_2O_3 surface in aqueous KCl was followed potentiometrically. The surface charge and potential were calculated as a function of the concentration of ions. The results indicate that the capacity of the Al_2O_3 double layer is not constant. Two adsorption sites with different dissociation constant were obtained from a suggested charge surface model at the point of zero charge.

The electrical conductance and electrophoretic mobility of Al_2O_3 particles in HCl, NaOH, NaCl and K_2SO_4 were measured. The point of zero charge at pH 9 was obtained satisfactorily by different methods.

REFERENCES

1 G. A. Parks and P. L. de Bruyn, *J. Phys. Chem.*, 66 (1962) 967.
2 R. J. Atkinson, A. M. Posner and J. P. Quirk, *J. Phys. Chem.*, 71 (1967) 550.
3 J. Yopps and D. W. Fuerstenau, *J. Colloid Sci.*, 19 (1964) 61.
4 P. L. de Bruyn and G. E. Agar, *Surface Chemistry of Flotation*, in *Froth Flotation*, 50th Anniversary Volume, A.I.M.E., N.Y. 1962, chap. 5.
5 G. Y. Onoda and P. L. de Bruyn, *Surface Sci.*, 4 (1966) 48.
6 T. Shedlovsky H. S. Brown and D. A. MacInnes, *Trans. Electrochem. Soc.*, 66 (1934) 165.
7 F. Z. Saleeb, Ph. D. Thesis, London University, (1962).
8 H. R. Kruyt, *Colloid Science*, Vol. I, Elsevier, New York, 1952.
9 D. C. Grahame, *Chem. Rev.*, 41 (1947) 441.
10 J. J. Bikerman, *Phil. Mag.*, 33 (1942) 384.
11 J. King Jr. and S. W. Benson, *Anal. Chem.*, 38 (1966) 261.
12 J. H. de Boer, J. M. H. Fortuin, B. C. Lippens and W. H. Meijs, *J. Catalysis*, 2 (1963) 1.
13 J. B. Peri, *J. Phys. Chem.*, 63 (1965) 211; 70 (1966) 1482.
14 A. K. Helmy, H. Sadek and S. K. Doss, *Kolloid-Z.*, 205 (1965) 104.
15 C. Dakshinamurti and D. E. Chandool, *Soil Sci.*, 102 (1966) 123.
16 G. S. Hartley and J. W. Roe, *Trans. Faraday Soc.*, 36 (1940) 101.

ELECTROANALYTICAL CHEMISTRY AND INTERFACIAL ELECTROCHEMISTRY
Elsevier Sequoia S.A., Lausanne – Printed in The Netherlands

INDUCTIVE OSCILLOMETRIC MEASUREMENTS*

ATHOS BELLOMO
Institute of Analytical Chemistry, University of Messina (Italy)
(Received February 23rd, 1970)

The first analytical oscillometric measurements using inductive measuring cells were performed in 1946 by Jensen and Parrack[1] with a TP-TG circuit[2]. Inductive or similar measurements were then developed as the instruments used were improved, as well as other practical researches[3-10].

The problem then arose of interpreting the results as a function of the relationships between the inductance, the cell-geometry, the conductivity and the concentration[11] of the solution to be tested.

The relationship existing between the different parameters is not a simple one, but a simplified interpretation can be achieved by considering the properties of the cell in terms of the corresponding simplified equivalent circuit[12-14] for the specific situation.

The chemical reaction occurs exclusively in the cell: the electrical elements connected to it have the function of translating the chemical properties of the sample into easily measurable variations in voltage, current, frequency or capacitance.

There have been other researches with inductive[15] or helicoidal[16] measuring cells, but only recently have Farkas and co-workers[17] examined inductive measuring cells from a theoretical point of view on the basis of Maxwell's equations.

It is now possible to calculate the impedance characteristics of an inductive measuring cell from the relation between the properties of the cell and the constants of the sample to be tested.

Since it was of interest to establish, in the case of oscillometric measurements, the relation between the geometrical properties of an inductive or capacitive measuring cell and the frequency variations[18] (Δ_f) of the oscillator with which the cell is coupled, we attempted to achieve by frequency measurements an understanding of the relation between the parameters of an inductive measuring cell and the conductivity as well as the concentration of the solution.

EXPERIMENTAL

Apparatus

The oscillometer was of laboratory construction of a non-tuned charge type[19] with stabilized voltage supply[20]. The induction coil L_1 of the oscillating circuit was wound around a ceramic support. The cell consisted of a glass tube and stirring was

* Presented at the 3rd International Symposium of Oscillometry at Horny Smokovec (September 1969), C.S.S.R.

effected by purified electrolytic hydrogen. The frequenziometric measurements were done by means of a Hallicrafter receiver type SX 122 connected to a Philips oscilloscope type G.M. 5600. The measurements were carried out in accordance with the technique of Blaedel and Malmstadt[21,22] as applied in our earlier work[23].

The interpretation of the relation between the sensitivity of the frequenziometric measurements and the characteristics of the induction coil L_1, is based on the theory of oscillometric inductive cells developed by Farkas and co-workers[17]. According to this the field intensity does not remain constant inside the substance but varies with the radius of the cylinder forming the cell which contains the solution. This has been verified by examining the relationship between the diameter d of the induction coil belonging to the oscillating circuit and the frequenziometric sensitivity s.

The concentration curves of Fig. 1, obtained for different d values of the induction coil L_1 containing the solution, have shown that, for the same number of turns, Δ_f varies as a function of d.

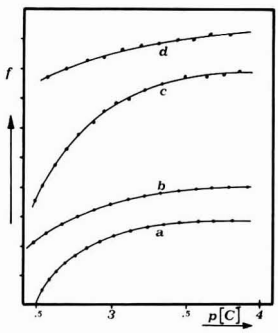

Fig. 1. Concn. curves of NaCl for different d values of L_1: (a) 2 cm, (b) 3 cm, (c) 4 cm, (d) 6 cm.

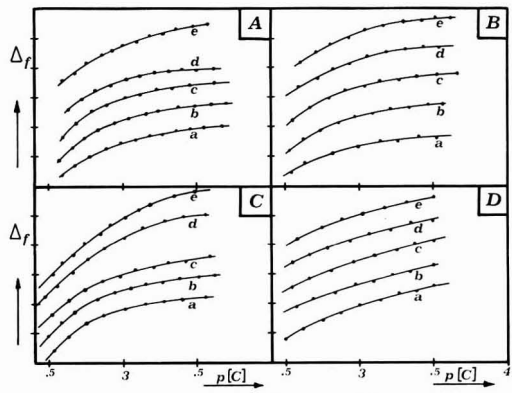

Fig. 2. Concn. curves obtained at constant d (4 cm) and increasing L_1: (A) 4.029 μH, (B) 9.066 μH, (C) 36.26 μH, (D) 64.47 μH. (a) NaCl, (b) $BaCl_2$, (c) $CuSO_4$, (d) $K_3[Fe(CN)_6]$, (e) $K_4[Fe(CN)_6]$.

Figure 2 shows concentration curves of electrolytes for constant d values and variable L_1. These curves show a direct relation between the frequency f and L_1 expressed[18] in μH.

The insert for Fig. 3 shows concentration curves for electrolytes (HCl) at constant d and increasing L_1 plotting the frequency f *vs.* p$[C]$; then for each curve the Δ_f is referred to a constant p$[C]$ value; in Fig. 3 the Δ_f is plotted *vs.* L_1 expressed in μH.

If the value of the inductance of the coil varies progressively for a given d value of the inductive measuring cell, the amplitude of the response curve also varies.

For analytical purposes the optimum Δ_f range falls in the region corresponding to the greatest frequency slope. The same concentration curves obtained with capacitive measuring cells show a wider Δ_f range because the effective electrical components are then the resistive and capacitive ones which, compared to L_1, cause a higher Δ_f[18]. This becomes evident when carrying out measurements in which the resistive or capacitive components predominate over the inductive ones[18].

The conductance G of an inductive measuring cell[5] is expressed by the equation:

$$G = \frac{RL_1^2}{R^2(L_1+L_2)^2+\omega^2 L_1^2 L_2^2} \quad (1)$$

where L_1 is the inductance of the coil, L_2 the self induction of L_1 and R the cell resistance.

For an acid–base titration series, the Δ_f of the frequenziometric titration curves having different L_1/C ratios at constant L_1 and d and increasing C values, have been plotted in Fig. 4.

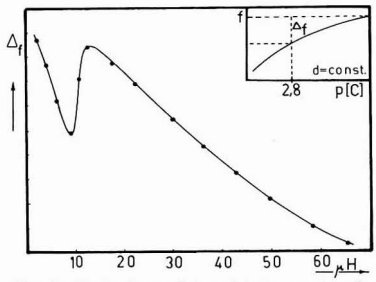

Fig. 3. Variation of Δ_f with L_1 maintaining p[C] and d constant.

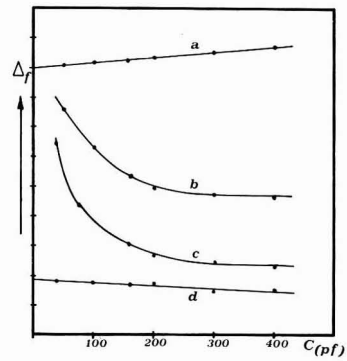

Fig. 4. Change in magnitude of Δ_f for different values of the L_1/C ratio. d Values: (a) 2 cm, (b) 3 cm, (c) 4 cm, (d) 6 cm. C, expressed in pF, is the capacity in parallel to L_1.

Figure 4 shows how the L_1/C ratio influences the frequenziometric sensitivity even for measurements with inductive measuring cells. This is in accordance with the observations of Cruse and Huber[14] and as we have already observed with capacitive measuring cells[24]. This has also been verified in the interpretation of anomalous curves[25]. A comparison with capacitive measuring cells is now possible. It was proved that the instrumental sensitivity, particularly in the case of frequency measurements, increases with the surface area of the electrodes and decreases as a function of the equation:

$$C = C_1 C_n/(C_1+C_n) \quad (2)$$

where, in the case of capacitive measuring cells, C is the total capacity in parallel to L_1, C_1 the surface capacity of the electrodes and C_n the resultant of all capacities in series with the cell.

In the case of inductive measurements a characteristic change of the frequenziometric sensitivity can be seen as the diameter of the induction coil L_1 increases, or as the coupling between the sample and the inductance varies. This is directly related to frequency measurements because, for a given number of turns and a constant length of coil, the inductance increases with the diameter of the coil while the frequency decreases. Frequency measurements for concentration curves of $n \gtrless n_1$ valent electrolytes, in cells of increasing diameter (Fig. 5) confirm that there is actually a maximum frequenziometric slope which corresponds to a specific d value (Fig. 5C).

The introduction into L_1 of the glass-tube containing the solution, gives rise to a concentration effect[1]. Electrolyte solutions placed into an inductance show a permeability μ_{eff}, while the inductive impedance varies with this permeability according to the following relationship:

$$Z = Z_0 \mu_{eff} \tag{3}$$

The frequenziometric sensitivity depends essentially on changes of inductance, since C expressed by:

$$f = (2\pi\sqrt{L_1 C})^{-1} \tag{4}$$

is constant.

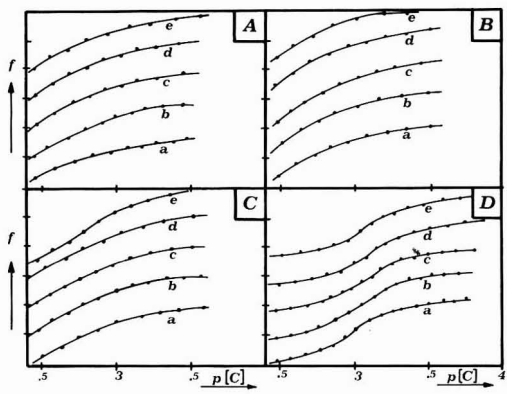

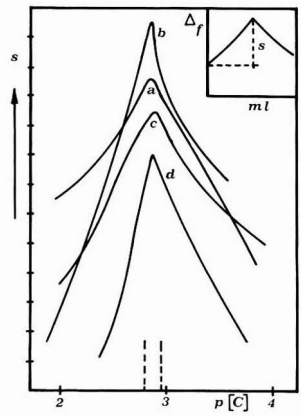

Fig. 5. Concn. curves of electrolytes for different d values of L_1. (A) 2 cm, (B) 3 cm, (C) 4 cm, (D) 6 cm. (a) NaCl, (b) $BaCl_2$, (c) $CuSO_4$, (d) $K_3[Fe(CN)_6]$, (e) $K_4[Fe(CN)_6]$.

Fig. 6. Relation between s_{max} and p[C] for d = const. as a function of L_1: (a) 4.029 μH, (b) 9.066 μH, (c) 20.39 μH, (d) 30.47 μH.

The L_1 variations derive from changes in permeability and conductivity of the solution which has been introduced. The capacitive component is also effected but to less extent, since on neutralizing a HCl solution placed into the induction coil L_1 of the oscillating circuit, it is possible to follow the neutralization reaction by capacity compensation in relation to the initial frequency assumed equal to zero. A certain part of the "loading effect" is therefore due to a capacitive component. All parameters considered contribute to Δ_f.

Furthermore, a series of titrations of an acid with a strong base, in the pH range 1.8–3.9, have been made using an inductive measuring cell. The sensitivity s of the measurements was defined as the variation in frequency from the start of the titration to the equivalence point. The inductances had different values but the same diameter. In each case the concentration range having the highest sensitivity was the same and equal to p[H^+] = 2.85 (Fig. 6).

Some interesting conclusions can be drawn from Fig. 6; for example, the sensitivity curves to through a maximum as the value of the inductance increases.

To a good approximation, the maxima of the sensivity curves all fall within the region corresponding to points of equal conductivity of the solution. An analogous correspondence can be observed with inductances having different d values.

These results show that using "external inductance" cells, the optimum concentration when titrating an electrolyte corresponds to a well defined conductivity and depends on the diameter of the induction coil L_1, going through a maximum of s (curve b).

With an "internal inductance" cell[26] the frequenziometric variations are wider[27] but the instrumental difficulties increase. In inductive measurements the frequenziometric sensitivity, in regard to variations of concentration, depends on the shape of the inductance containing the sample to be tested and presents more dependent variables than in capacitive measurements.

DISCUSSION

The dependence of the sensitivity s on the diameter d of the induction coil L_1, and the relation between the slope of the curves having frequency f and the amplitude of the induction coil L_1 with constant d value, as well as the frequenziometric sensitivity as a function of the magnitude of L_1, have been examined.

The relation between the conductivity by frequency measurements and the concentration of an electrolyte, as well as the change in s for different values of the L_1/C ratio have shown maxima of the frequenziometric slope for certain d values.

It becomes evident from the diagrams of s_{max} *vs.* the electrolyte concentration, in the case of d as a function of L_1, that the optimum concentration for the titration of the electrolyte to be tested, corresponds not only to a well defined conductivity, but also depends on the diameter d of the induction coil L_1, going through a maximum.

Hence it is possible to achieve a quantitative evaluation of the relation between the characteristics of the cell, the frequenziometric sensitivity and the concentration of the electrolyte.

The curves obtained with the inductive measuring cell reveal concentration ranges over which instruments are insensitive. In other ranges the results give a linear response with the concentration of electrolyte.

ACKNOWLEDGEMENTS

I am very grateful to Dr. A. Casale and Dr. D. De Marco for their useful and critical collaboration.

SUMMARY

The relations between the characteristics of an oscillometric "external inductance" type of cell and the frequenziometric sensitivity, when dealing with solutions of electrolytes, have been examined.

The measurements taken using different values of inductance having the same diameter have shown a maximum sensitivity for a given concentration. The results are compared with those obtained with capacitive measuring cells; each case the sensitivity passes through a maximum.

REFERENCES

1 F. W. JENSEN AND A. L. PARRACK, *Ind. Eng. Chem. Anal. Ed.*, 18 (1946) 595.
2 W. J. BLAEDEL AND H. V. MALMSTADT, *Anal. Chem.*, 22 (1950) 734.
3 F. W. JENSEN, G. M. WATSON AND L. G. VELA, *Anal. Chem.*, 23 (1951) 1327.
4 O. I. MILNER, *Anal. Chem.*, 24 (1952) 1247.
5 D. G. FLOM AND P. J. ELVING, *Anal. Chem.*, 25 (1953) 541.
6 I. P. DOWDALL, D. V. SINKINSON AND H. STRETCH, *Analyst*, 80 (1955) 491.
7 K. CRUSE, *Z. Elektrochem.*, 61 (1957) 1123.
8 F. J. SCHMIDT, *Anal. Chem.*, 29 (1957) 1060.
9 A. H. JOHNSON AND A. TIMNICK, *Anal. Chem.*, 30 (1958) 1324.
10 E. PUNGOR, *Oscillometry and Conductometry*, Pergamon Press, Oxford, 1965.
11 J. L. HALL, *Anal. Chem.*, 24 (1952) 1236.
12 S. PETOFÁLVI AND R. BERTRAM, Second Oscillometric Symposium, Veszprém, 1967.
13 J. FORMAN AND D. J. CRISP, *Trans. Faraday Soc.*, 42 (1946) 186.
14 K. CRUSE AND R. HUBER, *Hochfrequenztitration*, Monogr. in Angew. Chem. Ing. Tach., n. 69, Verlag Chemie, Weinheim, 1957.
15 K. NAKANO, T. KINDAICHI AND M. KOMIJA, Second Oscillometric Symposium, Veszprém, 1967.
16 H. STUHEC, Second Oscillometric Symposium, Veszprém, 1967.
17 F. FARKAS, O. KLUG, F. KOVACS AND M. GOMBOS, *Messtechnik*, 2 (1969) 46.
18 A. BELLOMO, G. D'AMORE AND O. KLUG, *Fundamentals of Oscillometry*, I-IV-MTA, Kemiai Tud. Ostz. Közl. 19, 1963, p. 57–63; 221–231.
19 A. BELLOMO, *Rass. Chim.*, 4 (1964) 167.
20 A. BELLOMO, *Atti Soc. Peloritana Sci. Fis. Mat. Nat.*, 2 (1956) 315.
21 W. J. BLAEDEL AND H. V. MALMSTADT, *Anal. Chem.*, 22 (1950) 743.
22 W. J. BLAEDEL AND H. V. MALMSTADT, *Anal. Chem.*, 22 (1950) 1413.
23 A. BELLOMO AND O. KLUG, *Z. Anal. Chem.*, 207 (1965) 93.
24 A. BELLOMO, S. SERGI AND O. KLUG, *Ann. Chim. (Rome)*, 55 (1965) 832.
25 A. BELLOMO AND E. BRUNO, *Atti Soc. Peloritana Sci. Fis. Mat. Nat.*, 4 (1959) 459.
26 M. F. C. LADD AND W. H. LEE, *Talanta*, 941 (1965) 12.
27 P. A. ZAGORETS, N. I. SMIRNOV AND V. I. ERMAKOV, *Russ. J. Phys. Chem., English Transl.*, 36 (1962) 1487.

ELECTROANALYTICAL CHEMISTRY AND INTERFACIAL ELECTROCHEMISTRY
Elsevier Sequoia S.A., Lausanne – Printed in The Netherlands

ANODIC STRIPPING VOLTAMMETRY WITH A GLASSY CARBON ELECTRODE MERCURY-PLATED *in situ*

T. M. FLORENCE

Chemistry Division, Australian Atomic Energy Commission Research Establishment, Lucas Heights, N.S.W. (Australia)

(Received September 19th, 1969)

INTRODUCTION

In recent years the literature on anodic stripping voltammetry using both the hanging mercury drop and thin mercury films has grown rapidly[1], but it is very doubtful whether practical applications of the technique to routine industrial analysis have kept pace with the number of research publications. Presently-available anodic stripping methods have some serious disadvantages for use in routine analysis. The hanging mercury drop electrode (HMDE) has relatively low sensitivity, and suffers from poor precision and particularly poor resolution of neighbouring waves. Thin mercury film electrodes offer improved sensitivity and excellent resolution, but in general the reproducibility of results is even less than that given by the HMDE[2-4]. The inconvenience and lack of reproducibility can be attributed almost entirely to the preliminary step of depositing the mercury film on an "inert" substrate such as platinum or nickel. It is difficult to prepare mercury films of consistent and uniform thickness, and even more difficult to preserve them in an active state for any length of time. Once exposed to air the electrode behaviour of mercury films becomes erratic[5]. Many of the substrates chosen for thin film stripping analysis introduce serious problems on their own. Platinum and nickel have strongly adherent surface oxide films, low hydrogen overpotentials, and a finite solubility in mercury. Carbon paste and wax-impregnated graphite electrodes, because of their mechanical properties, are inconvenient for use in routine analysis.

Glassy carbon is a recently-developed electrode material. Because of its hardness (Shore hardness of 100), good electrical conductivity, high hydrogen overpotential and chemical inertness, glassy carbon has already found considerable use in electroanalytical chemistry[6,7]. When polished metallographically it has a black, lustrous, mirror-like appearance. Using a polished glassy carbon substrate it was found that mercury could be electrodeposited, then completely removed simply by wiping with a paper tissue. A study was made of the simultaneous deposition of mercury and the trace metals being analysed, by adding mercuric nitrate to the sample solution and depositing at a potential where both Hg^{2+} and the trace metal ions are reduced. By this means a very thin mercury film is formed *in situ*, from which the trace metal can be anodically stripped. After completing the analysis the electrode is prepared for another sample by wiping off the mercury with a tissue. Mercury films produced in this way can be very thin, 0.001–0.01 μm, compared with the usual[2] film

thickness of 0.5–50 μm. Anodic stripping voltammograms obtained by this new technique show the highest resolution so far reported for stripping methods, and the sensitivity is also excellent. Reproducibility appears to be superior to other anodic stripping methods, with the precision of measurement approaching that of conventional polarography. The peak current calibration factor (μA 1 mol^{-1}) of a glassy carbon electrode for the determination of Pb^{2+} in 0.1 *M* KNO_3 remained constant to within $\pm 5\%$ over a period of three months.

The polished glassy carbon electrode with *in situ* mercury film deposition is applicable to a wide range of supporting electrolytes and sample types, and because of its simplicity and reliability is particularly suitable for routine analysis. This paper examines the effect of the experimental parameters on the determination of lead, and describes the application of the technique to the analysis of typical samples for copper, lead, and cadmium.

EXPERIMENTAL

Apparatus and reagents

Voltammeter. The voltammeter used in this work was built to the design of the ORNL model Q-2792 solid-state controlled-potential instrument[8]. For work with solid electrodes the DME filters were replaced with 50 Hz filters. A Hewlett–Packard type 7004A X–Y recorder was used with the voltammeter.

Constant-speed rotator. The rotator consisted of a d.c. motor controlled by a tachogenerator. A Helipot potentiometer allowed continuous selection of speeds from 50 to 4,000 rev. min^{-1} with a precision of $\pm 0.2\%$. The electrode was held in an O-ring chuck and rotated *via* a pair of gears and a self-lubricating bearing.

Cell. The glass voltammetric cell was 5 cm $\times$ 2.7 cm i.d., and fitted with a grooved Teflon cap. The cap was drilled to accept the rotating electrode, a platinum wire auxiliary electrode, a narrow ceramic-plug salt bridge, and a de-gassing tube. The salt bridge was filled with saturated KNO_3 and connected to a Beckman No. 39178 fibre junction SCE.

Room temperature was controlled at $25.0 \pm 0.5^\circ$ C.

Electrodes. Grade GC-20 glassy carbon discs, 0.5 cm high and 0.3 cm diameter, were supplied by Tokai Electrode Manufacturing Co., Ltd., Tokyo. The discs were metallographically polished on one plane face with diamond dust, then sealed into 25-cm lengths of 0.4 cm i.d. glass tubing using epoxy resin. Care was taken to avoid contaminating the exposed polished face with adhesive. A small quantity of mercury was placed inside the tube to contact the glassy carbon disc, and a platinum wire, around which the electrode rotated, dipped into the mercury and made contact with the voltammeter lead. Pyrolytic graphite electrodes were fabricated in the same manner, and the exposed face was smoothed with fine emery paper.

Metal ion solutions. A 1×10^{-2} *M* mercuric nitrate solution was prepared from triply-distilled mercury and high purity nitric acid. The solution was 1×10^{-2} *M* in free nitric acid. Standard metal solutions, 1×10^{-3} *M*, were prepared from reagent-grade nitrate or sulphate salts and kept in 0.1 *M* HNO_3.

Precautions taken to avoid contamination

With the very low metal concentrations used in anodic stripping voltammetry,

there is constant danger of errors caused by contamination or by adsorption of metal on container walls. All glassware was treated with a silicone repellent ("Repelcote", Hopkins and Williams, Ltd., England), and solutions for analysis were prepared just before use. Metal solutions were transferred with Eppendorf micropipettes, which have disposable plastic tips.

Water used throughout was demineralised, then distilled twice, first from potassium permanganate.

Typical experimental procedure

The determination of lead was carried out in the following manner. A 5-ml aliquot of 1 *M* KNO_3 was pipetted into a 50-ml volumetric flask, followed by 0.10 ml of mercuric nitrate solution. The lead solution was then added and the mixture diluted to volume with water. A 10-ml aliquot was pipetted into the voltammetric cell, which was then raised by a Labjack into position under the electrodes. With the electrode rotating to prevent gas bubbles adhering to its surface, the solution was sparged with argon for 10–15 min. At the end of this period a potential of -0.7 V was applied to the glassy carbon electrode (GCE) and a timer started simultaneously. After exactly 5 min deposition, an anodic scan from -0.7 to $+0.1$ V was applied at a scan rate of 3 V/min. The peak potential of the lead wave was at -0.46 V. The electrode potential was readjusted to -0.7 V, and a second 5-min deposition carried out. The anodic scan was then applied as before. The GCE was rotated at 2,000 rev. min^{-1} throughout the deposition and stripping steps. The concentration of Pb^{2+} in the sample was calculated from the height of the second anodic peak.

To prepare the GCE for another sample, it needs only to be rinsed with water then wiped 2 or 3 times with a soft paper tissue. This procedure effectively removes the thin mercury film.

RESULTS

Investigation of the various experimental parameters was carried out using Pb^{2+} in a 0.1 *M* KNO_3 (pH 4) supporting electrolyte. Varying the KNO_3 concentration from 0.005 to 1 *M* had no effect on the dissolution peak current (i_p) or the peak potential (E_p) of lead, and deposition potentials between -0.65 and -0.95 V led to the same values of i_p and E_p.

i_p vs. concentration of Pb^{2+}

The results in Table 1 show that peak current is proportional to lead concentration up to at least 1×10^{-6} *M* Pb^{2+}. Higher concentrations of lead were not investigated because direct controlled-potential derivative polarography can be used at these levels[8]. Figure 1 illustrates typical curves obtained for the anodic stripping of lead.

Precision of measurement was estimated by analyzing seven separate aliquots of a 2×10^{-7} *M* Pb^{2+} solution, and of a 5×10^{-9} *M* Pb^{2+} solution. The calculated relative standard deviations were $\pm 2.2\%$ and $\pm 7.5\%$, respectively, with a scan rate of 3 V/min, rotation speed of 2,000 rev. min^{-1}, and 10-min deposition. The second scan was used for analysis. The limit of detection was estimated by measuring i_p for lead in seven aliquots of a blank solution (0.1 *M* KNO_3) using 30-min deposition, 3 V/min scan rate, and 2,000 rev. min^{-1} rotation speed. The blank was equivalent to 1.1×10^{-9}

TABLE 1

RELATIONSHIP BETWEEN PEAK CURRENT AND LEAD CONCENTRATION
0.1 M KNO_3, 3 V/min, 2,000 rev. min^{-1}, 5-min deposition, 2×10^{-5} M Hg^{2+}, 25°

10^7 $C_{Pb^{2+}}$/mol l^{-1}	$i_p/\mu A$[a]	$-E_p/V$[a]	$b_{\frac{1}{2}}/mV$[d]	10^7 $i_p C_{Pb^{2+}}^{-1}$/μA l mol^{-1} [e]
nil	0.04	0.44	38	–
0.02	0.12	0.45	36	4.00
0.05	0.24	0.46	38	4.00
0.2	0.70	0.46	37	3.30
0.5	1.71	0.46	37	3.34
2	6.93[b,c]	0.46	37	3.45
5	17.5	0.47	37	3.49
10	35.4	0.47	36	3.54

[a] Measurements made on second scan. [b] Addition of 1×10^{-5} M Cu^{2+} and Fe^{3+} had no effect on i_p. [c] The variation of this peak current was within $\pm 5\%$ over 3 months. [d] Peak width at half-peak potential. [e] i_p corrected for blank value.

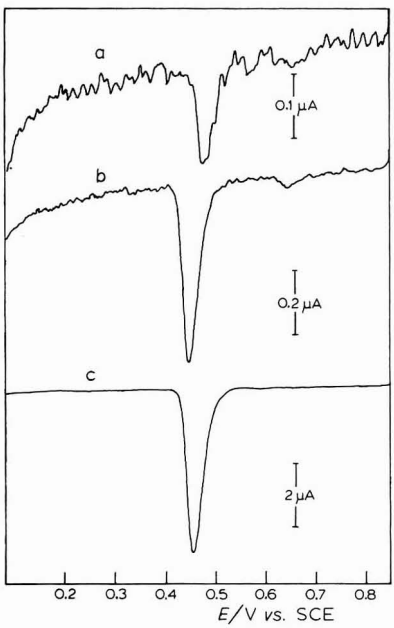

Fig. 1. Determination of lead. (a) blank, 20-min deposition; (b) 5×10^{-9} M Pb^{2+}, 10-min deposition; (c) 2×10^{-7} M Pb^{2+}, 7-min deposition. All in supporting electrolyte of 0.1 M KNO_3 plus 2×10^{-5} M Hg^{2+}, scan rate 3 V min^{-1}, 2,000 rev. min^{-1} rotation.

M Pb^{2+} with a relative standard deviation of $\pm 21\%$. The limit of detection, or minimum detectable difference between a mean sample and a mean blank reading, $(i_s - i_b)$, was calculated from,

$$(i_s - i_b) = 2\sqrt{2}\, S_b$$

where S_b is the standard deviation of the blank. The limit of detection is therefore estimated as 7×10^{-10} M Pb^{2+}.

i_p vs sweep number

Table 2 gives the results of seven successive 5-min depositions and anodic scans on one aliquot of a standard lead solution. Each deposition was commenced immediately after completion of the previous scan, without removing the electrode from the solution or interrupting stirring. It is apparent that the peak height is almost constant after the first scan.

TABLE 2

RELATIONSHIP BETWEEN PEAK CURRENT AND SWEEP NUMBER
0.1 *M* KNO_3, 3 V/min, 2,000 rev. min^{-1}, 5-min deposition, 2×10^{-5} *M* Hg^{2+}, 2×10^{-7} *M* Pb^{2+}, 25°

Sweep[a] *No.*	$i_p/\mu A$	$-E_p/V$	$b_{\frac{1}{2}}/mV$
1	6.00	0.48	35
2	6.79	0.47	34
3	6.85	0.47	34
4	6.87	0.46	35
5	6.91	0.46	36
6	6.90	0.45	35
7	6.94	0.45	35

[a] Successive depositions and scans on same solution.

i_p vs. mercury concentration

The effect of the initial concentration of Hg^{2+} on i_p is shown in Table 3. There was only a small decrease in i_p with decreasing Hg^{2+} concentration until, with less than 2×10^{-6} *M* Hg^{2+}, the anodic peak for lead diminished abruptly. This cut-off value of mercuric ion concentration appears to be independent of lead concentration, because similar results were obtained when a 2×10^{-8} *M* Pb^{2+} solution was used. Note that the deposition current is proportional to the concentration of mercuric ion.

TABLE 3

RELATIONSHIP BETWEEN PEAK CURRENT AND MERCURY CONCENTRATION
0.1 *M*, KNO_3 3 V/min, 2,000 rev. min^{-1}, 5-min deposition, 2×10^{-7} *M* Pb^{2+}, 25°

$10^5\ C_{Hg^{2+}}/mol\ l^{-1}$	$i_d/\mu A$[a]	$i_p/\mu A$[b]	$-E_p/V$	$b_{\frac{1}{2}}/mV$
nil	0.1	1.1	0.47	87[c]
0.05	0.15	1.5	0.50	40
0.1	0.20	1.5	0.49	39
0.2	0.25	5.20	0.48	32
0.4	0.45	5.80	0.48	35
1.0	0.75	6.21	0.48	37
2.0	1.5	6.87	0.47	35
10.0	7.0	7.42	0.46	38

[a] Deposition current. [b] Measurement made on second scan. [c] Distorted wave.

i_p vs. deposition time

Deposition times between one and 30 min were investigated and the results tabulated in Table 4. It is apparent that the anodic peak current for lead is proportional to deposition time. There seems to be no reason why longer deposition times could not be used if necessary.

TABLE 4

RELATIONSHIP BETWEEN PEAK CURRENT AND DEPOSITION TIME
0.1 M KNO_3, 3 V/min, 2,000 rev. min^{-1}, 2×10^{-5} M Hg^{2+}, 2×10^{-7} M Pb^{2+}, 25°

Deposition, t/min	$i_p/\mu A$[a]	$-E_p/V$	$b_{\frac{1}{2}}/mV$	$i_p t^{-1}/\mu A\ min^{-1}$
1	1.40	0.48	37	1.40
2	2.85	0.47	37	1.43
5	6.71	0.47	37	1.34
10	13.8	0.47	38	1.38
20	26.0	0.46	36	1.30
30	41.8	0.45	35	1.39

[a] Measurement made on second sweep.

i_p *vs. scan rate*

Table 5 shows the effect of scan rate, between 0.1 and 5 V/min, on anodic peak current. Because total deposition time depends on scan rate, all peak currents were corrected by a factor $5/(5+t)$, where t is the time in minutes taken to scan from -0.7 V to the peak potential, E_p. The corrected peak currents can then be compared directly.

TABLE 5

RELATIONSHIP BETWEEN PEAK CURRENT AND SCAN RATE
0.1 M KNO_3, 2,000 rev. min^{-1}, 5-min deposition, 2×10^{-5} M Hg^{2+}, 2×10^{-7} M Pb^{2+}, 25°

Scan rate, v/V min^{-1}	$i_p/\mu A$[a]	$i_p(corr)/\mu A$[b]	$-E_p/V$	$b_{\frac{1}{2}}/mV$	$i_p(corr)\ v^{-1}/\mu A\ min\ V^{-1}$
0.1	0.340	0.24	0.49	30	2.40
0.2	0.585	0.48	0.48	32	2.40
0.3	0.825	0.72	0.48	34	2.40
0.5	1.28	1.17	0.47	32	2.34
1.0	2.43	2.32	0.47	36	2.32
2.0	4.46	4.35	0.46	36	2.18
3.0	6.80	6.70	0.47	37	2.23
5.0	10.0	9.90	0.46	42	1.98

[a] Measurement made on second sweep. [b] Corrected for time taken to scan from start potential to peak potential.

i_p *vs. rotation speed*

Electrode rotation speeds of 500–3,000 rev. min^{-1} were tested, and it can be seen from Table 6 that both i_p and deposition current are proportional to the square root of the rotation speed.

Analysis of diverse samples

Thallium, cadmium, indium, lead, and copper all produce very well-formed anodic dissolution peaks in 0.1 M KNO_3 (Fig. 1), and peak height is proportional to metal ion concentration. The anodic peak for bismuth in 0.1 M KNO_3 is rather distorted, but still usable. A very sharp bismuth peak is obtained in a 0.1 M HCl supporting electrolyte.

TABLE 6

RELATIONSHIP BETWEEN PEAK CURRENT AND ROTATION SPEED
0.1 M KNO_3, 3 V/min, 5-min deposition, 2×10^{-5} M Hg^{2+}, 2×10^{-7} M Pb^{2+}, 25°

Rotation speed, r/rev. min^{-1}	$\sqrt{r/min^{-1}}$	$i_p/\mu A$[a]	$i_d/\mu A$[b]	$i_d\, r^{-\frac{1}{2}}/\mu A\ min^{\frac{1}{2}}$
500	22.4	3.57	0.9	0.040
1,000	31.6	5.25	1.2	0.038
1,500	38.7	5.75	1.5	0.039
2,000	44.7	6.80	1.7	0.038
2,500	50.0	7.80	1.9	0.038
3,000	54.8	8.81	2.0	0.037

[a] Measurement made on second sweep. [b] Deposition current.

TABLE 7

ANALYSIS OF DIVERSE SAMPLES
0.1 M KNO_3 supporting electrolyte

Sample[a]	$[Cu^{2+}]/ppb$	$[Pb^{2+}]/ppb$	$[Cd^{2+}]/ppb$	*% Recovery of* Pb^{2+} *spike*
Doubly distilled, demineralised water	1.2	0.2	< 0.1	102
Demineralised water	10	0.3	< 0.1	99
River water	18	1	3	99
Heavy water ex HIFAR reactor	32	0.8	0.1	98
KNO_3, A.R.	8	5	< 1	100
$ZnSO_4$, A.R.	1.5×10^3	2.7×10^2	< 10	105
$Th(NO_3)_4$, A.R.	70	1.2×10^2	< 10	98
$Zr(NO_3)_4$, technical	3.6×10^2	1.7×10^4	< 10	102

[a] 2×10^{-5} M Hg^{2+} added to sample solution.

All the samples analyzed had measurable amounts of copper and lead, and significant concentrations of cadmium were found in some. The results are summarized in Table 7.

DISCUSSION

Calculations show that with a Hg^{2+} deposition current of 1.3 μA for 5 min (Table 3), and a geometrical electrode surface area of 0.071 cm^2, the thickness of the mercury film is only 40 Å, or 12 atomic layers of mercury. The film thickness used in this work is therefore orders of magnitude less than that used by previous workers[2,5]. De Vries[9] has demonstrated that resolution of neighbouring waves improves as the film thickness decreases, and the excellent resolution shown in Fig. 2(d) undoubtedly results from the use of particularly thin mercury films. It is interesting to note from Table 3 that the anodic peak sensitivity for Pb^{2+} decreases abruptly at mercuric ion concentrations below 2×10^{-6} M. This concentration of Hg^{2+} corresponds to a film thickness of 4 Å, or one monolayer of mercury on the electrode. One possible inference from this result is that the deposited mercury is spread uniformly over the glassy carbon surface.

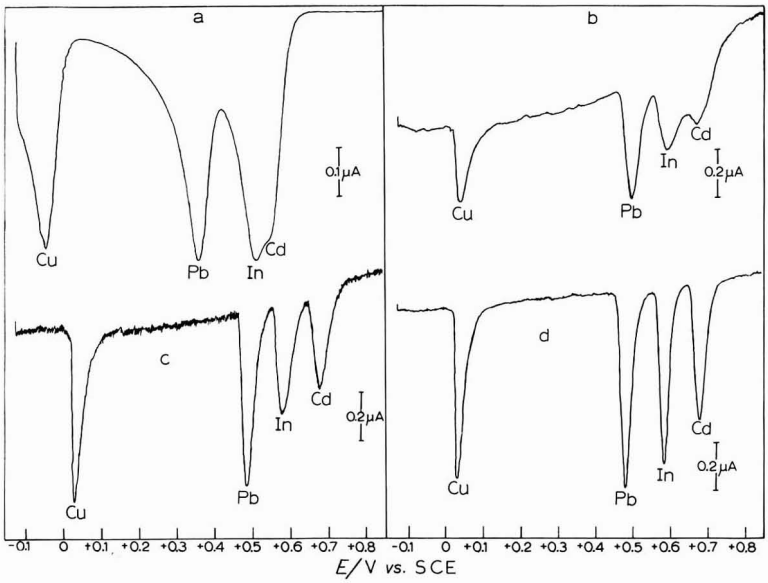

Fig. 2. Effect of substrate. (a) hanging mercury drop, 30-min deposition; (b) pyrolytic graphite electrode, 5-min deposition; (c) unpolished glassy carbon electrode, 5 min-deposition; (d) polished glassy carbon electrode, 5-min deposition.

All contained 2×10^{-7} *M* Cd^{2+}, In^{3+}, Pb^{2+}, and Cu^{2+} in 0.1 *M* KNO_3. Scan rate 0.3 V min^{-1}. Solutions for (b)–(d) also contained 2×10^{-5} *M* Hg^{2+}; rotation speed was 2,000 rev. min^{-1}.

Pyrolytic graphite and unpolished glassy carbon substrates are not as satisfactory as a polished GCE which gives complete resolution of Cd^{2+}, In^{3+}, Pb^{2+}, and Cu^{2+} waves (Fig. 2). Higher mercury deposition currents obtained at the first two electrodes confirm that their roughness factors are higher than that of the polished GCE, and reproducibility of results obtained at unpolished electrodes was poor.

The efficiency of removing mercury by wiping the polished surface was checked by measuring the mercury anodic dissolution wave at +0.45 V (0.1 *M* KNO_3). No wave could be detected after an electrode with a deposited film was wiped once with a wet, and once with a dry tissue.

Table 3 shows that the sensitivity of the determination of lead gradually increases with increasing Hg^{2+} concentration. However, very high mercury concentrations are inconvenient because the large deposition currents must be backed off electrically. The increase in i_p with scan number (Table 2) cannot be explained on the basis of mercury film thickness, since even when much higher initial Hg^{2+} concentrations are used the first scan always gives peak currents significantly smaller than those from successive scans. Apparently the first anodic scan is needed to condition the electrode surface.

As predicted by the theory of thin film electrodes[9], i_p was directly proportional to potential scan rate (Table 5) up to rates of 1 V/min, after which proportionality began to fail. This loss of proportionality at high scan rates can probably be attributed to the limited reversibility of the electrode reaction. The $b_{\frac{1}{2}}$ values (half-peak width) also increase at high scan rates, and for maximum resolution of neighbouring waves, scan rates of 0.3 V/min or less should be used (Fig. 2).

Lead in 0.1 *M* KNO_3 has a half-wave potential at a DME of -0.385 V, so the value for $E_p - E_{\frac{1}{2}}$, with a scan rate of 0.1 V/min, is -100 mV (Table 5). This value is indicative of the very thin film used, since De Vries' theory[9] predicts $E_p - E_{\frac{1}{2}}$ values of -40 mV and -60 mV for 4 μm and 1 μm films, respectively.

Rotation of the electrode improves sensitivity by increasing the amount of metal deposited on the electrode during the deposition step. Table 6 shows that, as expected, the deposition current is proportional to the square root of the rotation speed[10]. There is no advantage in stopping rotation before the anodic scan, and in fact peak heights are slightly higher if rotation is continued during the scan.

Mercury deposition *in situ* can be used with a wide range of supporting electrolytes. Well-formed anodic voltammograms were obtained in 0.1 *M* KNO_3, 0.1 *M* HNO_3, 0.1 *M* HCl, 0.1 *M* NaF, 0.25 *M* NH_4OH–NH_4Cl, 0.25 *M* triethanolamine–HCl, and 0.1 *M* sodium gluconate supporting electrolytes to which 2×10^{-5} *M* Hg^{2+} had been added. Lead, cadmium, thallium, indium, copper, and bismuth were readily determined, but the sensitivity towards zinc was very low in all solutions tested. This insensitivity of thin film electrodes for the determination of zinc has been reported previously[11], but has not been explained satisfactorily.

SUMMARY

An anodic stripping technique is described in which a very thin mercury film is formed on a polished glassy carbon substrate by adding mercuric nitrate to the sample solution and electrodepositing mercury and trace metals simultaneously. The trace metals are then anodically stripped from the mercury film which typically has a thickness of 0.001–0.01 μm. After the analysis the mercury film can be completely removed from the electrode by simply wiping with a tissue.

This new technique is highly sensitive, gives excellent resolution of neighbouring waves, and because of its simplicity and reliability is particularly suitable for routine analysis. Examples are given of the application of the method to the determination of copper, lead, and cadmium in diverse samples.

REFERENCES

1 E. Barendrecht, *Electroanal. Chem.*, 2 (1967) 53.
2 D. K. Roe and J. E. A. Toni, *Anal. Chem.*, 37 (1965) 1503.
3 K. W. Gardiner and L. B. Rogers, *Anal. Chem.*, 25 (1953) 1393.
4 R. Neeb, *Z. Anal. Chem.*, 180 (1961) 161.
5 S. P. Perone and K. K. Davenport, *J. Electroanal. Chem.*, 12 (1966) 269.
6 H. E. Zittel and F. J. Miller, *Anal. Chem.*, 37 (1965) 200.
7 T. Yoshimori, M. Arakawa and T. Takeuchi, *Talanta*, 12 (1965) 147.
8 H. C. Jones, W. L. Belew, R. W. Stelzner, T. R. Mueller and D. J. Fisher, *Anal. Chem.*, 41 (1969) 772.
9 W. T. de Vries, *J. Electroanal. Chem.*, 9 (1965) 448.
10 J. Heyrovský and J. Kůta, *Principles of Polarography*, Academic Press, New York, 1st ed., 1966, p. 111.
11 W. Kemula and Z. Galus, *Nature*, 184 (1959) 1795.

ELECTROANALYTICAL CHEMISTRY AND INTERFACIAL ELECTROCHEMISTRY
Elsevier Sequoia S.A., Lausanne – Printed in The Netherlands

OBSERVATIONS ON SOME APPARENT ANOMALIES IN THE YIELD OF STRIPPING OF Ag ON Pt. I

GIORGIO RASPI AND FRANCESCO MALATESTA

Istituto di Chimica Analitica ed Elettrochimica dell' Università di Pisa (Italy)

(Received February 12th, 1970)

It has been reported[1,4] that the charge consumed in the deposition could not be recovered in the stripping of Ag on Pt. Nisbet and Bard[2] observed that an appropriate "activating" treatment of the electrode surface resulted in a nearly 100% recovery of the charge consumed in the cathodic process, while oxidation or a prolonged use of the electrode without renewal of this treatment led to a significant diminution of the stripping yield. On the basis of the significant "retained" quantities of silver ($\cong$ 60 monolayers—calculated on the basis of bright electrode) these authors —excluding the possibility of oxidation of silver by the lower oxides of platinum— supposed a layer with Pt–O–Ag bonds which might have insulator properties at positive potentials and would inhibit the dissolution of the silver layers covering it.

Becker[3] ascertained that silver remains at the end of the stripping in the form of only partially destroyed crystals adherent to the platinum surface and found also mechanical silver losses under certain conditions.

Bixler and Bruckenstein[4] showed that the mechanism proposed by Nisbet and Bard was not valid. They observed that the differences between the anodic and cathodic quantity of electricity are very low, when a proper experimental technique is used, and could be completely explained by the capacitive contributions of the double layer charge. At preoxidized electrodes, still lower "yields" of stripping were found which has been interpreted by these authors as being due principally to cathodic contributions of the reduction of platinum oxides as well as to mechanical losses of silver.

Our measurements demonstrated that from doubtfully pure solutions (obtained with simply de-ionised water) the deposited silver usually does not dissolve completely during stripping because of pronounced but barely reproducible inhibition effects. From solutions of higher purity (obtained using bidistilled water) the differences between the quantity of silver theoretically deposited and that recovered in the stripping are much lower and demonstrate a specific dependence on the potential to which the electrode was polarized before performing the deposition.

Our measurements were made with a platinum microelectrode with periodical renewal of the diffusion layer[5], using a standard voltammetric technique, calculating —if necessary—a proper correction on the basis of the ohmic resistance of the cell. Some typical curves obtained when silver was deposited or dissolved are shown in Figs. 1a and 1b (the symbols used are explained in the Notation).

NOTATION

E^* equilibrium potential of the Ag^+/Ag (crystalline) couple; for very small amounts of deposited silver E^* does not correspond to the equilibrium potential of the Ag^+/Ag (deposited) couple
E_{ox} potential at which the electrode was maintained before starting the deposition
E_{dep} potential chosen for deposition at constant potential (Fig. 1b) equal to -0.400 V *vs.* SMSE if not otherwise indicated
E_{ip} potential at which the stripping was initiated (with a linear variation of the potential) when the deposition was carried out at the constant potential E_{dep} (Fig. 1b)
E_{fp} potential at which the stripping was finished
i_d mean limiting diffusion current of Ag (μA)
i_{fp} current observed at E_{fp}, measured with reference to the instrumental zero (μA)
t_{ox} time of treatment at E_{ox}
t'' time passed between the end of the treatment at E_{ox} and the beginning of that at E_{dep} (15 s if not otherwise indicated)
t_{dep} time at E_{dep}

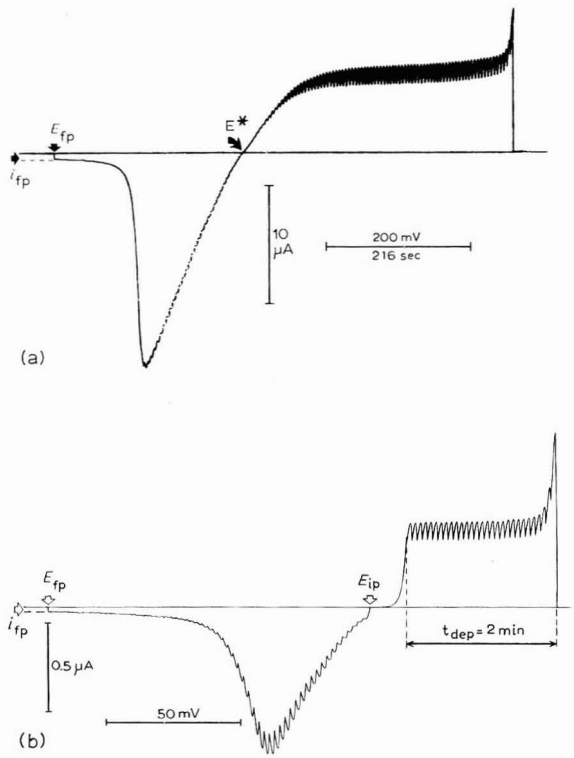

Fig. 1. Typical voltammetric curves obtained with a platinum microelectrode with periodic renewal of the diffusion layer when silver is deposited and stripped in 1 *M* $HClO_4$ soln. (a) Linear scanning of 2 V/36 min, $[Ag^+] = 1 \times 10^{-3}$ *M*; (b) deposition at controlled constant potential ($E_{dep} = -0.4$ V) and linear scanning stripping (1 V/36 min), $[Ag^+] = 4 \times 10^{-5}$ *M*.

t' time passed between the end of the deposition and the start of the stripping (30 s if not otherwise indicated)

q_c^0 $= i_d \times t_{dep}$ (μC), theoretical quantity of silver deposited at E_{dep}

q_c integral of the total observed cathodic current (resp. to the instrumental zero line) (μC)

q_a integral of the total anodic current observed up to E_{fp} (resp. to the instrumental zero line) (μC)

q_{Ag} quantity of silver at the electrode before the stripping was started (μC)

q'_{Ag} quantity of silver dissolved when the stripping was finished at E_{fp} (μC).

Symbols $>$ and $<$ when used before E refer to more positive and more negative potentials, respectively.

With rather concentrated ($[0.5\text{–}5] \times 10^{-3}$ M Ag^+, 1 M $HClO_4$) solutions it was observed that at potentials somewhat more negative than E^* the current slowly increases corresponding to a progressive increase of the surface of the electrode, while at potentials more negative by 200–300 mV than E^*, the current remains constant in time. A microscopic investigation (800 $\times$ magnification) of the deposits obtained at $E_1 = E^* - 20$ mV, $E_2 = E^* - 100$ mV and $E_3 = E^* - 300$ mV, respectively, shows a change in the structure of the deposit from well separated crystals (increasing surface during the deposition) to an apparently homogeneous deposit, the surface of which remains statistically unchanged on advancement of the deposition (Fig. 2a,b,c). This leads us to suppose that also in more dilute solutions the value of i_d remains constant with time if the potential is negative enough, and consequently the product $i_d t_{dep} = q_c^0$ (calculated on the basis of the concentration of Ag^+ ions) represents the quantity of silver deposited at the electrode during t_{dep}. Nevertheless the existence of a certain number of other contributions to the charge can be presumed (some of which play a significant role only at very small amounts of deposit) which cause the values of q_c^0, q_c, q_a, q_{Ag} and q'_{Ag} to be generally different from each other.

A. Capacitive contributions

The electrode maintained formerly at E_{ox} is brought to E_{dep}. After a period t_{dep} at E_{dep} and an interval t' at open circuit the potential is swept from E_{ip} to E_{fp}. Let us suppose that in the potential range used Ag^+ is the only depolarizer and further (for sake of simplicity) that at E_{fp} no trace of silver remains at the electrode. Evidently in the instant when E_{dep} is imposed a capacitive discharge can be observed which superimposes on the diffusion current of Ag for a short period; q_c would surpass q_c^0 because of a capacitive contribution which depends on the values chosen for E_{ox} and E_{dep} (Fig. 1b). During the period t' the potential of the electrode is shifted towards E^* with the deposition of a quantity of silver corresponding to the change in the capacitive charge. This effect leads to $q_{Ag} > q_c^0$ at the end of t'. In the course of the stripping up to E_{fp}, beside the dissolution of the quantity q_c^0 of silver, a further anodic "capacitive" contribution would exist (which includes also the dissolution of silver deposited during t') corresponding to the change in the electrode capacitive charge between the following two states: E_{dep}, electrode "silvered" and E_{fp}, electrode uncovered. Thus $q_a > q_c^0$ would result. Since the total process starts from the state E_{ox} (electrode uncovered) and terminates at the state E_{fp} (electrode uncovered), a difference corresponding to the change in the capacitive charge between these two states should exist between q_a and q_c. Therefore the relation $q_c \gtrless q_a$ corresponding to $E_{ox} \gtrless E_{fp}$ should

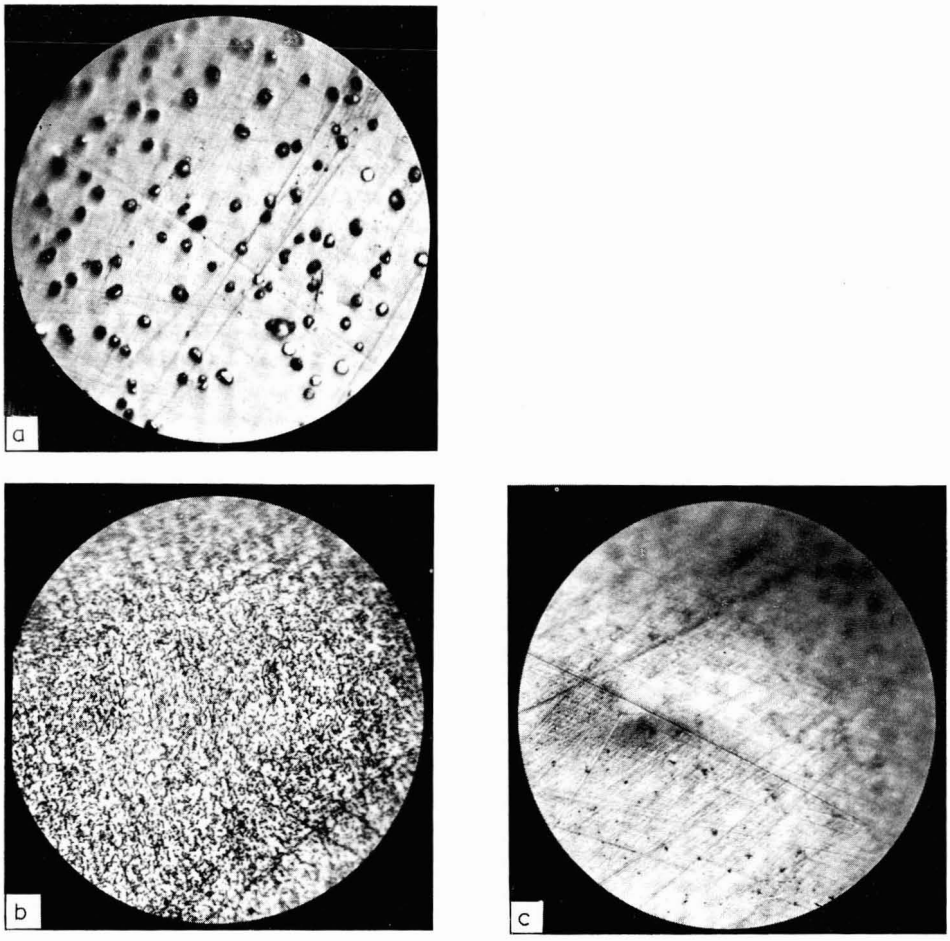

Fig. 2. Silver deposits (200–500 μC mm^{-2}) obtained with 1×10^{-3} *M* Ag^+ in 1 *M* $HClO_4$ soln.; E_{dep}: (a) -0.020 V *vs.* E^*, (b) -0.100 V *vs.* E^*, (c) -0.300 V *vs.* E^*.

exist. It should be noted that the simple capacitive effects cannot explain the occurrence of $q_a < q_c^0$. Further, the difference between q_c and q_a cannot be dependent on E_{ox} because of capacitive effects, at least not under our experimental conditions. Strictly speaking, the initial capacitive discharge at E_{dep} may initially cause (because of ohmic potential drop) silver deposition with a current i lower than i_d, but orientative calculations, based on an experimental evaluation of such an initial discharge, demonstrate that the phenomenon is interesting only at time intervals lower than the average error of determination of t_{dep}.

B. Pseudocapacitive contributions

If considerable differences exist in the surface oxidation state of the electrode at E_{ox}, E_{dep} and E_{fp}—other than the true capacitive contributions—these would lead to pseudocapacitive contributions causing differences in q_c^0, q_c and q_a in the same manner as has been described under A.

C. Incomplete reduction of substrate during deposition

If the deposition proceeds with a velocity such that the complete reduction of the underlying surface is hindered the situation will presumably be different from that indicated under B. The surface lying under the deposit would behave as an oxidant towards silver or would be electrochemically reduced while the silver is dissolved during stripping. The resulting effect will be a cathodic contribution which would result in a diminution in the absolute value of q_a. This is the first effect among those already considered which can justify theoretically the inequality $q_a < q_c^0$ and which permits a relation between q_a and E_{ox}.

D. Silver of activity less than one

According to the model of Rogers[6], a certain quantity of "monolayer" silver $M(E)$ is stable at the electrode surface at all potentials $E > E^*$. If contributions A, B and C are neglected for sake of simplicity and deposition of q_c^0 is performed at an electrode previously brought to equilibrium at E_{ox} we get $q_{Ag} = q_c^0 + M(E_{ox})$. Supposing that in the stripping equilibrium is reached at E_{fp}, the quantity of silver dissolved will be $q'_{Ag} = q_{Ag} - M(E_{fp}) = q_c^0 + M(E_{ox}) - M(E_{fp})$. This effect like effect C supplies a proof for $q_a < q_c^0$ at $E_{ox} > E_{fp}$, while at $E_{ox} < E_{fp}$ it leads to $q_a > q_c > q_c^0$ also because of simultaneous contribution of A and B. Effect D like C assumes a dependence of q_a on E_{ox}.

E. Mechanical losses

These may justify only diminutions in q_a both at $q_a < q_c$ and $q_a < q_c^0$. Their dependence on E_{ox}, however cannot be expected *a priori* but neither can it be excluded.

F. Overvoltages developing in initial periods of deposition

These effects may result in q_c^0 not representing the real quantity of silver deposited during t_{dep} and may lead therefore to $q_c < q_c^0$ and $q_a < q_c^0$. According to Bruckenstein[4] this effect could be verified by depositing silver (from solutions of $[1\text{–}5] \times 10^{-5}$ *M* Ag^+ in 0.1 *M* $HClO_4$) at 0 V (SCE) at an electrode maintained previously at 0 V (SCE) in a solution free of silver until a quantity of silver approximately enough for two monoatomic layers would deposit at the electrode.

G. Inhibition

According to the mechanism suggested by Nisbet and Bard[2] the dissolution of silver would cease when the remaining silver is no longer in direct contact with the platinum but joined by means of Pt–O–Ag bonds which show an insulator effect. As Bruckenstein[4] notes, a similar mechanism can hardly explain the effects referred to by Nisbet and Bard. A true inhibition mechanism caused by surface-active impurities would lead to analogous situations. Impurities which may be adsorbed at the surface of silver or built into the deposit, may not leave during the stripping process thus forming an inhibiting layer of increasing density which would increasingly diminish the rate of the dissolution and so only a part of the deposit would be dissolved at E_{fp}. A phenomenon of this type would increasingly develop as the deposition–stripping cycle is repeated and would lead to $q_a < q_c$ or $q_a < q_c^0$. However it is presumably possible that if a cleaning operation which may destroy or weaken the inhibiting layer is interposed at a given point of the deposition–stripping cycles, the reproduc-

tion of the quantity of silver retained previously at the electrode can be obtained and thus $q_a > q_c$. A dependence on E_{ox} cannot be expected *a priori* because the "history" of the electrode may be so complex that it may lead to completely irreproducible results.

H. Trace species which can be electrodeposited

a. If these give anodic deposits, the effect would be—according to the actual case—parallel to that of contributions B and C.

b. If these species give cathodic deposits and are present in the supporting electrolyte in a quantity which can disturb the measurements they can be taken into account by means of "blank" stripping experiments, with t_{dep} values much higher than those used commonly, and can be eliminated by pre-electrolysis at Pt cathodes of large surface.

I. Disturbing currents

These can be related to instrumental causes, and to non-depositable electroactive substances. They may be expected to influence the q_c and q_a values if these are determined relative to the instrumental zero line. A correction with a blank test may be insufficient since the base line with a silver-covered electrode can be markedly different from that measured with bright platinum.

K. Other depolarizers

The presence of foreign electroactive substances may cause another effect beside the inconveniences mentioned under I. If silver is not the unique depolarizer in the solution for the potential range investigated, contributions A and B would become dependent on t' (for the foreign reducible species) as well as C and D on t'' (reduction of the electrode or deposition of monolayer at open circuit after a reaction with oxidizable substances). A standardization of t' and t'', choosing these to be the shortest possible, allows the control of this effect and keeps it identical in each experiment of a given series (invariant additive contributions). A change in t' and t'' provides a possibility to determine the effects on q_c and q_a and to see whether these markedly influence the results.

EXPERIMENTAL

The following instruments and substances have been used:

1. Metrohm Polarecord type E 261.
2. Saturated mercury sulphate electrode of *ca.* 10 cm^2 surface.
3. Cell with platinum microelectrode with periodical renewal of the diffusion layer[5].
4. The cell was connected with a "lung" reservoir filled with the solution investigated by means of a glass bridge with two sintered filters. A salt bridge (ammonium nitrate in agar–agar gel) connected the "lung" with the saturated mercury sulphate electrode. A slight difference of level assured a slow streaming of the liquid from the cell to the "lung" preventing contamination. All ground joint contacts were fitted well enough not to require silicon greasing for tightening. The microelectrodes were treated before use (always once, if not otherwise indicated) with metallographic

alumina supported on chamois leather, then carefully washed, oxidized anodically in conc. HNO_3 for 3 min to the beginning of gas evolution, reduced in alcoholic KOH for a further 3 min to the beginning of H_2 evolution and finally kept for 5 min in conc. HNO_3 and then in conc. HCl. Between these various treatments they were carefully washed with bidistilled water.

5. $HClO_4$ from Carlo Erba of RP grade for preparation of the supporting electrolyte (1 and 0.1 M $HClO_4$) was generally not pre-treated. Experiments performed with $HClO_4$ previously electrolysed with Winkler electrodes up to gas evolution (48 h, each 200 ml of solution), with or without previously admixed silver (2.5 g/100 ml) in the form of perchlorate or nitrate, did not provide significantly differing results. Higher base currents were observed in the blank tests in the case of electrolytic pre-treatment in the presence of silver nitrate.

Experiments have been performed with various electrodes of area ranging between 2 and 6 mm^2. The qualitative results reported refer to an electrode of surface area estimated about 5.8 mm^2. The applied potential was changed with a speed of 1 V/36 min (0.4629 mV s^{-1}) and the recorder paper moved forward with the maximum velocity (4.16 cm min^{-1}) to enlarge the dimensions of the peaks. The integrals, q_c and q_a, were always determined with respect to the instrumental zero, also taking into account in q_a the contribution of the "tail" situated after the end of the peak itself (up to E_{fp}) (Fig. 1a,b). The presence of foreign substances electrodepositable in the potential range investigated (-0.500 to $+1.500$ V, SMSE) has been excluded after accurate blank stripping measurements.

The solutions were deaerated by bubbling N_2 through for 10 min before each series of measurements; the remaining traces of O_2 do not affect the results.

If not otherwise indicated t' was 30 s and t'' 15 s to ensure the constancy of contributions I and K which are not determined directly, for all measurements carried out with the same solution. The values of E_{ox}, E_{dep}, E_{ip} and E_{fp} were read off directly on the scale of the polarograph with an error of less than ± 5 mV.

The potential values reported in the present work refer to SMSE, if not otherwise indicated.

RESULTS AND DISCUSSION

1. Solutions prepared with bidistilled water

If silver is deposited at constant potential in the range of the limiting diffusion current from solutions prepared using water bidistilled from permanganate, the results are regularly reproducible. If the silver concentration is sufficient to allow an accurate reading of the cathodic deposition current ($[5\text{–}0.05] \times 10^{-3}$ M) it can be observed that q_c is higher than $q_c^0 = i_d \times t_{dep}$ because of an initial cathodic discharge effect which is higher the more positive the value of E_{ox} imposed previously. Such a discharge evidently does not represent an amount of deposited silver. At fixed t_{dep} values however it can be observed that the area of the anodic peak, q_a, decreases with increasing E_{ox}. The time t_{ox} should be long enough to assure the reproducibility of the results. In practice, if $E_{ox} = +1.0$ V, 5 or 7 min are sufficient for this purpose while if $E_{ox} < 0$ V the more dilute is the solution, the longer time t_{ox} should be: up to 30 min for a 2×10^{-6} M solution. Imposition of $E_{ox} = 0$ V brings complete reproducibility with very short t_{ox} duration if previously a deposit has been dissolved until $E_{fp} =$

0 V, while t_{ox} should be much longer and dependent on the dilution (30 min for 2×10^{-6} M solution) when the electrode had previously been oxidized at +1 V. In plots of q_a *vs.* t_{dep} for various E_{ox} values a family of parallel lines is obtained for different silver concentration (Fig. 3). The slope of these lines is sufficiently consistent

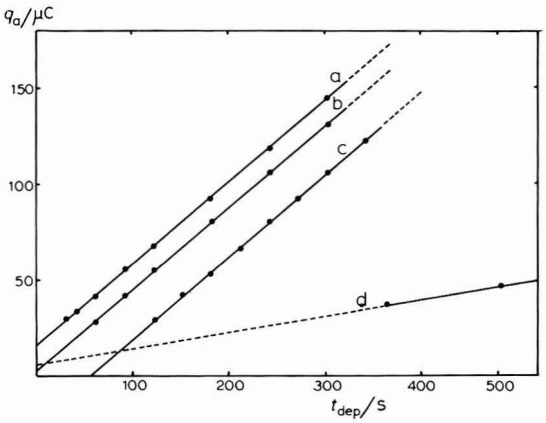

Fig. 3. Variation of q_a *vs.* t_{dep}: $[Ag^+] = 4 \times 10^{-5}$ M (a, b, c), 8×10^{-6} M (d); $E_{ox} = -0.125$ V (a, d), 0.00 V (b), +1.00 V (c). Line d was obtained from expl. data by ranging t_{dep} between 6 and 30 min.

with i_d (Table 1) thus excluding the possibility of significant relative losses. Thus the experimental value, q_a, differs from the theoretical quantity of silver deposited (q_c^0) only by additive constants which depend on E_{ox} and the concentration. The $q_a - q_c^0$ difference can be determined experimentally for each solution and for each value of E_{ox}, thus being represented by the ordinate at the starting point of the corresponding plot. The cases $E_{ox} = 0$, $E_{ox} < 0$ and $E_{ox} > 0$ ($E_{fp} = 0$ V) will be discussed separately below.

$E_{ox} = 0$ V. With this condition q_c and q_a are identical (Table 2). On the basis of the contributions introduced above, this identity is justified only if it is supposed that for $E_{ox} = 0$ V only those possibilities A, B, C and D would exist (the first two equal for

TABLE 1

Comparison of i_d values obtained from cathodic current (i_d [exptl.]) and i_d values obtained from q_a *vs.* t_{dep} plots (i_d [calcd.]). The i_d [exptl.] values are affected by an absolute error of about ± 0.05 μA, the i_d [calcd.] values are affected by a percentual error of about $\pm 1\%$.

$[Ag^+]$ /mmol l^{-1}	i_d[exptl.] /μA	i_d[calcd.] /μA	i_d[calcd.] $[Ag^+]^{-1}$ /μA l mmol^{-1}
1	10.8 (a)	10.7 (a)	10.7
3×10^{-1}	3.2_2(a)	3.23(a)	10.8
1×10^{-1}	1.1 (a)	1.07(a)	10.7
4×10^{-2}	0.4_4(a)	4.31×10^{-1}(a)	10.8
2×10^{-2}	(c)	2.17×10^{-1}(b)	10.8
8×10^{-3}	(c)	8.55×10^{-2}(b)	10.7
2×10^{-3}	(c)	2.15×10^{-2}(b)	10.8

(a) $E_{dep} = -0.400$ V. (b) $E_{dep} = -0.500$ V. (c) Undetectable.

TABLE 2

Comparison of q_c, q_a, q_c^0 for $E_{ox} = E_{fp} = 0$ V

$[Ag^+]$/ mol l^{-1}	t_{dep}/s	$q_c/\mu C$	$q_a/\mu C$	$q_c^0/\mu C$
1×10^{-3}	30	326	322	323
1×10^{-3}	60	650	648	645
3×10^{-4}	60	195	197	194
3×10^{-4}	180	580	588	581
1×10^{-4}	120	132	132	129
1×10^{-4}	180	196	193	194
4×10^{-5}	120	56	54	52
4×10^{-5}	180	82	81	78
4×10^{-5}	240	109	106	103

q_c and q_a, the others theoretically zero for $E_{ox} = E_{fp}$). The effects of the remaining contributions taking these into account in turn, can be considered negligible: the supposition that these can amount to zero by reciprocal compensation can be discarded on the basis of the results reported in Table 2. In this case the value of $q_a - q_c$ thus represents the sum of the capacitive and pseudocapacitive effects which is about 2–3 μC (2.7 μC from line b in Fig. 3).

$E_{ox} < 0$ *V*. As E_{ox} becomes more and more negative ($E^* < E_{ox} < 0$) the value of $q_a - q_c^0$ gradually increases up to values which are not yet explicable on the basis of capacitive contributions which certainly do not exceed 2–3 μC, observed at $E_{ox} = 0$.

B, D and I are the only contributions among the others which may cause an increase in the value of $q_a - q_c^0$. Considering the fact that the deposits are dissolved always in the same manner, contribution I should be negligible as in the case of $E_{ox} = 0$ previously examined. Contribution B, at constant E_{ox}, can increase only if the concentration of silver decreases, and consequently at E_{dep} the time interval during which the electrode surface can be reduced before it is covered by the deposit would be longer. Since such an increase does not appear (*cf.* the ordinates at the starting point of plots a and d in Fig. 3) contribution B can also be ruled out. Consequently it seems that the high values of $q_a - q_c^0$ are to be attributed solely to the existence of silver of less than unit activity.

$E_{ox} > 0$ *V*. The ordinate at the starting point of the plot obtained with $E_{ox} = +1.0$ V is clearly negative (line c, Fig. 3). This corresponds to the "loss" of a silver quantity quite significant compared with the deposit (24–28 μC, depending on the concentration of the solution). If the values of E_{ox} are in the range between 0 and +1.0 V the starting ordinates of the lines obtained are between the negative value mentioned above and the value of line b in Fig. 3. For $E_{ox} > +0.6$ V the starting ordinates will be independent of further changes in potential towards more positive values: it achieves a "limiting loss". The decrease in the stripping yield can generally be attributed to contributions I, K, C, E, F, G, Ha, D. Since the stripping of the deposits is performed in the same manner it is not reasonable to suppose that I and K can depend on E_{ox} and were therefore responsible for the low yields observed. The effect of oxidation at +1.0 V can be eliminated if 0 V potential is imposed for sufficient time before the deposition; in this case the behaviour of the electrode is the same

as would be observed when $E_{ox} = 0$ V is applied directly. Now in the case of dilute solutions the electrode remains at E_{dep} for an appreciable period before it becomes completely covered. Thus a significant decrease in the "losses" would be expected compared to those observed with more concentrated solutions. This could not be verified: the limiting loss decreases only slightly with decreasing concentration (from 28 to 26 μC for more concentrated solutions towards 26 to 24 for more dilute solutions of the series). Only the hypothesis that silver of activity less than unity is present up to very positive potentials can fully justify a behaviour such as this: the monolayer destroyed at +1.0 V would be re-formed "at the expense" of the silver deposited at E_{dep} and the whole quantity $M(0) - M(+1\text{ V})$ cannot be dissolved in the stripping.

2. Solutions prepared with deionized water

In solutions prepared with simply deionized water the regular behaviour described above cannot be verified. Generally the value of the $q_a - q_c$ difference is much larger and its dependence on the history of the system is so complicated that it appears to be practically irreproducible. The investigations were carried out with silver concentrations above 1×10^{-4} M, in 1 M $HClO_4$ and with rather large amounts of deposits (100–500 μC mm^{-2} of the electrode). Under such conditions the integrals q_c and q_a can diverge substantically from each other solely because of the effects of contributions E and D which are the only ones which can become more important with increasing amount of deposit. Whether deposition is carried out at constant potential and dissolution at linearly changing potential, or the whole voltammetric curve is recorded from E_{dep} to E_{fp} (with various E_{dep}—not necessarily in the range of the diffusion limiting current—and E_{fp} values), generally q_a values lower than q_c can be observed. q_a values near to 100% of q_c can be obtained in the first measurements after having immersed the electrode with pre-treated surface (*cf.* Experimental 4) in the cell, but the "yield" diminishes progressively in succeeding measurements. No rule has been found to predict after how many deposition–stripping cycles the decreases in yield would become serious or to estimate their magnitude. Apparently the phenomenon is strongly influenced by a number of parameters, *e.g.* duration in the cell (also in open circuit state), the quantity of the deposits formed, the imposed value of E_{fp}, the oxidizing conditions chosen to liberate the surface of the electrode from all traces of silver, the potential of deposition. The following conditions usually accelerate and increase these phenomena (causing a progressive decrease in the yield): oxidation of the electrode until oxygen evolution begins in the solution investigated; leaving the deposit to age for some time at the electrode at open circuit; deposition at potentials in the neighbourhood of E^*, addition of agar–agar to the solution; depositing very large quantities of silver. Generally the phenomenon manifests itself in a progressive increase of the anodic current i_{fp} (in absolute value) parallel with the deformation of the peak itself which will become increasingly flatter. The anodic current which should obey the equation

$$E = E^* + 0.059 \log(i_d - i)/i_d \qquad (1)$$

until the deposit retains a constant area and the process is controlled by diffusion, decreases greatly relative to the theoretical value (gradually as the experiments are repeated). After the maximum of the peak the current successively approaches the

value of i_{fp} instead of dropping rather steeply to zero, as can be observed with solutions prepared using bidistilled water. The relative "losses" are very significant with respect to the deposited quantity, and are of the order reported by Nisbet and Bard[2], or even higher. Though the existence of mechanical losses cannot be excluded *a priori*, a significant part of the silver which does not undergo anodic oxidation remains in fact at the electrode and accumulates in increasing quantities as the cycle is repeated. This can be observed also microscopically in the form of a crystalline layer which is rapidly destroyed if the electrode is immersed in cold conc. nitric acid. On the other hand the anodic dissolution of these amounts of silver in the cell is very slow and if the applied potential is progressively increased the current does not change notably with respect to i_{fp} observed at E_{fp}. The solutions concerned show evidence of the presence of impurities which are able to influence greatly the kinetics of the dissolution of silver. Besides the deviation from eqn. (1)—which is verified for deposits of Tl and Hg as well as (with good approximation) for those of silver in solutions prepared from bidistilled water—if a deposit of the type of that in Fig. 2c is dissolved at constant potential, the current does not remain constant for the given time and thereafter does not drop rapidly to zero (as occurs in solutions prepared with bidistilled water) but decreases gradually as an inhibiting surface layer would accumulate. With deposits of the type of Figs. 2a and b which theoretically could never follow eqn. (1), the recorded voltammetric curve shows a horizontal inflexion corresponding with E^* which cannot be brought into agreement with the variation of the surface of the deposit but which should be explained with slow kinetics of the electrode process. Though the effective surface area of the deposit at which the exchange reaction, $Ag^+ + e^- \rightleftharpoons Ag$ occurs, may remain lower (because of the more regular order in the crystal) than that in the case of deposits of the type of Fig. 2c which do not show such inflexion, it is necessary to suppose (in accordance with the known reversibility of the Ag^+/Ag couple) that it is dependent on the presence of some impurities. Having left a deposit to age for some time (from 2 h to some days) in the solution, this could not be dissolved without starting from potentials higher than about 10–30 mV more than expected. It is possible to deposit directly a very small amount of silver which in the stripping phase would be dissolved separately (Fig. 4). The effect is too strong to correlate it with a lattice stabilization and thus it must be connected with an accumulation of surface active impurities which are able to passivate the electrode in the open circuit state.

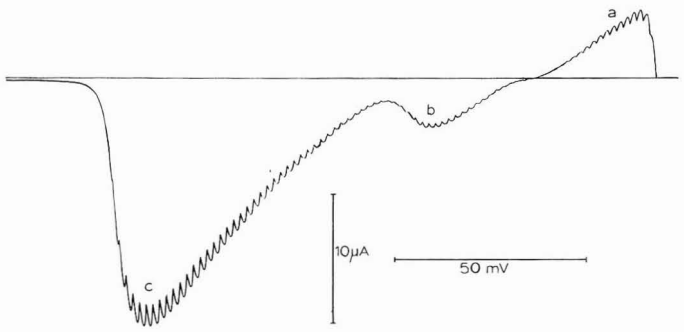

Fig. 4. Voltammogram with deposition (a) of a small amount of silver onto aged silver deposit, and consecutive stripping of fresh (b) and aged (c) deposits.

CONCLUSION

The highly anomalous yields in the stripping of silver in solutions prepared using simply deionized water are due to surface-active impurities which are capable of passivating the deposits. The results obtained with solutions prepared from bi-distilled water cannot be attributed to the presence of traces of impurities of this kind. The quantity of electricity in the anodic process (q_a) proves to be a function of the potential to which the electrode has been pre-polarized before deposition. The value of q_a may be greater than the quantity of silver deposited theoretically (q_c^0) when the potential of pre-polarization was more positive than that of equilibrium by only a few tens of millivolts: the difference can assume values which cannot be justified on the basis of only the capacitive contributions suggested previously[4]. If the electrode is pre-polarized at very positive potentials q_a would be lower than q_c^0.

Taking into consideration the various contributions which may cause changes in the values of q_a, only the one deriving from the existence of silver of less than unit activity is in complete accordance with the results obtained.

SUMMARY

Measurements have been made to resolve the anomalous yields observed in the stripping of silver at platinum by using a platinum microelectrode with periodic renewal of the diffusion layer. Taking into account the various contributions which may cause changes in the value of the quantity of electricity in the process, only that deriving from the existence of silver of less than unit activity is in complete accordance with experimental results.

REFERENCES

1 S. S. LORD JR., R. C. O'NEILL AND L. B. ROGERS, *Anal. Chem.*, 24 (1952) 209.
2 A. R. NISBET AND A. J. BARD, *J. Electroanal. Chem.*, 6 (1963) 332.
3 J. J. BECKER, *J. Electrochem. Soc.*, 111 (1964) 480.
4 J. W. BIXLER AND S. BRUCKENSTEIN, *Anal. Chem.*, 37 (1965) 791.
5 D. COZZI, G. RASPI AND L. NUCCI, *J. Electroanal. Chem.*, 6 (1963) 275; 6 (1963) 267; 12 (1966) 36.
6 J. T. BYRNE AND L. B. ROGERS, *J. Electrochem. Soc.*, 98 (1951) 457; L. B. ROGERS AND A. F. STEHNEY, *J. Electrochem. Soc.*, 95 (1949) 25; L. B. ROGERS, D. P. KRAUSE, J. C. GRIESS JR. AND P. B. EHRINGER, *J. Electrochem. Soc.*, 95 (1949) 32; J. C. GRIESS JR., J. T. BYRNE AND L. B. ROGERS, *J. Electrochem. Soc.*, 98 (1951) 447; J. T. BYRNE, L. B. ROGERS AND J. C. GRIESS JR., *J. Electrochem. Soc.*, 98 (1951) 452.

ELECTROANALYTICAL CHEMISTRY AND INTERFACIAL ELECTROCHEMISTRY
Elsevier Sequoia S.A., Lausanne – Printed in The Netherlands

OBSERVATIONS ON SOME APPARENT ANOMALIES IN THE YIELD OF STRIPPING OF Ag ON Pt

II. EXISTENCE OF TWO DIFFERENT MONOLAYERS OF SILVER ON PLATINUM

F. MALATESTA AND G. RASPI
Istituto di Chimica Analitica ed Elettrochimica dell' Università di Pisa (Italy)
(Received February 12th, 1970)

It is known that various metals can deposit from very dilute solutions at electrodes prepared from different metals[1-3]. This effect was first investigated by the school of Rogers. On the basis of simplified hypotheses the "theoretical" distribution of a metallic monolayer on the surface of another metal was calculated[4,5] and it was verified by means of ^{111}Ag that the deposition of silver from dilute solutions at Pt and Au electrodes was in accordance, at least qualitatively, with these hypotheses[6-8].

Re-investigating and possibly simplifying the hypotheses of Rogers, Nicholson[9] derived and tested the equation of dissolution of a monolayer at a stationary electrode under conditions of linear sweep of potential: it could be verified that this equation describes rather satisfactorily the dissolution of small quantities of Ag at Pt, less exactly that of Pb at Pt and even worse that of Cu at Pt. When Nicholson attempted to extend the equation calculated for the case of submonolayer deposits of nickel on platinum and gold[10] he observed the presence of two distinct oxidation peaks instead of only one, which he attributed to the heterogeneity of the electrode surface. Nevertheless this phenomenon seems to be rather general, since Perone observed multiple peaks in the dissolution of silver[11] and later of Hg[12] at graphite. Subsequently Vassos and Mark[13] when studying the initial steps of deposition of Cu on pyrolytic graphite observed three distinct peaks in the stripping which are due to the dissolution of the crystalline deposit, to a first "monolayer" deposit and to a second more stably bound "monolayer". Breiter[14] and somewhat later Bruckenstein[15] ascertained that copper also forms two different monolayers before it can produce crystalline deposits at Pt.

Our measurements, which have been designed to explain definitely the anomalous yields observed in the stripping of silver at platinum[16], demonstrate that also with Ag on Pt two deposits of "monolayer" type, clearly different from each other, can be obtained before the crystalline silver deposit. The more unstable of these monolayers is distributed in a rather restricted potential range which is confined by the deposition range of crystalline silver. The other is destroyed at very positive potentials and yields only very flattened peaks in the stripping which can be easily masked by the base line current. Thus these peaks cannot be readily observed directly; this explains why they have not been identified until now, although the measurements of the school of Rogers showed the existence of small quantities of silver which could not be removed from the electrode even under much more drastic conditions than

those expected to be necessary for the monolayer.

According to our results, the anomalous yields observed when the cathodic and anodic quantities of electricity in deposition and stripping of silver on platinum were compared, depend in effect (if there are no particular impurities in the solution) on the presence of these monolayers of silver. The capacitive contributions do exist[17] but are of appreciably less importance. Under the conditions chosen by us no mechanical losses were present.

EXPERIMENTAL

The symbols adopted and the names of the various contributions are as in the previous work[16]. The experimental method was essentially the same: 0.1 M $HClO_4$ solutions prepared with water bidistilled from neutral permanganate were used exclusively with silver concentrations ranging between 2×10^{-4} and 2×10^{-6} M. All depositions were performed at a constant potential of -0.500 V *vs.* SMSE, sufficient to assure the attainment of the limiting current even with the most dilute solutions of the series. All the quantitative results refer to an electrode of area geometrically estimated as 5.8 mm^2. In all the experiments the stripping was performed proceeding from $E_{ip}=E^*+15$ mV to $E_{fp}=0$ V, the potential changing at a rate of 1 V in 36 min (0.463 mV s^{-1}). In recording the anodic peaks the same instrumental sensitivity was always used (5×10^{-9} A mm^{-1} of ordinate) to compensate instrumental errors. Deposition time was regulated according to the concentration to obtain deposits always of the order of 50–200 μC, comparable with the effects to be investigated. Thus t_{dep} was varied from 60 s, for the most concentrated solutions of the series ($[1–2]\times10^{-4}$ M) to 30 min for the most dilute solutions (2×10^{-6} M), with an error of about 0.3 s. Under the conditions chosen, in the recording 1 μC corresponded to about 1.4 cm^2 (1.386 cm^2); thus the errors introduced by integration were at most fractions of a microcoulomb.

Integrals of the anodic peaks, q_a, were determined always with respect to the instrumental zero, including the contribution of the "tail" after the true peak (up to E_{fp}). In this manner not only are all the various capacitive and pseudocapacitive contributions (together with those caused by silver of less than unit activity) included in q_a up to E_{fp} but also those due to base line disturbing currents (contribution I, ref. 16). Nevertheless the latter appear to be equal for all the anodic peaks obtained in a given solution, at t_{dep}, E_{ip}, E_{fp}, for which the variation in q_a as functions of E_{ox} can be independent of the existence of disturbing base line currents. In the course of our experiments contributions I were always very small and therefore did not introduce in any case appreciable errors if the working conditions were chosen in a manner to retain the silver constituting a second monolayer at the electrode.

RESULTS AND DISCUSSION

It has been shown in the previous work[16] that if the values of q_a are plotted *vs.* the corresponding t_{dep} values at a given E_{ox}, a straight line is obtained the slope of which represents i_d. The possibility of determining precisely the value of i_d in this manner makes it convenient to plot the values of the difference $q_a-q_c^0$ *vs.* E_{ox} by simply determining the values of q_a at various E_{ox} and subtracting from these the corre-

sponding calculated values of q_c^0. The observed shape is reported in Fig. 1, for three different concentrations. If only contributions A, B, C and D [16] are taken into account, all the plots $q_a - q_c^0 = f(E_{ox})$ should coincide at $E_{ox} = E_{fp}$. In reality the presence of contributions other than A, B, C and D (as well as presumably I) causes the value of $q_a - q_c^0$ for $E_{ox} = 0$ V to be not exactly identical for all solutions but shows oscillations of ± 1 μC. Since these deviations are small enough to be neglected in Fig. 1, the plots there were drawn arbitrarily to coincide at $E_{ox} = 0$ V. This displacement corrects empirically the difference due to an incomplete reproducibility of the base line currents but does not introduce any preconception about the significance of the results which are derived from the form of the curves and not from their position relative to the horizontal zero axis. It can be pointed out that if a different value is chosen for E_{dep}, or for the position of the instrumental zero line for carrying out the integration, this would only cause a parallel displacement of all the curves upwards or downwards. An analogous effect would be caused by variations in E_{fp}, but then the curves would

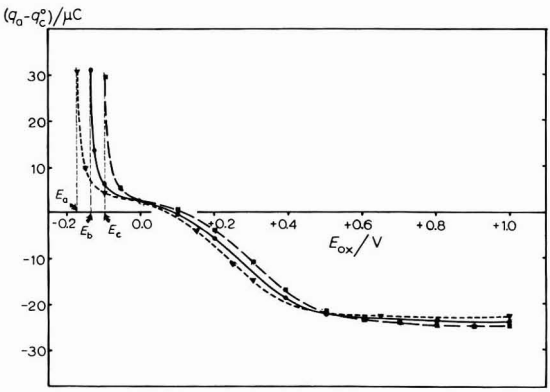

Fig. 1. $q_a - q_c^0$ dependence on E_{ox} for silver deposits in 0.1 M $HClO_4$ solns. $E_{fp} = 0.000$ V; $E_{dep} = -0.500$ V. (▼) 8×10^{-6} M Ag^+, $t_{ox} = 7$ min ($E_{ox} > 0$ V), 30 min ($E_{ox} < 0$ V), $E^* = E_a = -0.175$ V; (●) 4×10^{-5} M Ag^+, $t_{ox} = 7$ min ($E_{ox} > 0$ V), 15 min ($E_{ox} < 0$ V), $E^* = E_b = -0.135$ V; (■) 2×10^{-4} M Ag^+, $t_{ox} = 7$ min ($E_{ox} > 0$ V), 7 min ($E_{ox} < 0$ V), $E^* = E_c = -0.095$ V.

coincide at a new value of E_{ox} (equal to E_{fp}). Neither could E_{dep} be chosen as being much more positive than -0.500 V if we want to guarantee that the deposition occurs in the range of the diffusion limiting current even with the most dilute solutions of the series, nor much more negative to avoid the reduction of hydrogen which distorts the values of q_a. Neither could E_{fp} be chosen much more negative than 0 V if we would like to insure the dissolution of all silver even in more concentrated solutions in which E^* is not particularly negative, nor as being positive by choice because beyond a given limit the residual currents increase rapidly and thus q_a would include a contribution I, of order commensurable with q'_{Ag}.

In the curves shown in Fig. 1 a trend can be observed of an increase of $q_a - q_c^0$ towards very positive values (up to about 30 μC) if E_{ox} approaches E^* (this last value can be precisely determined by short-circuiting the electrode with an electrically silvered auxiliary microelectrode in the same solution). In the previous communication [16] it has been suggested that the particularly high values of $q_a - q_c^0$ observed for $E_{ox} < 0$ V depend on the presence of silver of less than unit activity at the electrode

surface. In agreement with this hypothesis the potential at which a certain amount of monolayer silver should be stable at the electrode, should be displaced according to the Nernst equation by changing the concentration of silver in the solution. The curves reported in Fig. 1 demonstrate just such a displacement of about 40 mV relative to each other corresponding to the value calculated (41 mV) for the actual silver concentrations.

With suitable concentration ($[5–1] \times 10^{-5}$ *M* in silver for the type of electrode used by us[18] with a periodic renewal of the diffusion layer of 4–5 s) and potentials between 0 V and E^*, the deposition of the monolayer can be directly observed. After having changed the potential from $E_{ox} = 0$ V to an E_1 value chosen in this range (0 V–E^*), a cathodic current flow can be observed (after a short initial discharge) with lower intensity than i_d, which shows the typical regular periodic oscillations characteristic of processes controlled by diffusion at the electrode employed by us (Fig. 2). This current decreases after a certain period to zero and its total integral,

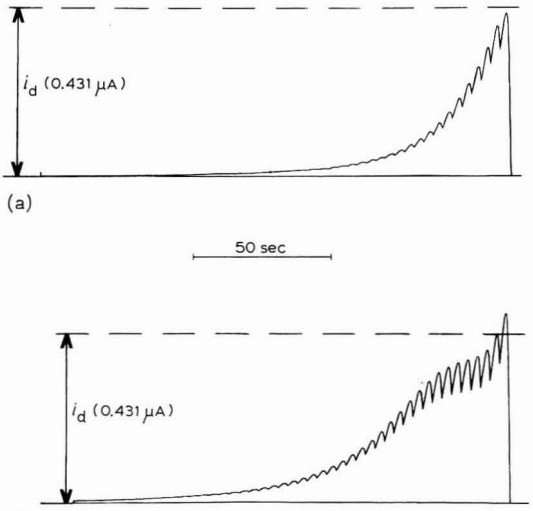

Fig. 2. Deposition of less than unit activity silver at potential $E_1 > E^*$ in 0.1 *M* $HClO_4$, 4×10^{-5} *M* Ag^+ soln. (a) $E_{ox} = 0.000$ V, $E_1 = -0.120$ V; (b) $E_{ox} = +0.100$ V, $E_1 = -0.130$ V.
Observed charges: (a) 9.6 μC, (b) 19.7 μC.

including the more intensive initial discharge, agrees to within 10% with the difference between $q_a - q_c^0$ for $E_{ox} = E_1$ and $q_a - q_c^0$ for $E_{ox} = 0$ V in the same solution. If the electrode is stripped at this point from E_1 to 0 V a very suppressed peak can be observed, the integral of which is equal to that of the preceding one. If a more negative value is chosen for E_1 or a more positive one for E_{ox}, the value of the cathodic integral increases (as expected) without the intensity of the observed cathodic current surpassing the value of i_d: it simply remains nearly constant for a longer period before it falls to zero (Fig. 2a,b). All this is in perfect agreement with the hypothesis that at E_1 silver of less than unit activity is deposited.

The form of the $q_a - q_c^0$ curves shown in Fig. 1 demonstrates that the amount of

silver constituting the monolayer identified above, decreases nearly exponentially with increasing potential, reaching zero at about +150 mV *vs.* E^*, in correspondence with the nearly horizontal section in which the yield depends only slightly on the potential (first plateau). The next successive diminution of the value of $q_a - q_c^0$, until the situation is reached of limiting loss which remains constant even beyond the potential range of the initial O_2 discharge (second plateau), should therefore be attributed to different reasons:

C. (or H.a) oxidizing effect of the substrate, incompletely reduced at E_{dep};

D. existence, even after the first plateau, of appreciable amounts of silver of less than unit activity (in such a case there would be a "second monolayer", M′, noticeably more noble than the one already identified);

E. mechanical losses of silver with characteristic dependence on E_{ox};

F. incomplete deposition because of the effect of overpotentials being higher the more positive is the previously imposed potential, E_{ox};

G. inhibition, because of the effect either of surface-active impurities or of the mechanism suggested by Nisbet and Bard[19];

I, K. disturbing currents and presence of foreign non-electrodepositable, electroactive species which in the actual dissolution process may carry cathodic contributions depending on the pre-imposed value of E_{ox}.

It has been already assumed in the preceding work[16] that the negative values of $q_a - q_c^0$ observed for $E_{ox} > 0$ V should be connected only with the existence of silver of less than unit activity on the electrode. Nevertheless, stronger evidence for this dependence is given by the following series of experiments (Table 1):

α. In a silver-free perchlorate solution the electrode is polarized to +1.0 V for 10 min, then to 0 V for 20 (40) min. Then the circuit is opened and the desired quantity of silver ions are introduced. After waiting for 5 min (proved to be sufficient for complete mixing) the deposition is started at −0.500 V for a t_{dep} period which is suitable to the actual concentration. Then the stripping peak is recorded from E_{ip} to $E_{fp} = 0$ V, measuring the integral, $q_a(\alpha)$.

β. In the same solution, which now contains Ag^+, the electrode is polarized again for 10 min at +1.0 V, then for 20 min (40 min if the solution is very dilute, *e.g.* 2×10^{-6} *M* Ag^+) at 0 V. After waiting for 5 min with open circuit, the deposition is carried out as under α and the integral $q_a(\beta)$ is determined.

γ. Immediately thereafter the oxidation at +1.0 V is repeated for 10 min, then deposition is performed directly at E_{dep} as under α and the deposit is dissolved in the usual manner, determining thus the integral $q_a(\gamma)$.

δ. Control. It is proved that 20 min (40 min with more dilute solutions) is

TABLE 1

$[Ag^+]$ /mol l^{-1}	$[q_a(\beta) - q_a(\gamma)]$ /μC	$[q_a(\delta) - q_a(\gamma)]$ /μC	$[q_a(\beta) - q_a(\alpha)]$ /μC	$[q_a(\alpha) - q_a(\gamma)]$ /μC
2×10^{-4}	27.5	27.2	5.8	21.7
4×10^{-5}	26.8	26.3	6.7	20.1
1×10^{-5}	24.4	24.6	11.7	12.7
5×10^{-6}	24.4	25.0	15.2	9.2
2×10^{-6}	24.0	24.6	19.2	4.8

sufficient to achieve the equilibrium by comparing $q_a(\beta)$ with $q_a(\delta)$, where δ stands for a peak obtained in the following manner: after having performed stripping of a preceding deposit (*e.g.* γ or β or α) up to $E_{fp}=0$ V, the potential is left at 0 V for some time (2–20 min), then deposition is carried out by the usual method at -0.500 V, the stripping peak is recorded and the integral $q_a(\delta)$ is determined. It can be observed that 20 min at 0 V is generally enough to obtain $q_a(\beta)=q_a(\delta)$ but in the case of particularly dilute solutions longer time is required (40 min for 2×10^{-6} M Ag^+).

The only hypothesis which explains why $q_a(\alpha)<q_a(\beta)$ should always be obtained (see Table 1) is the supposition that in procedure β silver of less than unit activity is deposited*. The existence of a "second monolayer" of silver on platinum is thus evident.

The charges corresponding to the two "monolayers", from Fig. 1, are practically equal to each other and amount to nearly 27 μC. If a cross-section commensurable with that of crystalline silver is attributed to a silver atom in the monolayer, 1 mm^2 of the monolayer corresponds to nearly 2.24 μC. This means that either our electrode had an effective elementary surface of at least 12 mm^2 (against 5.8 mm^2 evaluated geometrically) or the so-called "monolayers" are not of true monoatomic character.

It can be seen in Table 1 that the value of $q_a(\beta)-q_a(\gamma)$ decreases with decreasing concentration. This is due partly to the fact that $E_{fp}=0$ V was always imposed: then all the $q_a-q_c^0=f(E_{ox})$ curves coincide with each other at $E_{ox}=0$ V. Since the amount of "monolayer" silver present at the electrode at $E_{ox}=0$ V is the lower the more dilute is the solution, it is logical that the difference $q_a(\beta)-q_a(\gamma)$ decreases with decreasing concentration. An influence of the effect C or of other contributions different from D is partly possible in the more concentrated solutions of the series, nevertheless it is evident that this is very small in our case.

The typical distribution of silver on the electrode should be determined from the curves shown in Fig. 1 (differentiating *vs.* E_{ox}) as a function of the potential. Nevertheless this calculation is not exact because the experimental points are distributed within too broad error limits, especially in the range between 0 V and $+0.6$ V. The "first monolayer" occurs only in a rather restricted potential range which is adjacent to the range in which the crystalline silver is stable and for which the dissolution of crystalline silver and the silver of the first monolayer cause one common peak in a normal stripping test. The second monolayer shows a quasi-statistical distribution, with a maximum at about $+0.450$ V *vs.* E^*, in such a broad potential range that it can give rise to very flattened peaks generally masked by the base currents which are very sensitive in this range (at least with the solutions used by us). The situation is therefore much less favourable than has been described by Vassos and Mark[13] for copper at pyrolytic graphite or by Bruckenstein[15] for copper at platinum, in so far as it is not easy to identify the peaks due to dissolution of (i) the crystalline deposit, (ii) the first

* According to this supposition $q_a(\alpha)=q_a(\gamma)$ should also have been observed, but this condition could not be realized since during the 5 min waiting time after the introduction of silver in procedure α, a certain amount of silver of the second monolayer deposits "spontaneously" (either causing a displacement of the electrode potential from 0 V towards more positive values, with an eventual oxidation of the platinum surface, or because of the reaction with depolarizing impurity substances). Thus in this case $q_a(\alpha)$ must decrease and approach to $q_a(\gamma)$ with diminishing silver concentration (the maximum quantity of silver which can be deposited in 5 min is limited by the actual diffusion current and thus by its concentration), as can be seen in Table 1.

and (iii) the second monolayer in the voltammetric curve.

The possibility of obtaining double peaks in the stripping has been described in the previous communication[16] in so far as a "fresh" deposit is formed over a preceding aged deposit in rather impure solutions. This is not due to the presence of silver of different activity but is a kinetic phenomenon due to the passivation of the older deposit (impurities). In fact, those amounts of silver which cause the second peak cannot be deposited at potentials more positive than E^*.

In the course of our measurements it has been observed that so long as the "second monolayer" is present on the electrode, the disturbing currents due to the presence of foreign substances can be neglected practically over the whole potential range $+0.200$ to -0.500 V. This is proved by: (a) the low value of i_{fp} and further by the possibility of obtaining negligible currents after a certain period necessary to achieve the equilibrium in the whole range between $+0.200$ V and E^*; (b) the identity of q_a with q_c for $E_{ox}=0$ V $(=E_{fp})$ observed for different concentrations[16]; (c) the proportionality without additive constants between i_d and the silver concentration in the solution. Nevertheless in silver-free solutions both anodic and cathodic base line currents of a certain intensity can be observed. The species which cause these currents are not electrodepositable. It has been proved (by variation of t') that the reducible species were not able to oxidize the silver chemically (at least in appreciable amounts) in the period between the end of the deposition and the end of stripping; however such species were electroreducible between E^* and E_{fp} in silver-free solutions onto smooth platinum. By imposing potentials positive enough to destroy the second monolayer in silver solution, the current changed rapidly, reaching the anodic values observed in silver-free solutions. In supporting electrolytes at less positive potentials anodic currents can already be observed. If after the (at least partial) destruction of the second monolayer less positive potentials were imposed, a base line current, initially equal to that observable in silver-free solution, was superposed on the current due to the deposition of silver until a sufficient quantity of it was deposited. This explains why the deposition of the second monolayer has not been directly observed but only a part of the deposition of the first: in fact, if the second monolayer is absent the deposition is masked.

CONCLUSION

In confirmation of the previous work[16], it has been possible to show definitely that the apparent anomalies in the yield found in the stripping of silver at platinum in perchlorate solutions prepared with bidistilled water, are due to silver of appreciably lower activity than crystalline silver.

Silver gives three distinct types of deposit on platinum: the first two, containing silver amounts commensurable with that of monoatomic layers, can deposit at more positive potentials than that of the Ag^+/Ag(crystalline) couple (E^*).

It is not very reasonable to compare directly the charge measured in the stripping (q_a) with the experimental value of the integral of the cathodic current (q_c): in fact, the latter is strongly mixed with the base line currents if the deposition is performed on an electrode from which previously the second monolayer of silver had also been eliminated. On the other hand, the difference between q_a and another experimentally determinable quantity, q_c^0, is significant; the physical meaning of q_c^0 is the quantity

of silver deposited on the electrode in the range of the diffusion limiting current.

It was found impossible to determine quantitatively, because of the base line currents, the dissolution of the more "noble" fractions of silver present on the electrode. Therefore it should be found, and is found in fact, that integrating the stripping peaks q_a is lower than q_c^0 if the pre-treatment of the electrode (E_{ox}, t_{ox}) before deposition eliminated the fractions mentioned before. *Vice versa*, if the pre-treatment of the electrode assures the presence of silver only slightly greater than this fraction on the electrode before deposition, the values of q_a would surpass these of q_c^0. Small capacitive (and eventually pseudocapacitive) contributions cause q_a to be slightly larger than the quantity of silver dissolved in the course of the stripping (q'_{Ag}). Under our experimental conditions noticeable effects which could be attributed to mechanical losses, to oxidation of the silver deposited or to other causes, were not found.

The existence of the second monolayer of Ag on Pt could be due to the surface formation of solid solutions (in the case of the Ag–Pt system in particular, the phase diagrams are rather complex[20]), as also for the Cu–Pt system[14,15]. Nevertheless a second monolayer of Ag[11], Hg[12] and Cu[13] seems to be present also on graphite, and for these systems the solubility of carbon even in the molten metal is very low; thus it is difficult to suppose a formation of solid solutions in the cold.

SUMMARY

It has been possible to explain the apparent anomalies in the yield found in the stripping of silver at platinum electrodes in perchlorate solutions as due to silver of appreciably lower activity than crystalline silver. Silver yields three distinct types of deposit on platinum: the first two, containing silver amounts commensurable with that of monoatomic layers, can deposit (and may be stripped) at more positive potentials than crystalline silver.

REFERENCES

1 G. HEVESY, *Physik. Z.*, 12 (1912) 715.
2 K. F. HERZFELD, *Physik. Z.*, 13 (1913) 29.
3 M. HAÏSSINSKY, *J. Phys. Chem.*, 43 (1946) 21.
4 L. B. ROGERS AND A. F. STEHNEY, *J. Electrochem. Soc.*, 95 (1949) 25.
5 J. T. BYRNE AND L. B. ROGERS, *J. Electrochem. Soc.*, 98 (1951) 457.
6 L. B. ROGERS, D. P. KRAUSE, J. C. GRIESS JR. AND P. B. EHRLINGER, *J. Electrochem. Soc.*, 95 (1949) 32.
7 J. C. GRIESS JR., J. T. BYRNE AND L. B. ROGERS, *J. Electrochem. Soc.*, 98 (1951) 447.
8 J. T. BYRNE, L. B. ROGERS AND J. C. GRIESS JR., *J. Electrochem. Soc.*, 98 (1951) 452.
9 M. M. NICHOLSON, *J. Am. Chem. Soc.*, 79 (1957) 7.
10 M. M. NICHOLSON, *Anal. Chem.*, 32 (1960) 1058.
11 S. P. PERONE, *Anal. Chem.*, 35 (1963) 2091.
12 S. P. PE ONE AND W. J. KRETLOW, *Anal. Chem.*, 37 (1965) 968.
13 B. H. VASSOS AND H. B. MARK, *J. Electroanal. Chem.*, 13 (1967) 1.
14 M. W. BREITER, *J. Electrochem. Soc.*, 114 (1967) 1215.
15 G. W. TYNDALL AND S. BRUCKENSTEIN, *Anal. Chem.*, 40 (1968) 1051.
16 G. RASPI AND F. MALATESTA, *J. Electroanal. Chem.*, 27 (1970) 283.
17 J. W. BIXLER AND S. BRUCKENSTEIN, *Anal. Chem.*, 37 (1965) 791.
18 D. COZZI, G. RASPI AND L. NUCCI, *J. Electroanal. Chem.*, 12 (1966) 36.
19 A. R. NISBET AND A. J. BARD, *J. Electroanal. Chem.*, 6 (1963) 332.
20 M. HANSEN, *Constitution of Binary Alloys*, McGraw-Hill, New York, Toronto, London, 2nd edn., 1958, pp. 43–45.

ELECTROANALYTICAL CHEMISTRY AND INTERFACIAL ELECTROCHEMISTRY
Elsevier Sequoia S.A., Lausanne – Printed in The Netherlands

THE RELATIONSHIP BETWEEN THE AMOUNT OF ADSORBED HYDROGEN AND THE POTENTIAL OF THE HYDROGEN ELECTRODE

THOMAS C. FRANKLIN, MASAHIKO NAITO[1], TAKUJI ITOH[2] AND DONALD H. McCLELLAND[3]

Chemistry Department, Baylor University, Waco, Texas (U.S.A.)

(Received February 9th, 1969; in final form April 6th, 1970)

A previous study from this laboratory[1] followed the effect of poisons on the potential of the hydrogen electrode. It is well known that the hydrogen electrode gives erratic results when used to measure pH in solutions that contain so-called electrode poisons. This seemed[1] to be caused by changes in the amount of hydrogen adsorbed on the platinized platinum electrode. Further studies[2-6] have improved the technique for measuring the amount of adsorbed hydrogen and results obtained have indicated that the process was not as simple as was first indicated. For this reason a more extensive study was made of the relationship between the amount of adsorbed hydrogen and the potential of the hydrogen electrode.

EXPERIMENTAL

The amount of adsorbed hydrogen was measured by a previously described coulometric technique[6]. The apparatus is pictured in Fig. 1. The cell was a simple "H" cell with the chambers separated by a fritted glass disk. In most experiments, hydrogen was electrolytically generated on the test electrode until the potential between it and the reference electrode reached a specific value. The current was then turned off; the potential was read using a high impedance digital voltmeter and then a polarogram was obtained for the oxidation of hydrogen present at the surface of the electrode at that particular voltage using a large platinum gauze electrode as a counter electrode. The area under the maxima in the polarogram is a direct measure of the amount of hydrogen oxidized. The time between the interruption of the cathodic current and the polarographic measurement did not seem to be particularly important as long as the polarographic measurement was made directly after the measurement of the potential. The potential variations with time were attributable entirely to changes in the amount of adsorbed hydrogen. The area and potential measurements for the hydrogen saturated electrode were measured immediately after the cathodic current was turned off.

In some cases the voltage was measured between the test electrode and the platinized platinum gauze electrode in a hydrogen saturated solution (an NHE). In other cases a reference calomel electrode was inserted in the cell and the voltage

Present addresses: [1]Mitsuitoatsu Chemicals, Inc. Yokohama, Japan; [2]Toa Nenryo Kogyo K. K., Tokyo, Japan; [3]Gates Rubber Company, Denver, Colorado.

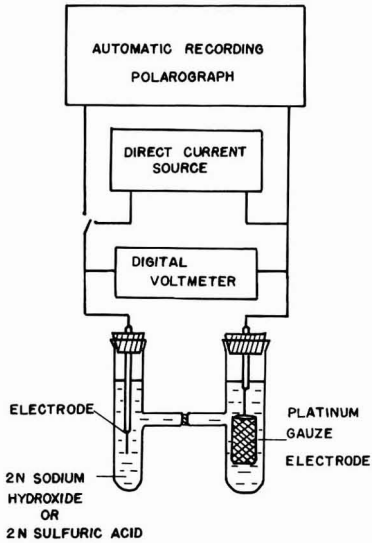

Fig. 1. Block diagram of experimental arrangement.

was measured between the test electrode and the calomel reference. This study was limited to bright and platinized platinum wires. The electrolyte solution was 2 *N* sodium hydroxide, sulfuric acid or perchloric acid. The solution, was, in different experiments, saturated with hydrogen, helium or nitrogen. The hydrogen adsorbed on platinum was varied in different experiments by:

1. Electrolytically charging the electrode with hydrogen until different potentials were reached.

2. Decreasing the amount of hydrogen dissolved in solution by bubbling helium or nitrogen through the solution.

3. Addition of electrode poisons.

The platinum was platinized from a solution around 3% in chloroplatinic acid. The platinum plating conditions ranged from zero amount plated to very heavy deposits; from a plating current density ranging from approximately 10 mA cm^{-2} to 10^3 mA cm^{-2}; from no lead acetate added up to about 0.5% added. The size of the base platinum electrode varied from wires sheared off even with the glass up to wires approximately 5 cm long and to small foils about $\frac{1}{2}$ cm square. Although the base electrode was pretreated in several different ways before plating, the most common method was merely to chemically etch the surface with *aqua regia*.

Some of the experiments were performed in highly purified solutions but most were performed in solutions prepared directly from chemicals that were the purest available commercially. The results obtained in both types of solutions were comparable. The first experiments performed on each electrode were usually the determination of the equilibrium amount of hydrogen adsorbed at hydrogen pressures of 1 atm. If the area under the current potential curves did not reproduce after the first few runs to within $\pm 3\%$ the system was cleaned out and a new electrode and new solutions were used.

A study was made of the effect of sweep rate on the current–voltage curve and

it was found that as long as the sweep rate stayed above 0.2 V min^{-1} the area under the current–voltage curve stayed constant indicating that there was negligible contribution from diffusion of hydrogen to the electrode during the voltage sweep. For this reason, the voltage sweep was maintained between 0.25–0.50 V min^{-1}. In studying the effect of additives on the hydrogen electrode the same experimental procedure used in the absence of the additive was used with additive placed in the solution with the electrode.

Method of calculating the fraction of the surface covered with hydrogen

Figure 2 shows a typical current–voltage curve for the oxidation of hydrogen at a platinized platinum electrode in 2 *N* sulfuric acid. A similar curve was obtained in perchloric acid solutions. The determination of the amount of hydrogen adsorbed on these electrodes is complicated by the fact that the current–voltage curves for the oxidation of hydrogen adsorbed on platinum exhibit several maxima. These maxima are caused by the oxidation of hydrogen that differs in the energy of bonding between the hydrogen and the platinum[3,5,7]. The difference in bonding energy would cause each of these forms of hydrogen to have different E^0 values. For this reason an attempt was made to study the relationship between potential and coverage for each form of adsorbed hydrogen*. The hydrogen oxidation curve was separated into three major forms. The method of separation is shown in Fig. 3.

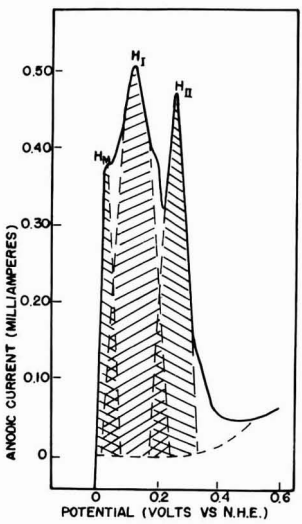

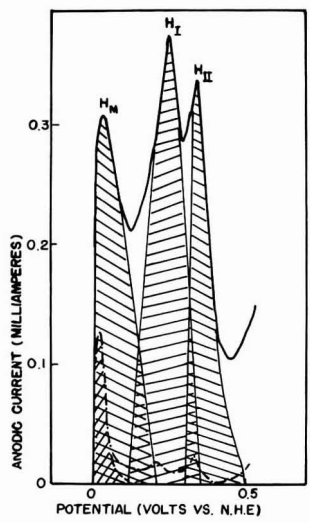

Fig. 2. A typical current–voltage curve for the oxidation of hydrogen at the platinized platinum electrode in 2 *N* sulfuric acid.

Fig. 3. Typical current–voltage curves for the oxidation of hydrogen at platinum electrodes in 2 *N* sodium hydroxide. (---) Platinized platinum, (-·-) bright platinum.

* It should be noted that Petrii *et al.*[8] have experimentally verified, using the differential forms of the equations, the reversibility existing between H^+ and adsorbed atomic hydrogen on platinized platinum in potassium chloride–hydrochloric solutions. It should also be pointed out that current–voltage curves in hydrochloric acid solutions do not show the sharp separation into two peaks observed in H_2SO_4 [9] indicating that possibly in this system it is not necessary to separate the hydrogen into three forms.

Triangles were drawn from the peak to the base so that the sum of the currents of the overlapping triangles would approximate the current–voltage curve obtained experimentally. This was usually accomplished by allowing the two triangles to intersect at the potential of the minimum at a current half as high as the minimum current. This is essentially the equivalent of the drawing of a line from the minimum perpendicular to the potential axis. θ's were calculated for each region. For example, θ_M, at a particular potential was obtained by dividing the amount of hydrogen found as Form I by the amount of hydrogen found as Form I when the platinum was at equilibrium with hydrogen under a pressure of 1 atm in the absence of additives. θ_I and θ_{II} were calculated in a similar manner.

Figure 3 shows typical current–voltage curves for the oxidation of hydrogen in 2 *N* sodium hydroxide using bright and platinized platinum. The various θ's were calculated in the same way as indicated above.

The hydrogen electrode in the absence of additives

Normally the Nernst equation for the hydrogen electrode is written in terms of the fugacity of the hydrogen gas in equilibrium with the electrode. The actual electron transfer process, however, is

$$M + nH^+ + ne \rightleftharpoons MH_n$$

where M–H_n refers to the adsorbed hydrogen and n is the number of hydrogens adsorbed on a site; $n=1$ for atomic hydrogen and $n=2$ for molecular hydrogen. If this electron transfer process is a rapid equilibrium process, then thermodynamically there should be associated with it a Nernst-type equation[10,11] of the following form at 25.0°C

$$E = K - (0.059/n)\log[\theta/(1-\theta)[H^+]^n]$$

where θ is the fraction of the surface covered with adsorbed hydrogen and $(1-\theta)$ is the fraction of the surface that is bare. (It should be recognized that for any value of n greater than one the reaction is composed of a series of steps and one is assuming with this equation that all steps prior to the rate-determining step are essentially at equilibrium[12]). At constant hydrogen ion concentration this equation will reduce to

$$E = K' - (0.059/n)\log[\theta/(1-\theta)] \quad (I)$$

or at low coverages

$$E = K' - (0.059/n)\log H_{adsorbed} \quad (I')$$

It should thus be possible from plots of the potential of the electrode *vs.* $\log[\theta/(1-\theta)]$ or $\log H_{adsorbed}$ to determine first of all whether the electron exchange process over the whole hydrogen region is reversible and, secondly, if it is reversible, to determine the value of n. Straight line plots with appropriate slopes would indicate reversibility. Slopes of -0.030 V would indicate that the adsorbed hydrogen is molecular, whereas, slopes of -0.059 V would indicate that the adsorbed hydrogen is atomic.

RESULTS AND DISCUSSION OF RESULTS

Figures 4 and 5 show typical examples of the results obtained on platinized

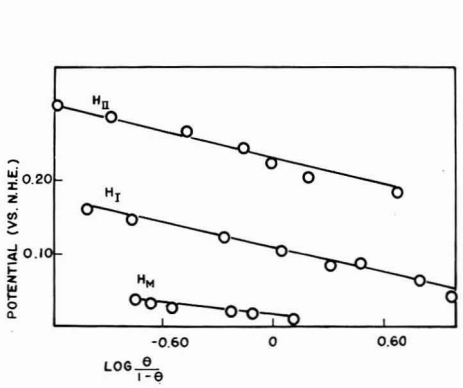

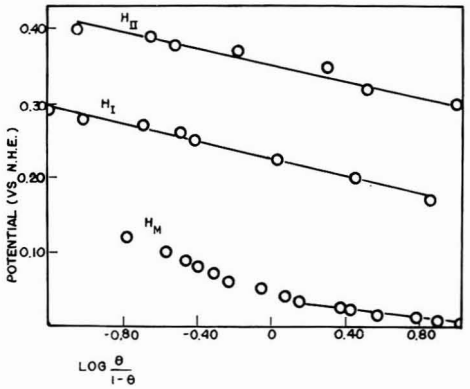

Fig. 4. The effect of adsorbed hydrogen on the potential of a platinum black electrode in 2 *N* perchloric acid.
Fig. 5. The effect of adsorbed hydrogen on the potential of a platinum black electrode in 2 *N* sodium hydroxide.

platinum. The results are summarized in Table 1. On going from still electrodes to electrodes rotated at 600 r.p.m. there was essentially no change in the height or areas associated with H_I or H_{II}. There was a slight change in the total area which was caused entirely by change in H_M. For example in one experiment the total area in arbitrary units upon rotation decreased from 469 to 455. This could be regarded as within the 5% error that had been set as the maximum error in the area measurements. However, this small drop was consistent from experiment to experiment with and without additives present.

TABLE 1

THE FORMULA OF HYDROGEN ADSORBED ON PLATINUM

Metal	*Solution*	*Slope/V*	*Hydrogen form*
Black Pt			
H_M	2 *N* $HClO_4$	−0.29	Molecular
H_I	2 *N* $HClO_4$	−0.059	Atomic
H_{II}	2 *N* $HClO_4$	−0.059	Atomic
H_M	2 *N* NaOH	Uncertain	(?)
		−0.030	Molecular
H_I	2 *N* NaOH	−0.059	Atomic
H_{II}	2 *N* NaOH	−0.059	Atomic
Bright Pt	2 *N* H_2SO_4	−0.031	Molecular[a]
Bright Pt	2 *N* NaOH	−0.029	Molecular

[a] In this case a straight line with a slope of −0.031 V was obtained from a plot based on eqn. (I′) indicating that the maximum coverage of the electrode by hydrogen was relatively small. In all other cases eqn. (I) was used indicating that at maximum coverage the electrode was essentially completely covered.

On bright platinum there is only one maximum and the slope in both acidic and basic solutions was approximately −0.030 V indicating that molecular hydrogen is exchanging electrons with the metal. It should be pointed out that it is not possible

in this experiment to distinguish between adsorbed molecular hydrogen and molecular hydrogen in solution adjacent to the electrode. The fact that in basic solutions it was necessary to plot potential *vs.* $\log[\theta/(1-\theta)]$ in order to obtain a straight line with a reasonable slope implies that the equilibrium was an adsorption equilibrium. On the other hand the fact that H_M decreased slightly on rotation indicates that the peak is at least in part caused by the oxidation of hydrogen in the diffusion layer.

On platinized platinum in acidic and basic solutions the last two maxima gave lines with slopes of approximately -0.059 V (Figs. 4 and 5) indicating that these two forms of hydrogen are atomic in nature. In acidic solutions the form of hydrogen oxidized first gives a line of -0.029 V slope (Fig. 4). In basic solution this form of hydrogen gives a slope at high coverages of -0.30 V (Fig. 5). This indicates that this form of hydrogen is molecular in nature over the potential range of its existence in acidic solutions and at high coverages in basic solutions. It can be seen in Fig. 5 that the single peak on bright platinum corresponds in potential to the H_M peak on the black platinum.

The effect of additives on the hydrogen electrode

The introduction of foreign substances into the solution in contact with the hydrogen electrode can affect the electrode in three ways.

1. The simple elimination of hydrogen adsorption sites by the adsorption of the additive.

2. The removal of the adsorbed hydrogen by direct reaction with the hydrogen

$$M-H+\text{Add.} \rightarrow M+H\ \text{Add.},$$

where Add. refers to the additive and H Add. refers to the reduced additive.

3. The removal of the adsorbed hydrogen by indirect oxidation of the hydrogen, *i.e.*, an electron transfer reaction from the hydrogen through the electrode to the additives.

$$MH \rightarrow M+H^+ + e$$

$$\text{Add.} + e \rightarrow \text{Add.}^-$$

$$\text{Add.}^- + H^+ \rightarrow H\ \text{Add.}$$

It would be expected that, if the electron exchange reaction between the adsorbed hydrogen and the metal is rapid, the first two mechanisms of poisoning of the electrode would not alter the relationship between potential and coverage from that given in eqn. (I) for H_I and H_{II}.

$$E = K - 0.059 \log[\theta/(1-\theta)]$$

However, an additive that behaves as indicated in the third mechanism will act essentially the same as an anodic current oxidizing the hydrogen and the relation between potential and coverage must be taken from electrode kinetics.

When such a reacting ion, for example ceric ion Ce^{4+}, is used as an additive in acidic solutions, the following reactions will proceed at the surface of the electrode, M.

$$MH + H_2O \underset{k_1}{\overset{k_{-1}}{\rightleftharpoons}} M + H_3O^+ + e \tag{1}$$

$$Ce^{4+} + e \overset{k_2}{\rightarrow} Ce^{3+} \tag{2}$$

$$MH + Ce^{4+} + H_2O \rightarrow M + H_3O^+ + Ce^{3+} .$$

The net rate of reaction (1) is given by the expression[1,2],

$$\text{rate (per unit area)} = k_1\theta \exp[(1-\beta)\eta F/RT] - k_{-1}c_{H_3O^+}(1-\theta)\exp(-\beta\eta F/RT)$$

where θ is the fraction of the surface covered with hydrogen, η is the overvoltage, and β is the transfer coefficient. This rate must be equal to the rate of reaction (2). If the concentration of the additive is small, reaction (2) is diffusion controlled and then the rate of reaction (2) per unit area is given by the following equation,

$$\text{rate (per unit area)} = k_2[Ce^{4+}]$$

where k_2 is equal to the diffusion coefficient, D, divided by the thickness of the diffusion layer, δ, $(k_2 = D/\delta)$.

Equating these two rates, which is equivalent to a steady-state assumption, one obtains, after assuming that β is equal to $\frac{1}{2}$ and rearranging the equation, the overpotential, η, as

$$\eta = -(2\,RT/F)\ln\theta + (2\,RT/F)\ln\tfrac{1}{2}\{K_2 + (K_2^2 + 4\,K_1\theta(1-\theta))^{\frac{1}{2}}\} \tag{II}$$

where K_1 is equal to $\{(k_1/k_{-1})\cdot c_{H_3O^+}\}$ and K_2 is equal to $\{(k_2/k_{-1})\cdot[Ce^{4+}]\}$.

When θ approaches unity or zero, eqn. (II) reduces into

$$\eta = -(2\,RT/F)\ln\theta + (2\,RT/F)\ln K_2 . \tag{II'}$$

The maximum deviation, $\Delta\eta_{max}$, of eqn. (II) from eqn. (II') occurs at the point of half coverage $(\theta = \frac{1}{2})$ and is expressed by the equation,

$$\Delta\eta_{max} = (2\,RT/F)\ln\tfrac{1}{2}\{1 + (1 + K_1/K_2^2)^{\frac{1}{2}}\}$$

If K_1/K_2^2 is small compared with unity, $(1 + K_1/K_2^2)^{\frac{1}{2}}$ is approximately equal to $1 + K_1/2\,K_2^2$, $(1+x)^{\frac{1}{2}} = 1 + \frac{1}{2}x$ if x is small compared with 1) then $\Delta\eta_{max}$ is given by the expression

$$\Delta\eta_{max} = (2\,RT/F)\ln(1 + K_1/4\,K_2^2) \doteqdot (RT/F)(K_1/2\,K_2^2)$$

Since K_2 is proportional to the ceric ion concentration, this equation indicates that the maximum deviation, $\Delta\eta_{max}$ between eqns. (II) and (II') is decreased with increasing concentration of ceric ion.

These derivations show that in the higher concentrations of ceric ion eqn. (II') can be used in place of the more complicated eqn. (II) for expressing the overpotential over the whole potential range.

Equation (II') can be further simplified at 25°C to the following expression,

$$\eta = 0.118\log K_2 - 0.118\log\theta$$

$$= A_2 - 0.118\log\theta , \tag{II''}$$

where A_2 is a constant when the concentration of the ceric and hydronium ions are kept constant.

A plot of the potential *vs.* the logarithm of coverage, θ, should thus give a straight line with a slope of -0.118 mV if an electrochemically reducible compound is added to the solution at 25.0°C.

Experimental verification of eqn. (II)

Ceric sulfate was selected as the additive, platinized platinum as the electrode, and 2 *N* sulfuric acid as the medium in order to check experimentally the validity of the above equations. Figures 6 and 7 show typical examples of the experimental results.

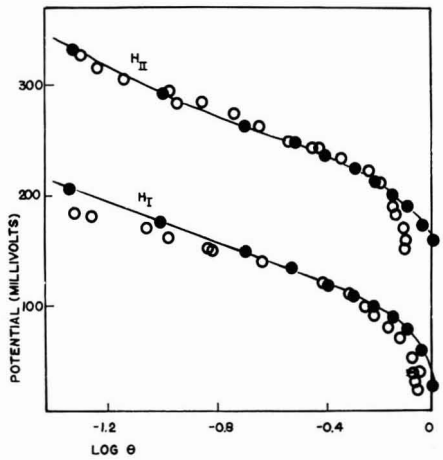

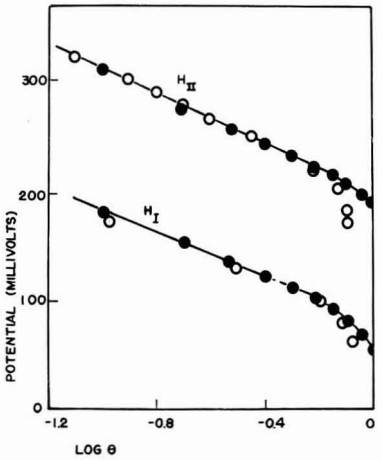

Fig. 6. The effect of adsorbed hydrogen on the potential of a platinum black electrode in 2 *N* sulfuric acid in the presence of 4.0×10^{-7} *M* ceric sulfate. (●) Calcd. value, (○) exptl. data.

Fig. 7. The effect of adsorbed hydrogen on the potential of a platinum black electrode in 2 *N* sulfuric acid in the presence of 4.0×10^{-3} *M* ceric sulfate. (●) Calcd. value, (○) exptl. value.

From these data the constants K_1 and K_2 in eqn. (II) for both the weakly and strongly adsorbed hydrogen can be calculated. In the calculation of K_1 and K_2, the data at the extreme ends of the curve were neglected because the experimental error is relatively large in the determination of the amount of each form of hydrogen in these regions. This is true because in these regions there is appreciable oxidation of another form of hydrogen; for example, as the amount of weakly adsorbed hydrogen gets small there is appreciable oxidation of strongly adsorbed hydrogen.

The computation was done using an IBM 1620 computer by means of an iterative least squares program. The result of the computation are tabulated in Table 2.

Using these two constants K_1 and K_2 for eacn concentration of ceric ion, the theoretical values of hydrogen overpotential at various ceric sulfate concentrations were calculated, and these theoretically calculated values are also plotted in Figs. 6 and 7.

It can be seen that there is good agreement between the data obtained experimentally and the values calculated theoretically.

It is, however, observed in Table 2 that the constants vary with the concentration of the ceric ion. In other words, although the results at a constant cerium(IV)

TABLE 2

THE CALCULATED VALUES OF THE CONSTANTS, K_1 AND K_2, FOR WEAKLY AND STRONGLY ADSORBED HYDROGENS

Ce^{4+}/ mol l^{-1}	H_I			H_{II}		
	$K_1 = \frac{k_1}{k_{-1}} c_{H^+}$	$K_2 = \frac{k_2}{k_{-1}}[Ce^{4+}]$	$\frac{k_2}{k_{-1}}$	$K_1 = \frac{k_1}{k_{-1}} c_{H^+}$	$K_2 = \frac{k_2}{k_{-1}}[Ce^{4+}]$	$\frac{k_2}{k_{-1}}$
0	68	0	—	5800	0	—
4.0×10^{-7}	44.3	1.78	4.5×10^6	2140	21.5	5.4×10^7
4.0×10^{-5}	34.8	2.17	5.4×10^4	1460	26.1	6.5×10^5
3.0×10^{-4}	31.2	2.61	8.7×10^3	910	30.2	1.0×10^5
4.0×10^{-3}	24.7	2.87	719	650	38.4	9.6×10^3
2.33×10^{-2}	19.5	3.16	136	500	42.3	1.8×10^3

concentration are consistent, the constants are more complex than are indicated by this simplified model.

The determination of the mechanism of action of different additives

As indicated in the last section, the relationship between potential and coverage in the presence of additives that block the electrode or react directly with the adsorbed hydrogen is given by eqn. (I) for adsorbed atomic hydrogen

$$E = k - 0.059 \log [\theta/(1-\theta)] \qquad (I')$$

For the third mechanism of poisoning, reduction by electron transfer process, the relationship was shown to be given by eqn. (II) which is approximately given by the expression

$$E = k - 0.12 \log \theta \qquad (II')$$

Several additives were selected for study to experimentally verify eqns. (I') and (II'). Table 3 summarizes the information obtained. Acetonitrile which is known to be catalytically reduced under these conditions[13,14] was selected as an example of a substance that would probably be hydrogenated by direct addition of hydrogen atoms. It was expected that *n*-butanol would not be reduced under these conditions and it was selected as an example of a substance that would act by blocking the electrode

TABLE 3

THE EFFECT OF DIFFERENT MECHANISMS OF POISONING OF HYDROGEN ELECTRODES ON THE EXPERIMENTALLY DETERMINED SLOPE OF THEIR GRAPHS

Catalyst	*Additive*	*Slope/V*	*Mechanism*
Platinum H_I	Acetonitrile	−0.063	Hydrogen addition
Platinum H_I	Ceric sulfate	−0.12	Electron transfer
H_{II}	Ceric sulfate	−0.10	Electron transfer
Platinum H_I	n-Butanol	−0.062	Blocking and decomposition
Platinum H_I	Acrylonitrile	−0.059	Hydrogen addition
H_{II}	Acrylonitrile	−0.12	Electron transfer
Platinum H_I	Quinone	−0.062	Hydrogen addition
H_{II}	Quinone	−0.062	Hydrogen addition

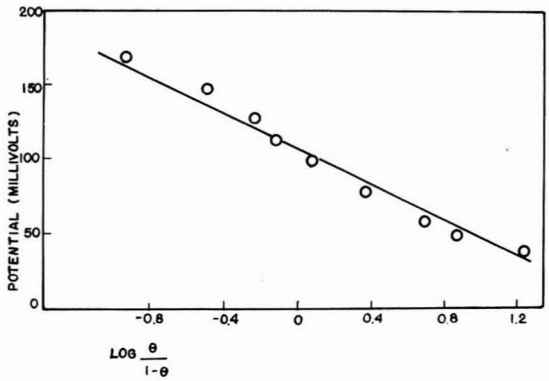

Fig. 8. The effect of adsorbed hydrogen on the potential of a platinum black electrode in 2 *N* sulfuric acid in the presence of n-butyl alcohol.

(Fig. 8). In both cases, in agreement with theory, $E - \log [\theta/(1-\theta)]$ plots gave straight lines with slopes of approximately -0.059 V. As explained in the previous section, ceric sulfate was selected as an example of a substance that was probably reduced under these conditions by an electron transfer process and the results were found to agree with the theory. Two other substances that are reduced at platinum electrodes were studied because, in their cases, there was a question about the mechanism of reduction. The slopes of the different plots indicated that quinone was reduced by hydrogen addition at both high and low coverages of hydrogen; acrylonitrile was reduced at low hydrogen coverages by an electron transfer process and at high coverages by direct addition of hydrogen atoms[14].

It should be pointed out that all of the additives reported in this study have been only moderately to weakly adsorbed. For this reason it has not been necessary to include in the equations a term involving coverage of the additive.

ACKNOWLEDGEMENT

Grateful acknowledgement is given to The Robert A. Welch Foundation for the support given to the major portion of the research reported in this paper.

SUMMARY

An investigation was made of the relationship between the amount of adsorbed hydrogen and the potential of the hydrogen electrode both in the presence of and in the absence of different types of additives.

It was experimentally demonstrated that in the absence of additives or in the presence of additives that blocked the electrode or were hydrogenated by direct addition of hydrogen atoms the relation between potential and θ, the fraction of the surface covered with hydrogen, was

$$E = K - (RT/F) \ln [\theta/1-\theta]$$

If an additive is hydrogenated by an electron transfer process, it was shown that

the relationship was

$$E = E^0 - (2\,RT/F)\ln\theta + (2\,RT/F)\ln\tfrac{1}{2}[K_2 + \{K_2^2 + 4\,K_1\theta(1-\theta)\}^{\frac{1}{2}}]$$

where K_1 and K_2 include rate constants and the concentration of the additive.

REFERENCES

1 T. C. FRANKLIN AND R. D. SOTHERN, *J. Phys. Chem.*, 58 (1954) 951.
2 M. BREITER, C. A. KNORR AND V. VOLKL, *Z. Elektrochem.*, 59 (1955) 681.
3 T. C. FRANKLIN AND S. L. COOKE, JR., *J. Electrochem. Soc.*, 107 (1960) 556.
4 F. A. MATSUDA AND T. C. FRANKLIN, *J. Electrochem. Soc.*, 112 (1965) 767.
5 F. G. WILL, *J. Electrochem. Soc.*, 112 (1965) 451.
6 T. C. FRANKLIN AND D. H. MCCLELLAND, *J. Phys. Chem.*, 67 (1963) 2436.
7 A. N. FRUMKIN in P. DELAHAY (Ed.), *Advances in Electrochemistry and Electrochemical Engineering*, Vol. 3, New York, Interscience Publishers, 1963.
8 O. A. PETRII, R. V. MARVEL AND A. N. FRUMKIN, *Electrokimiya*, 3 (1967) 116.
9 T. C. FRANKLIN AND M. KAWAMATA, *J. Phys. Chem.*, 71 (1967) 4213.
10 M. W. BREITER, *Am. N.Y. Acad. Sci.*, 101 (1963) 709.
11 M. W. BREITER, *J. Electroanal. Chem.*, 8 (1964) 449.
12 B. E. CONWAY, *Theory and Principles of Electrode Processes*, New York, The Ronald Press Company, 1965, chap. 6.
13 B. FORESTI AND S. MUSMECI, *Boll. Sedute Accad. Giovenia Sci. Nat. Catania*, 5 (1959) 330.
14 T. C. FRANKLIN AND N. F. FRANKLIN, *Plating*, 51 (1964) 890.

Elsevier Sequoia S.A., Lausanne – Printed in The Netherlands

SHORT COMMUNICATIONS

Anomalous faradaic impedance of the nickelocene–nickelocinium system in acetonitrile

This study was aimed at examining the impedance behaviour of a mercury electrode in solutions containing a simple redox couple of which one or both components was adsorbed. Interest in such systems stems from a desire to establish kinetic and adsorption parameters in cases where impedance analysis does not correspond to classical derivations, *i.e.* in the absence of adsorption. The various theories for reactions involving adsorption have recently been reviewed[1].

The series of di-π-cyclopentadienyl metal sandwich compounds was considered promising in providing a suitable model system since these compounds are oxidised in a single electron transfer step[2-5] with both oxidised and reduced species soluble. The reaction is polarographically reversible[2-5] and therefore likely to display a faradaic admittance. Preliminary experiments with ferrocene (di-π-cyclopentadienyl iron) indicated that impedance measurements with this system would be difficult since the anodic wave occurred close to the start of mercury dissolution in either mixed or non-aqueous solvents (ferrocene and its analogues are not water soluble). In this region, double layer capacities were either steeply dependent on potential in a pure solvent or, in a mixed solvent, were dependent on frequency as a result of adsorption/desorption processes of the solvent species.

Nickelocene (di-π-cyclopentadienyl nickel) has a standard potential[2-4] about 0.4 V cathodic to that of ferrocene and was therefore chosen for further work. Acetonitrile was found to be a suitable solvent although satisfactory polarographic results were obtained only after purification (two distillations from P_2O_5 followed by two distillations from anhydrous K_2CO_3). Nickelocene, which decomposes quite rapidly in air, was purified by vacuum sublimation at 100°C and stored under vacuum. Experiments were carried out at 25°C in a base solution of 1 *M* $NaClO_4$ in acetonitrile.

For impedance measurements, a low resistance dropping mercury electrode of construction similar to that described previously[6] was used, the fine tip being siliconized by exposure to dichlorodimethylsilane vapour in order to reduce frequency dispersion in capacity measurements. Both blunt and fine tipped electrodes were used for polarography. A cylindrical platinum counter electrode was used in the impedance measurements. A large non-polarizable electrode consisting of a silver sheet, about 1 cm^2, in acetonitrile containing 1 *M* $NaClO_4$ and about 0.1 *M* $AgClO_4$ was used both as a reference electrode and as the counter electrode in polarographic measurements. Its potential was standardized regularly against another silver electrode (0.01 *M* $AgClO_4$, 1.0 *M* $NaClO_4$ in acetonitrile) to which all potentials are referred. The large reference electrode was connected to the cell *via* a salt bridge incorporating glass sinters, the total cell resistance with this arrangement being about 1500 Ω. The electrode impedance was measured as a series equivalent circuit using a variable ratio Wien a.c. bridge over the frequency range 150–4000 Hz.

Nickelocene gave an anodic wave corresponding to its one-electron oxidation to nickelocinium ion, with $E_{\frac{1}{2}} = -0.370 \pm 0.005$ V *vs.* 0.01 *M* Ag^+/Ag independent of nickelocene concentration and plots of *E vs.* $\log [i/(i_d - i)]$ having slopes of 62 ± 2 mV. There was considerable scatter in calculated diffusion coefficients for nickelocene, probably because a rather wide range of capillary characteristics was used. Mean values were $(2.0 \pm 0.5) \times 10^{-5}$ cm^2 s^{-1} using the Ilkovič equation and $(1.45 \pm 0.3) \times 10^{-5}$ cm^2 s^{-1} using the Koutecký equation. The choice of a correct value is discussed below.

Solutions containing nickelocinium ion were prepared from nickelocene solutions by electrolysis at constant current in stirred solution using the cylindrical platinum electrode as an anode. The course of the oxidation was followed polarographically, solutions containing both species giving a composite anodic/cathodic wave with no halt at zero current. So long as the current used for oxidation was not too high, nickelocinium ion seemed to be the only product, the yield agreeing well with the charge passed. Calculations using the variation of anodic and cathodic wave heights during oxidation gave a value for $(D_R/D_O)^{\frac{1}{2}}$ of 1.10 ± 0.01 where D_R and D_O are the diffusion coefficients of the reduced and oxidized forms. The smaller value of D_O is presumably due to the stronger solvation of the charged species. During oxidation the solution colour changed from an initial blue-green to yellow-green for a half-oxidized solution. In some runs the observation of small changes in diffusion currents and equilibrium potentials over a period of hours suggested that irreversible decomposition of the nickelocinium ion was occurring. The instability of this species could explain the less than satisfactory reproducibility found at times during this work.

Two kinds of faradaic impedance measurements were carried out, one at equilibrium with both species present in the bulk solution and the other at the half-wave potential of the anodic wave for nickelocene alone. Equilibrium measurements were performed in solutions having equal anodic and cathodic diffusion currents, *i.e.* $c_O^b D_O^{\frac{1}{2}} = c_R^b D_R^{\frac{1}{2}}$ where c^b refers to bulk concentration. The potentials of the two measurements were the same and the impedance behaviour was similar for the two cases. They are discussed together below.

When the impedance, measured over a range of frequencies, was analysed according to the classical method of Randles[7], anomalous behaviour was found in that the reactive component of the faradaic impedance exceeded the resistive component. This behaviour is similar to that found for a number of rapid electrode reactions[8-14] for which reactant adsorption is presumed to account for the departure from classical theory. When such adsorption is not too strong, its effect has been represented[9-12] by a frequency independent capacitance C_a acting in parallel with the "normal" faradaic impedance. Accordingly, the present measurements were analysed in order to see if this simple equivalent circuit was applicable. The initial assumption was that the electrode reaction was diffusion controlled and the steps used in the calculations were as follows (Fig. 1). The measured impedance, corrected for solution resistance, was converted to a parallel circuit, C_p and R_p. The assumption of diffusion control requires that R_p be the resistive part of a Warburg impedance and this can be tested[14] by examining the frequency dependence of $R_p\omega^{\frac{1}{2}}$, ω being the angular a.c. frequency. Satisfactory independence of frequency for this quantity was found in all cases.

The reactive part $C_{W,p}$ of the Warburg impedance is given by the condition $\omega R_p C_{W,p} = 1$. The difference $C_p - C_{W,p}$, denoted by C_t, should then comprise the sum

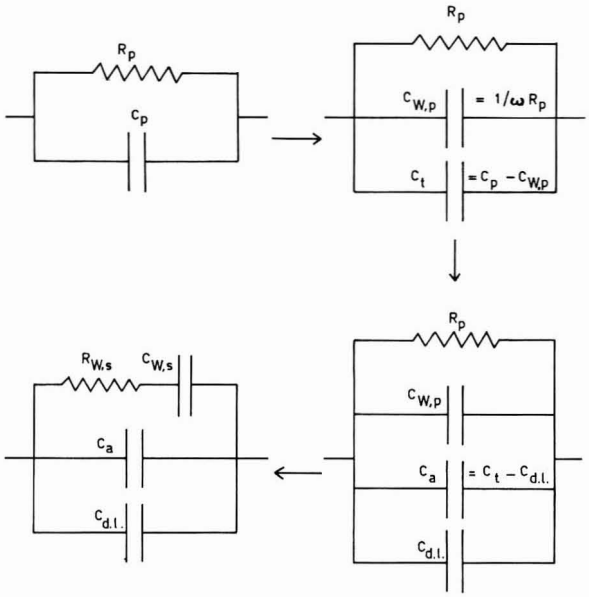

Fig. 1. Steps used in analysis of faradaic impedance components.

of the double layer capacity in the absence of reactants, C_{dl}, and the adsorption capacity, C_a. Adsorption capacities calculated by this method were independent of frequency within experimental error, a result consistent with the assumptions made in carrying out the analysis. Correspondingly, when the impedance analysis in terms of series components was carried out using a mean value of $C_a + C_{dl}$ in place of C_{dl} alone, the Randles plots, $R_{W,s}$ and $(\omega C_{W,s})^{-1}$ *vs.* $\omega^{-\frac{1}{2}}$, were linear, coincided and passed through the origin, as expected for a Warburg impedance.

An equivalent method of analysing results in terms of electrode admittance was used by Timmer *et al.*[14]. In the case of a reversible system with weak reactant adsorption they calculated an apparent double layer capacity C_{app} using

$$\omega C_{app} = Y'' - Y' \tag{1}$$

where Y'' and Y' are the imaginary and real components of the admittance. It can be seen that, in terms of the impedance components used here,

$$Y' = (R_p)^{-1} \quad \text{and} \quad Y'' = \omega C_p \tag{2}$$

Hence

$$C_{app} = C_p - (\omega R_p)^{-1} = C_p - C_{W,p} \tag{3}$$

C_{app} is therefore equivalent to the present $C_a + C_{dl}$.

The concentration dependence of the adsorption capacitance is shown in Fig. 2. Here the concentration is the sum of the bulk concentrations of nickelocene and nickelocinium ions; the actual surface concentration of each species is, for all practical purposes, half this value. The error bars give an indication of the constancy of C_a over the frequency range used rather than an estimate of the accuracy of the results. Apart

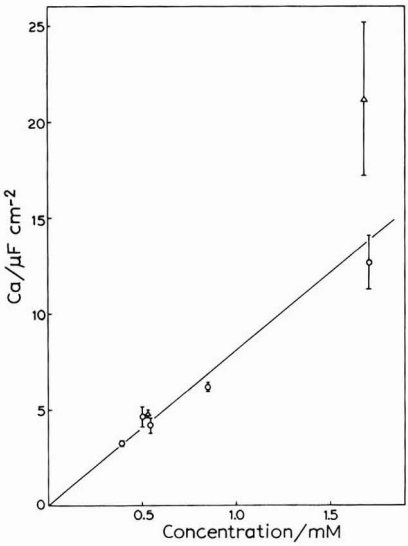

Fig. 2. Concentration dependence of adsorption capacitance C_a. (△) Polarographic, (○) bulk generation of nickelocinium ion.

from the discordant point at 1.68 mM, for which we are unable to offer an explanation, the dependence of C_a on concentration seems to be linear, a finding similar to the reported behaviour of the $Tl^+/Tl(Hg)$ system[10].

The double layer capacity on either side of the admittance peak was examined in order to detect any effects due to adsorption of reactants. A significant lowering was found on the cathodic side indicating the adsorption of nickelocene. On the anodic side, a slight lowering of capacity suggested that nickelocinium ion was also adsorbed; poor reproducibility, however, makes this conclusion uncertain.

As a further test of the applicability of the adsorption capacity—Warburg impedance model to the nickelocene system, the consistency of Warburg slopes with polarographic diffusion results was examined. The Warburg slope σ, obtained either from the Randles plot of $R_{W,s}$ and $(\omega C_{W,s})^{-1}$ *vs.* $\omega^{-\frac{1}{2}}$ or from the relation[14] $R_p\omega^{\frac{1}{2}} = 2\sigma$, is given by

$$\sigma = \frac{RT}{2^{\frac{1}{2}}F^2}\left(\frac{1}{c_O D_O^{\frac{1}{2}}} + \frac{1}{c_R D_R^{\frac{1}{2}}}\right) \tag{4}$$

where the c's are surface concentrations (averaged over the period of the a.c.). We consider two cases:

(1) Bulk generation of oxidised form, impedance measured at equilibrium. Here, surface and bulk concentrations are equal and $c_O^b D_O^{\frac{1}{2}} = c_R^b D_R^{\frac{1}{2}}$. Further, c_R^b is related to the initial nickelocene concentration, $c_{R,i}^b$, by

$$c_R^b = c_{R,i}^b/[1 + (D_R/D_O)^{\frac{1}{2}}] = c_{R,i}^b/2.1 \tag{5}$$

Hence

$$\sigma_1 = \frac{2.1\sqrt{2}\,RT}{F^2 c_{R,i}^b D_R^{\frac{1}{2}}} \tag{6}$$

(2) Polarographic generation of oxidised form[6].

$$\sigma_2 = \frac{2\sqrt{2}\,RT}{F^2 c_R^b D_R^{\frac{1}{2}}} \tag{7}$$

Diffusion coefficients calculated using eqns. (6) and (7) were in reasonable agreement giving $D_R^{\frac{1}{2}} = (3.25 \pm 0.3) \times 10^{-3}$ cm $s^{-\frac{1}{2}}$ (or $D_R = (1.06 \pm 0.2) \times 10^{-5}$ cm^2 s^{-1}). This is much less than the values calculated earlier from diffusion current data but the disagreement can be at least partly resolved as follows. We start with the assumption that the Koutecký equation is more likely to be applicable than the Ilkovič equation. Now, when the results which led to the mean value (Koutecký) of D_R quoted earlier are examined, it is found that they are divided into two groups. For blunt electrodes with drop times of 4–5½ s, $D_R^{\frac{1}{2}} = (3.56 \pm 0.15) \times 10^{-3}$ cm $s^{-\frac{1}{2}}$ while for sharp electrodes with drop times of 6–10½ s $D_R^{\frac{1}{2}} = (4.05 \pm 0.15) \times 10^{-3}$ cm $s^{-\frac{1}{2}}$. With the former type of electrode, the Koutecký equation is supposed[15] to predict limiting currents quite accurately whereas the unshielded, long drop-time electrodes are likely to give limiting currents closer to those for "first drops" in undepleted solutions and therefore yield values of $D_R^{\frac{1}{2}}$ 10–20% too high[15], as actually found. We therefore conclude that the lower D_R is probably the most reliable value from limiting current data and that the polarographic and impedance results are consistent.

To conclude, we find that with systems containing nickelocene and nickelocinium ion in the bulk of the solution as well as with *in situ* polarographic generation of the oxidised form, the faradaic impedance behaviour can be described by a diffusion controlled Warburg impedance in parallel with a frequency independent capacitance which is attributed to the involvement of adsorbed reactants. This result suggests that a lower limit of about 10 cm s^{-1} can be placed on the rate constant for the charge transfer process. Such a high rate constant is not unexpected in view of the simplicity of the process and the presumably small energy required to rearrange the solvent sheaths of these large species. The kinetics of the homogeneous electron exchange between ferrocene and ferricinium ion has been investigated[16] and the rate constant at 25° found to be $> 7 \times 10^6$ l mol^{-1} s^{-1}. Using the established correlation[17] between electrochemical (k_{el}) and chemical (k_{ex}) electron transfer rate constants, $(k_{ex}/10^{11})^{\frac{1}{2}} \sim k_{el}/10^4$, we calculate that for the ferrocene system $k_{el} > \sim 100$ cm s^{-1}. Thus, there is order of magnitude agreement between the lower limits of electrochemical rate constants for these closely related systems.

Acknowledgement

We should like to thank the Science Research Council for a grant (1964–66) supporting this work.

Department of Physical Chemistry,
The University,
Bristol, BS8 1TS (England)

T. Biegler*
Roger Parsons

1 R. Parsons, in P. Delahay (Ed.), *Advances in Electrochemistry and Electrochemical Engineering*, Wiley, New York, 7 (1970) 171.
2 J. A. Page and G. Wilkinson, *J. Am. Chem. Soc.*, 74 (1952) 6149.

* Present address: CSIRO, Division of Mineral Chemistry, Port Melbourne, Victoria, Australia 3207.

3 G. WILKINSON, P. L. PAUSON AND F. A. COTTON, *J. Am. Chem. Soc.*, 76 (1954) 1970.
4 J. TIROUFLET, E. LAVIRON, R. DABARD AND J. KOMENDA, *Bull. Soc. Chim. France*, (1963) 857.
5 A. A. VLČEK, *Collection Czech. Chem. Commun.*, 30 (1965) 952.
6 T. BIEGLER AND H. A. LAITINEN, *Anal. Chem.*, 37 (1965) 572.
7 J. E. B. RANDLES, *Discussions Faraday Soc.*, 1 (1947) 11.
8 H. A. LAITINEN AND J. E. B. RANDLES, *Trans. Faraday Soc.*, 51 (1955) 54.
9 R. TAMAMUSHI AND N. TANAKA, *Z. Physik. Chem. Frankfurt*, 28 (1961) 158.
10 M. SLUYTERS-REHBACH, B. TIMMER AND J. H. SLUYTERS, *Rec. Trav. Chim.*, 82 (1963) 553.
11 M. SLUYTERS-REHBACH AND J. H. SLUYTERS, *Rec. Trav. Chim.*, 83 (1964) 967.
12 J. R. GALLI AND R. PARSONS, *J. Electroanal. Chem.*, 10 (1965) 245.
13 B. TIMMER, M. SLUYTERS-REHBACH AND J. H. SLUYTERS, *J. Electroanal. Chem.*, 15 (1967) 343.
14 B. TIMMER, M. SLUYTERS-REHBACH AND J. H. SLUYTERS, *J. Electroanal. Chem.*, 18 (1968) 93.
15 L. MEITES, *Polarographic Techniques*, Interscience, New York, 2nd ed., 1965, chap. 3.
16 D. R. STRANKS, *Discussions Faraday Soc.*, 29 (1960) 73.
17 R. A. MARCUS, *J. Phys. Chem.*, 67 (1963) 853.

Received March 9th, 1970

J. Electroanal. Chem., 27 (1970) 314–319

The cathodic evolution of hydrogen on ruthenium and osmium electrodes

Introduction

No straightforward study of the hydrogen evolution reaction (her) on solid osmium or ruthenium electrodes appears to have been reported[1] nor does much electrochemical data of any kind exist for these metals[2].

Experimental

(i) Instrumentation

Steady state measurements were obtained potentiostatically using a Chemical Electronics TR 40-3A potentiostat, with output current monitored on a Sangamo Weston S82 DC ammeter and electrode potentials measured with a Keithley 600A electrometer. Ohmic overpotentials were measured with a Solartron CD1400 oscilloscope and recorded on a Telford camera. Roughness factors were measured by the a.c. capacitance bridge technique using a Wayne Kerr 221A Universal bridge with low impedance adaptor Q221A operating at 1592 Hz. Pre-electrolysis was carried out with a Farnell constant current/constant voltage source, model C2.

(ii) Electrodes

Osmium. A vacuum melted button of 99.9% osmium, 0.8 cm diameter was supplied by International Nickel Co.

Ruthenium. A cylinder of 2 cm^2 area on the end face, prepared by powder metallurgical techniques was also supplied by International Nickel as 99.7% purity.

Both electrodes as used in this work, were mounted in a p.t.f.e. cup, showing 0.2 cm^2 of superficial area to the electrolyte. A p.t.f.e. tube screwed into the cup enabling a connection to be made to the back of the metal sample.

Pre-electrolysis, counter and reference electrodes. These were constructed of platinum supplied by Johnson Matthey Ltd. The pre-electrolysis electrode was a

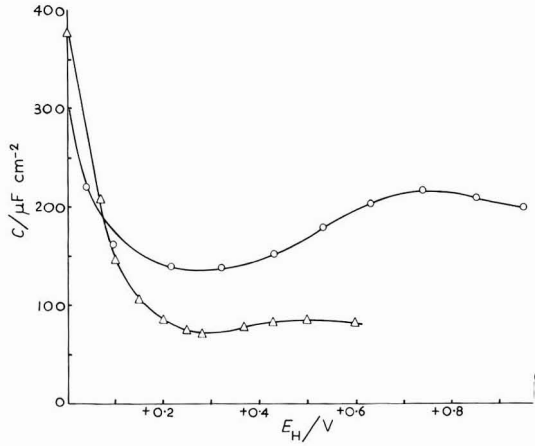

Fig. 1. Variation of the differential capacitance with electrode potential in 1 *N* hydrochloric acid at 25 ± 1°C. (○) ruthenium, (△) osmium.

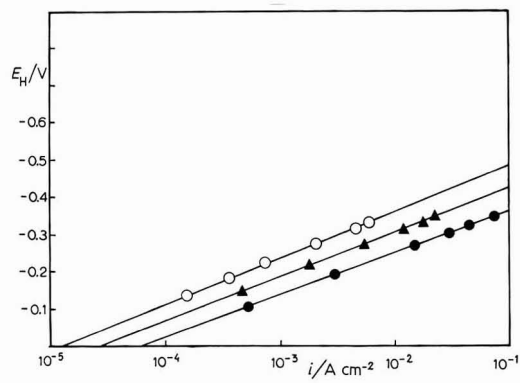

Fig. 2. Current density–potential curve for the hydrogen evolution reaction in hydrochloric acid and sodium chloride soln. of constant ionic strength at 25 ± 5°C on ruthenium. (●) pH 0.0, (▲) pH 0.75, (○) pH 1.45.

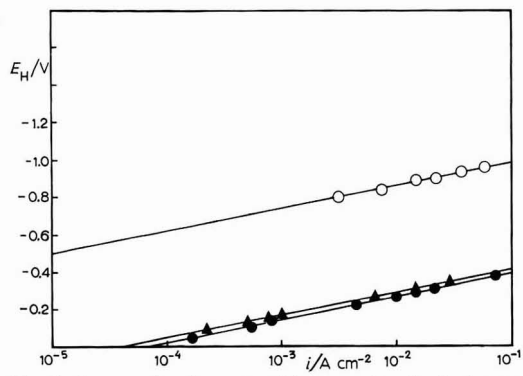

Fig. 3. Current density–potential curves for the hydrogen evolution reaction in hydrochloric acid and sodium chloride solns. of constant ionic strength at 25 ± 5°C on osmium. (●) pH 0.14, (▲) pH 0.65, (○) pH 10.3.

large Pt gauze cage 5 cm high, 3 cm diameter. Counter and reference electrodes were platinised with a chlorplatinic acid + lead acetate solution.

(*iii*) *Solutions*

These were prepared from AristaR HCl, AnalaR NaCl (B.D.H.) and conductivity water from a Fisons conductivity water still. Alkaline solutions were prepared *in situ* by pre-electrolysis (without use of hydrogen counter electrode) of NaCl solutions. These are less contaminated than commercial alkalis. pH values were measured before and after each run.

(*iv*) *Gases*

B.O.C. hydrogen was used, purified by passage through an Engelhard "Deoxo" catalytic purifier.

(*v*) *Cell*

This was a three-compartment cell of conventional design fitted with a Luggin capillary. In addition, the counter electrode had facility for purging, and was housed in a fritted compartment, thus being separated from the working electrode by two frits and two separate gas purge streams. In the working electrode compartment, the large Pt gauze cage was used for pre-electrolysis and was so fitted that it could be raised above the level of the solution during the actual experiments.

(*vi*) *Cleansing of the cell*

Hot water and detergent were used, followed by immersion for several hours in hot chromic acid. This was followed by washing for several hours in a steam/water mixture from the conductivity water still.

(*vii*) *Purification of solutions*

After cleansing of the cell, the solution was transferred into it and H_2 was bubbled into all compartments, not only to remove traces of dissolved oxygen but also to equilibrate the reference and working electrodes and to fuel the hydrogen oxidising counter electrode. With the working electrode positioned, the pre-electrolysis electrode was lowered into the solution through the gas-tight slide facility provided. Pre-electrolysis was continued for 24 h at 10 mA. pH variations were obtained at constant ionic strength using both chlorine evolving and hydrogen consuming counter electrodes.

(*viii*) *Measurement procedure*

After pre-electrolysis, the large cage electrode was withdrawn, still under applied e.m.f. The following potential sequence was then potentiostatically applied to the working electrode: (a) +1.0 V for 10 s, (b) −1.0 V for 1.0 min. This cycle was repeated at least six times, with final cathodic pulse 10 min in duration. The rest potential was then observed.

A series of steady state current–potential curves were then obtained with both increasing and decreasing overpotentials. Steady state was arbitrarily defined as the point at which current changed by less than 10% per h. Ohmic overvoltage corrections were made when the steady state had been reached.

Determination of ohmic overvoltage. This was made by interruption of the applied e.m.f. with a mercury wetted reed relay (model ERG-1HAW 6V) and recording the event oscillographically. At higher current densities, the electrode surface became covered with gas bubbles, reducing the area available for the reaction and causing current fluctuations. This led to difficulties in determination of ohmic drops, since the time and condition of the electrode at interruption are variable. To overcome this, the following procedure was adopted. A large number of ohmic drops were measured at a given potential, leading to a value for η_Ω which refers to i_{mean} at that potential. The ohmic drop relating to i_{max} (at the same given potential) is then given by: $\eta_\Omega \cdot i_{max}/i_{mean}$, and the i_{max} values are the ones plotted in the graphs.

(*ix*) *Determination of true electrode area*

Electrode interfacial capacitances were measured over the range 0.0–0.9 V RHE (Fig. 1).

Results

Figure 1 shows capacitance measurements on the Os and Ru electrodes. By taking the minimum capacitance on Hg electrodes[3] in HCl as 15 μF cm^{-2} the roughness factors for Os and Ru are 4.6 and 8.9, respectively. Figures 2 and 3 show

TABLE 1

REACTION PARAMETERS FOR HYDROGEN EVOLUTION ON Os AND Ru

Metal	*pH*	*Temp./°C*	*Rest potl./mV*	$10^4\ i_0/A\ cm^{-2}$	$(\partial\eta/log\ i)_{c_{H^+}}/V$
Os	0.0	25±1	4	1.05±0.1	−0.120
	0.0	45±1	1	1.2 ±0.3	−0.124
	0.0	65±1	−2	1.6 ±0.3	−0.129
	0.14	25±5	3	0.75±0.3	−0.122
	0.65	25±5	0	0.75±0.6	−0.121
	10.30	25±5	2	0.75±0.6	−0.120
Ru	0.0	25±1	−1	0.45±0.1	−0.117
	0.0	50±1	−2	0.68±0.3	−0.121
	0.0	70±1	3	1.76±0.3	−0.127
	0.0	25±5	1	0.6 ±0.3	−0.113
	0.75	25±5	−2	0.6 ±0.3	−0.118
	1.45	25±5	1	0.56±0.1	−0.123

current *vs.* voltage (ohmic free) plots. Table 1 gives data extracted from the graphs. The following kinetic derivatives were determined for both Os and Ru.

$$(\partial\eta/\partial \log i)_{c_{H^+}} = 2.3\ RT/F \qquad (\partial\eta/\partial \log c_{H^+})_i = 0$$

$$(\partial \log i/\partial \log c_{H^+})_\eta = 0 \qquad (\partial \log i/\partial \log c_{H^+})_\phi = 0.5$$

Variation of i_0 with temperature was also determined and was found to be small. An apparent energy of activation of 6 kcal is found for ruthenium and 2 kcal for osmium*.

* 1 kcal = 4.184 J.

The above facts, together with experimental evidence of high hydrogen coverage quoted in ref. 2 indicate the operation of a Volmer–Heyrovský type atom–ion mechanism on both metals.

Department of Chemistry and Applied Chemistry A. T. Kuhn
University of Salford, P. M. Wright
Salford M5 4WT, Lancashire (England)

1 R. D. GILES, J. A. HARRISON AND H. R. THIRSK, *J. Electroanal. Chem.*, 20 (1969) 47.
2 M. W. BREITER, *Electrode Processes in Fuel Cells*, Springer Verlag, Berlin, 1969, New York, chap. VI and refs.; G. P. KHOMCHENKO AND T. N. STOYANOVSKAYA, *Vestn. Mosk. Univ. Ser. II Khim.*, 19 (1964) 44; *idem*, *Russ. J. Phys. Chem. English Transl.*, 38 (1964) 227; G. P. KHOMCHENKO, N. G. UL'KO AND G. D. VOVCHENKO, *Soviet Electrochem.*, 3 (1967) 288.
3 D. C. GRAHAME, *J. Electrochem. Soc.*, 98 (1951) 343.

Received March 23rd, 1970

Preliminary note

The congruence of the adsorption isotherm and the model of the double layer New results regarding ethyl bromide

SERGIO TRASATTI and GIOVANNA OLIVIERI
Laboratory of Electrochemistry, University of Milan, Via Venezian 21, 20133 Milan (Italy)
(Received 20th June, 1970)

The problem of the correct choice of the electrical variable for the description of the adsorption of organic substances on electrodes has been recently discussed very widely[1-4]. No consensus of opinion has been so far achieved.

Behind the choice of the electrical variable there is the assumption of a well defined model for the adsorption layer. If q^M, the charge on the metal, is used as suggested by Parsons[5], the potential is a linear function of the coverage:

$$E_\theta = E_0(1-\theta) + E_1\theta \tag{1}$$

In this case, the adsorption layer can be represented by two series capacitors. In particular, at $q^M = 0$, this model predicts a linear shift of the potential of zero charge with θ:

$$\Delta E_{z,\theta} = \Delta E_{z,1}\cdot\theta \tag{2}$$

Frumkin and Damaskin[6-8] suggest the potential to be the correct electrical variable to be used. The charge on the metal is thus a linear function of θ:

$$q^M_\theta = q^M_0(1-\theta) + q^M_1\cdot\theta \tag{3}$$

In this case, the model of the surface layer corresponds to two parallel capacitors. In particular, this model predicts for the zero charge potential shift a more complicated variation with θ:

$$\Delta E_{z,\theta} = \Delta E_{z,1}\cdot\theta / \{(C_0/C_1)(1-\theta) + \theta\} \tag{4}$$

where C_0 and C_1 are capacities.

In practice, a clear distinction between these two models seems to be possible only when the isotherm is congruent[9], *i.e.* when the constants of the isotherm do not depend on the electrical variable. Parsons *et al.*[1] have found for C_4 diols that eqn. (1) and eqn. (3) are verified at the same time, while neither holds in the case of other substances, in particular butanol. Frumkin *et al.*[2] suggest, on the contrary, that the behaviour of saturated aliphatic compounds with only one functional group is better described by eqn. (3). and one method suggested to verify that is the use of eqn. (4), particularly when $C_0 \gg C_1$.

We have studied the adsorption of ethyl bromide on mercury from 0.1 *M* KCl aqueous solutions. It has been recently found that the presence of specifically adsorbed anions does not influence the possible congruence of the isotherm[10,11], or the shape of the $\Delta E_z - \theta$ relationship[10].

Electrocapillary curves for 17 solutions of ethyl bromide from 0.0053 *M* to 0.0745 *M* were measured using a Lippmann electrometer. Ethyl bromide was purified by distillation.

The electrocapillary curves become flatter as the ethyl bromide concentration is increased, which suggests that $C_0 \gg C_1$. The curves were differentiated by means of a computer programme described by Parsons *et al.*[12]. Detailed results of this work will be published later on.

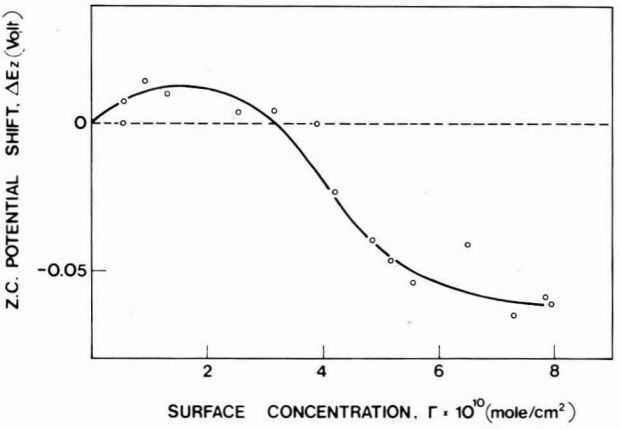

Fig.1. Shift of the potential of zero charge of mercury due to adsorption of ethyl bromide from 0.1 *M* KCl aqueous solution.

Fig.1 shows the zero charge potential shift, ΔE_z, as a function of the surface excess of ethyl bromide calculated by graphical differentiation of ξ *vs.* log *a*, where *a* was put equal to the molar concentration. It is possible to see clearly that the behaviour of E_z cannot be described by either eqn. (2) or eqn. (4). In this case, the variation of E_z with the coverage can only be accounted for by the assumption that the orientation of the adsorbed molecule changes with θ. At small coverages, for $\theta \to 0$, E_z is positive because ethyl bromide is almost completely flat on the surface. When $\theta \to 1$, the molecule is perpendicular with the negative end of the dipole toward the metal. In fact, q^{M}_{max}, the charge at which the surface pressure curves ($\Phi = \xi - \xi_{base}$ *vs.* q^{M}) show a maximum, is about $-2\ \mu C\ cm^{-2}$ for $\theta \to 0$ and about $+1\ \mu C\ cm^{-2}$ for $\theta \to 1$. The maximum adsorption at $-2\ \mu C\ cm^{-2}$ indicates that a small coverage there is negligible contribution by the adsorbed dipole[13], *i.e.* the molecule may be considered as flat on the surface. At high coverage, the maximum adsorption is shifted toward more positive charges because of the interaction of the negative end of the adsorbed dipole with the surface. In effect, the maximum value of Γ is consistent with a projected area of 21 $Å^2$ which corresponds to a perpendicular molecule. At high coverage, a reorientation of adsorbed water by the strongly oriented ethyl bromide dipoles, or an

interaction of the latter with adsorbed negative charges cannot be excluded, which might account for the apparent "saturation" value of ΔE_z. The isotherm has been found to be congruent neither with respect to the charge nor with respect to the potential.

If we take 21 Å^2 as the saturation area, the adsorption seems to be described by a Frumkin isotherm with A, corresponding to attraction, changing with q^M with a minimum at about $-2\ \mu C\ cm^{-2}$. Since marked deviations from this isotherm are observed at $\theta > 0.5$, it is possible that the orientation of the adsorbed molecules is roughly constant for lower coverages.

Existing results[1,11] seem to indicate that the congruence of the isotherm is possible only in the case of molecules which lie flat on the surface, the orientation of which cannot therefore change either with θ or with the electrical variable.

Damaskin[14] reports the case of various aliphatic compounds for which A changes linearly with E, *i.e.* the isotherm is not congruent with respect to the potential. This author suggests that this behaviour is due to non-equipotentiality of the plate of the two parallel capacitors on the solution side, and not to change in orientation of the adsorbed dipoles. The present results seem to suggest that in the case of ethyl bromide the cause of non-congruence and of variation of A with the electrical variable may be mainly the reorientation of the adsorbed molecules. A similar suggestion appears possible also in the light of the variation of E_z with the surface excess for some aliphatic alcohols[15].

REFERENCES

1 E. Dutkiewicz, J.D. Garnish and R. Parsons, *J. Electroanal. Chem.*, 16 (1968) 505.
2 A.N. Frumkin, B.B. Damaskin and A.A. Survila, *J. Electroanal. Chem.*, 16 (1968) 493.
3 R. Parsons, *Rev. Pure and Appl. Chem.*, 18 (1968) 91.
4 B.B. Damaskin, *Elektrokhimiya*, 5 (1969) 771.
5 R. Parsons, *J. Electroanal. Chem.*, 7 (1964) 136.
6 A.N. Frumkin, *Z. Phys.*, 35 (1926) 792.
7 B.B. Damaskin, *J. Electroanal. Chem.*, 7 (1964) 155.
8 A.N. Frumkin and B.B. Damaskin in J. O'M. Bockris (Ed.), *Modern Aspects of Electrochemistry, Vol. III*, Butterworths, London (1964).
9 R. Parsons, *Proc. Roy. Soc. (London)*, 261A (1961) 79.
10 S. Trasatti, submitted for publication.
11 R. Parsons and F.G.R. Zobel, *Trans. Faraday Soc.*, 62 (1966) 3511.
12 J. Lawrence, R. Parsons and R. Payne, *J. Electroanal. Chem.*, 16 (1968) 193.
13 K. Müller, *J. Res. Inst. Catal., Hokkaido Univ.*, 14 (1966) 224.
14 B.B. Damaskin, *Elektrokhimiya*, 1 (1965) 1123.
15 R.G. Barradas and P.G. Hamilton, *Can. J. Chem.*, 43 (1965) 2468.

Vol. 27 No. 2 JOURNAL OF ELECTROANALYTICAL CHEMISTRY SEPTEMBER 1970
AND INTERFACIAL ELECTROCHEMISTRY

CONTENTS